UNIVERSIDADE FEDERAL DE SANTA CATARINA
CENTRO TECNOLÓGICO
PROGRAMA DE PÓS-GRADUAÇÃO EM ENGENHARIA MECÂNICA

Edmilton Oliveira Stein

MODELING AND ANALYSIS OF A PUMP CONTROLLED SYSTEM FOR SPEED GOVERNOR IN HYDROELECTRIC POWER PLANTS

Florianópolis
2025

Edmilton Oliveira Stein

MODELING AND ANALYSIS OF A PUMP CONTROLLED SYSTEM FOR SPEED GOVERNOR IN HYDROELECTRIC POWER PLANTS

Dissertação submetida ao Programa de Pós-Graduação em Engenharia Mecânica da Universidade Federal de Santa Catarina para a obtenção do título de Mestre em Engenharia Mecânica.
Orientador: Prof. Victor Juliano De Negri, Dr. Eng.
Coorientador: Prof. Marcos Paulo Nostrani, Dr. Eng.

Florianópolis

2025

Ficha de identificação da obra

Stein, Edmilton Oliveira
MODELING AND ANALYSIS OF A PUMP CONTROLLED SYSTEM FOR SPEED GOVERNOR IN HYDROELECTRIC POWER PLANTS / Edmilton Oliveira Stein ; orientador, Victor Juliano De Negri, coorientador, Marcos Paulo Nostrani, 2025.
137 p.

Dissertação (mestrado) - Universidade Federal de Santa Catarina, Centro Tecnológico, Programa de Pós-Graduação em Engenharia Mecânica, Florianópolis, 2025.

Inclui referências.

1. Engenharia Mecânica. 2. Electro-hydrostatic actuators. 3. Speed governor. 4. Hydroelectric power plants. 5. Hydraulic systems. I. De Negri, Victor Juliano. II. Nostrani, Marcos Paulo. III. Universidade Federal de Santa Catarina. Programa de Pós-Graduação em Engenharia Mecânica. IV. Título.

Edmilton Oliveira Stein

MODELING AND ANALYSIS OF A PUMP CONTROLLED SYSTEM FOR SPEED GOVERNOR IN HYDROELECTRIC POWER PLANTS

O presente trabalho em nível de mestrado foi avaliado e aprovado por banca examinadora composta pelos seguintes membros:

Prof. Antonio Carlos Valdiero, Dr. Eng.
EMC – Universidade Federal de Santa Catarina

Prof. Antonio Dourado, Dr. Eng.
CTJ - Universidade Federal de Santa Catarina

Certificamos que esta é a **versão original e final** do trabalho de conclusão que foi julgado adequado para obtenção do título de mestre em Engenharia Mecânica.

____
Coordenação do Programa de Pós-Graduação

____
Prof. Victor Juliano De Negri, Dr. Eng.
Orientador

____
Prof. Marcos Paulo Nostrani, Dr. Eng.
Coorientador

Florianópolis, 2025.

This thesis is dedicated to my Lord and Savior, Jesus Christ, to my wife Emilly Stein, to my parents, Milton Stein and Marta Stein, and to all those who in some way collaborated with this work.

AKNOWLEDGEMENTS

First and foremost, I would like to thank God for His lovingkindness toward me, for providing me with wisdom and understanding where I had none, for granting me health, and for encouraging me to complete this thesis.

I am deeply grateful to my parents, Milton Stein and Marta Stein, for their unwavering belief in me and for supporting me, not only financially, but throughout this journey. I also want to express my heartfelt thanks to my wife, Emilly Stein, for standing by my side during this challenging time and understanding the many hours and sleepless nights that I went into completing this work.

I am equally grateful to my advisors, Victor De Negri and Marcos Nostrani, for their guidance and insightful advice. I would also like to extend this gratitude to all my teachers and professors who paved the way for me to reach this point.

Finally, my sincere thanks to all who contributed in some way to this accomplishment, with special mention to my friend and classmate, Ruben Bolaños.

RESUMO

Esta dissertação aborda as ineficiências e limitações dos sistemas hidráulicos tradicionais usados nos reguladores de velocidade de turbinas Francis em usinas hidrelétricas. Em particular, destaca-se a necessidade desses sistemas por grandes volumes de fluido hidráulico, o que apresenta desafios ambientais e de manutenção significativos. Além disso, os componentes complexos dos reguladores de velocidade convencionais são difíceis de modernizar e manter, com peças de reposição muitas vezes sendo caras ou indisponíveis em virtude de uma fabricação personalizada para cada planta. Buscando sanar esses problemas, esta pesquisa propõe um sistema descentralizado baseado em atuadores eletro-hidrostáticos (EHA). Essa abordagem elimina a necessidade de uma válvula distribuidora e reduz significativamente o volume de fluido hidráulico necessário. O estudo começa com uma breve revisão bibliográfica sobre usinas hidrelétricas, com foco nas turbinas Francis e seus reguladores de velocidade, seguida de uma revisão das configurações de EHA, identificando uma arquitetura adequada para reguladores de velocidade em usinas hidrelétricas com turbinas do tipo Francis. O sistema proposto utiliza exclusivamente produtos comerciais disponíveis, o que simplifica a implementação e reduz os custos de manutenção. A modelagem do sistema, realizada utilizando os softwares Hopsan e Matlab Simulink, avalia o desempenho da nova arquitetura. Os resultados mostram que o sistema é capaz de atender as necessidades comuns de reguladores de velocidade, como limitação de sobrevelocidade e mudanças rápidas de posição causadas por pequenas flutuações na demanda de energia pela rede elétrica. Além disso, a arquitetura simplificada do sistema proposto facilita a manutenção ao eliminar componentes complexos, aumentando sua adaptabilidade para futuras modernizações e manutenções.

Palavras-chave: Atuadores eletro-hidrostáticos, regulador de velocidade, Turbina Francis, usina hidrelétrica, hidráulica.

RESUMO EXPANDIDO

Introdução

A crescente demanda por energia elétrica no Brasil é suprida em sua maior parte por hidrelétricas que, segundo EPE (2021), foram responsáveis por cerca de 64% da energia elétrica gerada em 2020. Esse cenário coloca em pauta a necessidade de melhorias na eficiência dos processos de geração, transformação e distribuição de energia elétrica no país. Em 2020, o Brasil perdeu mais de 100 TWh em eletricidade, uma quantidade considerável se comparada ao total gerado (621,2 TWh) e aos 25,1 TWh importados no mesmo ano. Uma maior eficiência poderia, portanto, contribuir para a independência energética do país. A predominância da energia elétrica produzida em hidrelétricas no Brasil se deve em parte ao elevado potencial hídrico do país, com uma abrangente malha hídrica e vasto território.

Dentre os principais componentes de uma usina hidrelétrica é possível destacar barragem, reservatório, tomada d'água, vertedouro, casa de força, conduto forçado, chaminé de equilíbrio ou câmara de carga e tubo de sucção (HENN, 2006). Por intermédio destes componentes a energia potencial, armazenada na forma de grandes reservatórios de água, é transformada em eletricidade. Ou seja, a barragem armazena a água para formar um reservatório que serve como fonte de energia potencial, enquanto o conduto forçado direciona a água, transformando a energia potencial em cinética que, ao passar pelas turbinas, gera eletricidade por meio de um gerador elétrico.

Um regulador de velocidade é o responsável por controlar a quantidade de energia elétrica gerada no conjunto turbina/gerador, assim como, manter sua frequência constante independentemente da demanda por energia elétrica ou quantidade de água armazenada no reservatório. Geralmente, o controle de velocidade é feito por sistemas hidráulicos, cuja escolha é devido a suas características intrínsecas, como baixa relação peso/potência, altas velocidades e acelerações, variação contínua de força, torque e velocidades, além de ser autolubrificado e possuir boa robustez mesmo em condições ambientais adversas (LINSINGEN, 2016).

Contudo, os sistemas hidráulicos convencionais apresentam desvantagens, como baixa eficiência devido à característica de fornecimento contínuo de vazão pela bomba e à dissipação de energia por atrito viscoso. Outra característica desses sistemas é a quantidade de fluido hidráulico armazenado em suas tubulações, visto que, em muitos casos, o local onde a energia hidráulica é gerada fica distante do atuador que está realizando trabalho. O que implica em custos elevados, além de ser um agravante de impactos ambientais gerado pela óleo hidráulico de origem mineral. Além disso, esses sistemas estão sujeitos a riscos econômicos, visto que os fluidos minerais utilizados são finitos e caros, além de gerarem problemas de descarte.

Buscando mitigar estes problemas, esta dissertação propõe a descentralização do sistema hidráulico dos reguladores de velocidade em usinas hidrelétricas, utilizando atuadores controlados diretamente pela bomba. Neste cenário, cada função da planta seria individualmente gerida por um sistema controlado pela bomba, formando um sistema semiaberto e mais eficiente, em que a unidade primária de conversão também atua como unidade de controle, eliminando a necessidade de válvulas de controle. Isso reduz o consumo de energia, uma vez que esta, reduz a dissipação de energia por meio de válvulas de alívio.

O sistema descentralizado controlado por bomba apresenta várias vantagens em comparação com os sistemas centralizados convencionais, como a eliminação da válvula distribuidora. Muitas dessas válvulas, por terem arquitetura antiga e operarem há décadas, não têm peças de reposição no mercado, sendo muitas vezes caras e difíceis de substituir. Estes sistemas também necessitam de menos fluido hidráulico, já que todos os componentes estão próximos entre si, reduzindo a necessidade de longas tubulações e mitigando impactos ambientais em casos de vazamento. Além disso, eles facilitam a manutenção e a segurança, pois cada atuador possui sua própria fonte de conversão de energia, sendo assim, em caso de dano a um sistema, os outros não são comprometidos.

Portanto, o estudo visa avaliar a viabilidade técnica de substituir o sistema de controle de velocidade das turbinas Francis, atualmente operado por sistemas hidráulicos convencionais, por um sistema descentralizado com atuadores controlados pela bomba. A adoção desse modelo poderia reduzir o consumo de óleo hidráulico, melhorando a eficiência e diminuindo o impacto ambiental das usinas hidrelétricas.

Objetivos

O objetivo desta dissertação de mestrado é projetar um circuito hidráulico adequado para reguladores de velocidade, utilizando um atuador controlado por bomba aplicável a turbinas hidráulicas do tipo Francis, que são encontradas em usinas hidrelétricas. O projeto inclui a modelagem do sistema hidráulico e posterior análise de sua resposta dinâmica visando avaliar seu tempo de abertura, resposta a transientes no consumo de energia pela rede elétrica, bem como resposta à um cenário de emergência.

Os seguintes objetivos são definidos para atingir o objetivo principal desta dissertação de mestrado:

- Identificar as principais configurações possíveis de atuadores eletro-hidrostáticos, bem como suas características por meio de uma revisão de literatura sobre o assunto;
- Propor uma arquitetura de um atuador controlado por bomba aplicável a reguladores de velocidade;
- Selecionar os principais componentes para o sistema proposto para avaliar sua viabilidade;
- Modelar o sistema por meio de um software de modelagem e análise de sistemas multidomínio;
- Simular o sistema modelado;
- Avaliar a resposta dinâmica do sistema em relação ao tempo de abertura do servomotor, resposta à transientes no consumo de energia elétrica pela rede elétrica, assim como, em um cenário de emergência.

Metodologia

Com o objetivo de obter a base teórica suficiente para desenvolver a seguinte dissertação, foi realizada uma revisão bibliográfica sobre hidrelétricas, dando ênfase para os reguladores de velocidade de turbinas do tipo Francis. Seguindo para atuadores eletro-hidrostáticos e atuadores controlados por bombas. Para tal, foram utilizados livros e artigos científicos cujos temas abordam estes assuntos.

Posteriormente, foi elaborado uma arquitetura para o sistema hidráulico com uma pré-seleção de seus principais componentes, para que assim, possa ser desenvolvido uma modelo por meio dos softwares Matlab/Simulink e Hopsan. Por meio destes, é analisado o comportamento do sistema proposto para comparação com padrões definidos por norma e dados experimentais de testes em uma usina hidrelétrica existente.

Por fim, um esquema completo utilizando componentes de prateleira é elaborado para demonstrar a viabilidade técnica da arquitetura proposta.

Resultados e discussões

Como resultado é obtida uma arquitetura de um atuador controlado por bomba com objetivo de controle das pás do sistema diretor de turbinas Francis. Esta arquitetura é analisada quanto a seu desempenho no tempo de abertura, resposta a variações no consumo de energia elétrica e tempo de fechamento em modo de emergência. Ainda, é realizada uma comparação entre os dados simulados e experimentais obtidos em uma usina existente, fornecidos por uma empresa parceira.

O procedimento típico para avalição de servomotores em turbinas hidráulicas é posicioná-lo na posição central em relação ao seu curso e, em seguida, aplicar pequenos degraus de posição para avaliação de sua resposta dinâmica. Dessa forma, o primeiro teste realizado foi avaliar o sistema com os modelos matemáticos de atrito de LuGre e o modelo da carga típica em um servomotor. Em que o servomotor é posicionado no centro de seu curso para posterior aplicação de uma entrada em degrau de 5% do curso do cilindro. Para avaliação da resposta de servomotores, tipicamente, é realizado em água morta, ou seja, com o sistema sem cargas externas.

Em seguida, foi conduzida uma análise de desempenho do sistema em água morta (ausência de carga externa). O atuador é posicionado no centro de seu curso e é aplicado diferentes amplitudes de entrada de posição para avaliar a resposta do sistema. Sendo essas 10%, 5% e 3% do curso do atuador. Por intermédio da simulação é possível observar que o sistema proposto possui um erro em regime permanente e um tempo de acomodação menor em comparação ao sistema original.

Outro ponto de análise é a possibilidade de cavitação no sistema. A simulação demonstra que durante os testes a pressão nas portas de sucção da bomba nunca caem abaixo do limite crítico para cavitação. Esse resultado indica que o sistema proposto consegue operar sem danos por cavitação, aumentando sua durabilidade e confiabilidade.

Além das análises de desempenho e cavitação, destaca-se a arquitetura do novo sistema, que, por ser controlada por bomba e descentralizada, possibilita uma significativa redução no volume de óleo necessário no acumulador e na tubulação. Comparado ao sistema convencional, há uma diminuição de 4.054 m³ para 0,087 m³ de óleo no acumulador, e de 0,848 m³ para 0,058 m³ no volume total de tubulação. Essa simplificação não só facilita a manutenção do sistema, como também reduz a necessidade de componentes exclusivos, aumentando a confiabilidade e o acesso a peças de reposição.

Os resultados da simulação indicam que o novo sistema hidráulico é capaz de atender as dinâmicas de resposta de um sistema já existente e implementado. Além disso, a economia significativa de óleo reforça a eficácia e sustentabilidade do projeto. A simplificação na arquitetura também facilita a manutenção e aumenta a confiabilidade do sistema.

Conclusão e trabalhos futuros

Esta dissertação de mestrado apresenta uma visão geral de uma usina hidrelétrica e seus principais componentes, com ênfase no regulador de velocidade. Após analisar um sistema hidráulico típico para este tipo de máquina, é proposto um sistema moderno e descentralizado, permitindo que cada função opere de forma independente. Para isso, um atuador eletro-hidrostático é empregado para cada função da usina e a uma pressão maior do que a da usina analisada.

Uma revisão bibliográfica dos atuadores eletro-hidrostáticos foi concebida para obter a base teórica necessária para selecionar o melhor projeto para a aplicação. Uma nova arquitetura é proposta, cuja análise de desempenho compreende as avaliações do tempo de abertura, bem como a resposta dinâmica e sua capacidade de resposta a emergências. Todas as simulações e análises são conduzidas via simulação utilizando os softwares Hopsan e Matlab/Simulink, com os principais modelos descritos neste trabalho.

Após a realização das simulações é possível concluir que o sistema é capaz de atender pequenas variações no fornecimento de energia elétrica da mesma maneira que o sistema original, assim como, abrir as pás do distribuidor no devido tempo e realizar fechamentos de emergência com segurança.

Outra contribuição significativa é a redução do consumo de óleo, proporcionada pela possibilidade do posicionamento do equipamento mais próximo do local da aplicação e, em decorrência de seu tamanho reduzido quando comparado ao sistema convencional. Além disso, apresenta outra vantagem por meio da eliminação da válvula distribuidora, que muitas vezes é desenvolvida especificamente para cada planta com alta precisão e, portanto, cara e de difícil manutenção.

Além disso, este trabalho introduz um método para evitar intermitência excessiva em válvulas de retenção operadas por piloto usadas para compensar vazamentos e diferenças de área em cilindros hidráulicos diferenciais. Isso é obtido por meio das válvulas direcionais operadas por piloto.

Finalmente, um circuito hidráulico completo é apresentado, demonstrando a viabilidade do projeto usando componentes disponíveis comercialmente.

Após uma análise mais aprofundada nesta dissertação, os seguintes trabalhos são propostos:

Criar uma bancada de testes e dimensionar o sistema para aplicação em uma usina de energia, uma vez que esta dissertação abrange apenas resultados de simulação. Portanto, validála por meio de resultados experimentais contribuiria muito para uma mais profunda compreensão desses sistemas.

Como o presente trabalho empregou um controle PI com um perfil de carga específico, o desenvolvimento de estratégias de controle para atuadores controlados via deslocamento volumétrico da bomba com diferentes perfis de carga e configurações de circuito traria uma grande contribuição.

Aprimorar o método de seleção de bombas de deslocamento variável para aplicação em atuadores eletro-hidrostáticos para incorporar uma dinâmica mais adequada ao seu prato.

Investigar e desenvolver uma solução para manutenibilidade em relação a filtragem manutenção de temperatura de sistemas hidráulicos que trabalham em circuito fechado ou semiaberto.

Palavras-chave: Atuadores eletro-hidrostáticos, regulador de velocidade, Turbina Francis, usina hidrelétrica, hidráulica.

ABSTRACT

This thesis addresses the inefficiencies and limitations of traditional hydraulic systems used in speed governors for Francis turbines in hydroelectric power plants. Particularly, their need for large volumes of hydraulic fluid, which presents significant environmental and maintenance challenges. Additionally, the complex components of conventional speed governors are difficult to modernize and maintain, with replacement parts often being expensive or unavailable. To address these issues, this master's thesis proposes a decentralized system based on electro-hydrostatic actuators (EHA). This approach eliminates the need for traditional control valves and significantly reduces the hydraulic fluid required. The study begins with a brief literature review on hydroelectric power plants, focusing on Francis turbines and their speed governors, followed by a review on EHA configurations, identifying a suitable architecture for speed governors in hydroelectric power plants. The proposed system relies solely on off-the-shelf products, simplifying implementation and reducing maintenance costs. The system modelling, performed using Hopsan and Matlab Simulink, assesses the performance of the new architecture. The results show that the system effectively manages common challenges in speed governors, such as overspeeding and fast position changes caused by minor fluctuations in electrical power demand. Furthermore, the proposed system's simplified architecture makes maintenance easier by eliminating complex components, enhancing its adaptability for future modernization and maintenance.

Keywords: electro-hydrostatic actuators, speed governor, Francis turbines, hydroelectric power plants, hydraulic systems.

LIST OF FIGURES

LIST OF TABLES

CONTENTS

1 INTRODUCTION

The large demand for electricity in Brazil, of which hydroelectric power plants are responsible for supplying approximately 64% in 2020, according to EPE (2021), reinforces the need to increase the efficiency of electricity generation, transformation and distribution. The electricity lost in the country in 2020 surpassed 100 TWh from a total of 621.2 TWh generated, which hydraulic energy was responsible for 396.4 TWh. Moreover, the electricity lost is about four times the imported in the same year (25.1 TWh). Therefore, better system efficiency could help Brazil achieve energy independence.

Brazilian hydroelectric potential (Figure 1), among other factors, makes this the predominant source of energy in the country. In addition, hydroelectric power plants are able to provide large-scale clean and renewable energy, as mentioned by Eick (2010).

Hydroelectric plants typically comprise a dam, reservoir, water intake, spillway, power house, penstock, stand-pipe or loading chamber and draft tube (HENN, 2006). In summary, the dam stores water creating a reservoir as a potential energy source, then the penstock directs it in the form of kinetic energy to the power house, which converts it into electricity. There are also other auxiliary systems such as stop-logs, whose purpose is to cut off the water supply in an emergency or for maintenance. Details of the remaining systems will be presented in Section 2.1.

Figure 1 - Electricity generation in Brazil by source in 2020.

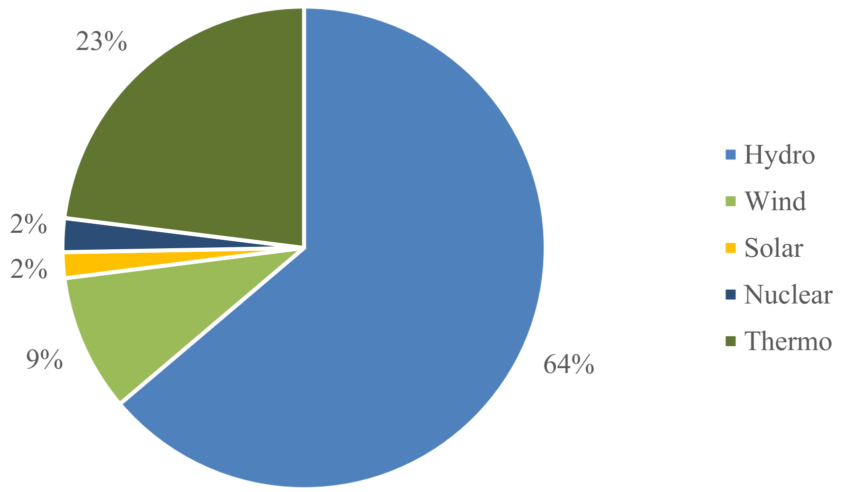

Source: Based in EPE (2021).

Hydraulic turbines are the components responsible for transforming hydraulic energy into electric energy. A hydroelectric power plant may contain one or more turbines, which must operate at a given frequency and as efficiently as possible regardless of their load or head. In order to do so, a component known as a speed governor is used. Although there are researches using pneumatic technology to control the speed of hydroelectric power plants turbines such as seen in Mendoza (2006), typically, their speed control is achieved by hydraulic systems. This is due to characteristics such as those mentioned by Linsingen (2016), which are their low power-to-weight ratio, high speeds and accelerations, continuous variation of force, torque and speeds, being self-lubricated, and robust to harsh environmental conditions.

As presented in Linsingen (2016), conventional hydraulic systems generally consist of a primary conversion unit (PCU), limiting and control unit (LCU), secondary conversion unit (SCU) and storage and conditioning (SC), as can be seen in Figure 2. Typically, the PCU comprises a hydraulic pump that is driven by an electric motor or internal combustion engine. This unit is responsible for providing flow rate to all actuators in the system. At the LCU, hydraulic energy is conditioned through valves, which, are controlled using external action or signal feedback in order to control the actuators that are in the secondary conversion units. The SCU is responsible for converting hydraulic energy to mechanical energy to the system. Finally, the SC is composed of a reservoir, filters and heat exchangers. The SC interacts with the environment through heat exchangers, with the LCU by receiving hydraulic energy from all actuators and the pump, and with the PCU receiving the already conditioned hydraulic fluid.

Conventional hydraulic systems have the disadvantage of low energy efficiency in some cases due to two main factors: – The need for a continuous flow rate by the pump, which mostly returns to the reservoir without performing any useful work (ALLE *et al.*, 2016). – The dissipation of energy by the friction resulting from the viscosity of the fluid in contact with pipe walls, load losses in valve orifices and internal leakage (LINSINGEN, 2016).

Another disadvantage in conventional hydraulic systems is the possibility of having a large amount of hydraulic fluid stored in pipelines used to transport it from the primary conversion unit to all actuators in the network. The amount of oil stored depends on the physical distance between the hydraulic elements. This results not only in an increase in cost due to a large amount of oil and pipes needed but mainly in an environmental impact generated by its production, risks of leakage into the environment and disposal.

Furthermore, conventional hydraulic systems are more susceptible to economic risks as cited by Gelinski *et al.* (2016), because the mineral-based hydraulic fluid is a finite resource.

Although there are alternatives for less polluting and renewable hydraulic fluids such as those presented in Ekman & Börjesson (2011), they have a high cost when compared to mineral-based hydraulic fluids, restricting their use to specific applications.

Figure 2 - Generic hydraulic system.

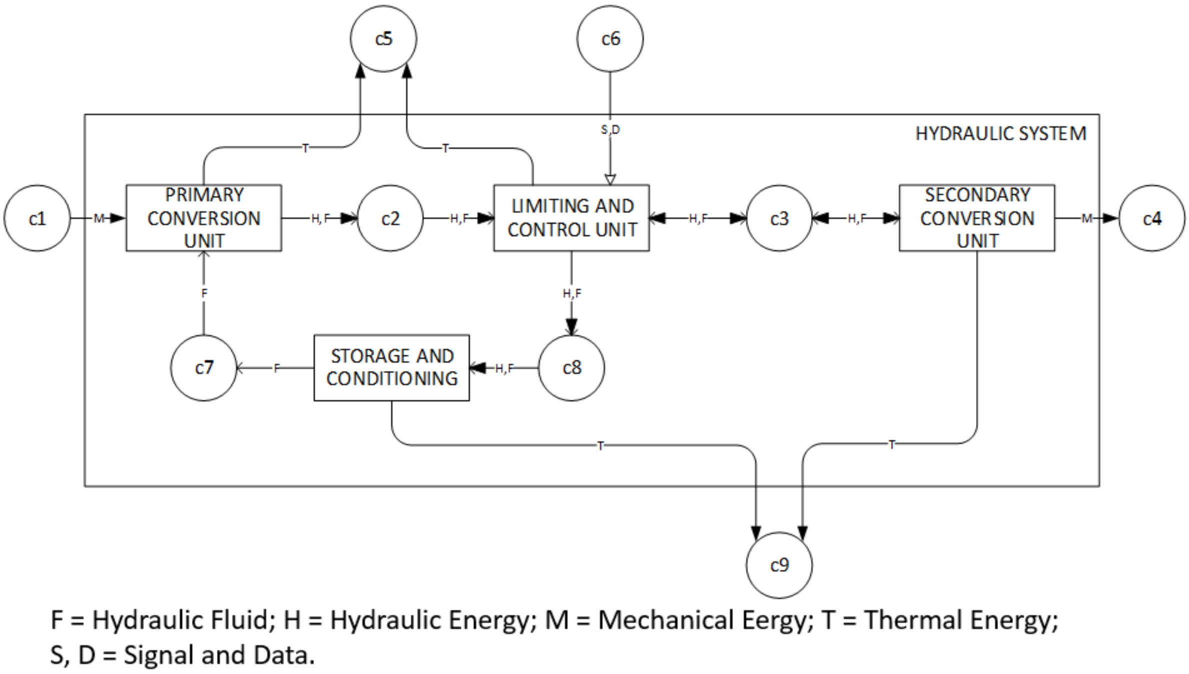

Source: Adapted from Linsingen (2016).

In a centralized design, a single large hydraulic unit is responsible for powering all major functions of the plant. In this setup, a pump charges an accumulator, which provides flow rate at a specified pressure range to most of the power plant components, such as the speed governor, brake system, bypass valve, and inlet valve. Figure 3 presents a simplified hydraulic circuit diagram of this typical design. This configuration requires a considerable volume of hydraulic fluid in the pipelines and presents challenges in installation and maintenance due to the size of the components and the complexity of the hydraulic circuit. Additionally, a failure in one system can lead to a complete shutdown of the entire plant.

In this context, this master's thesis proposes the decentralization of the hydraulic system used in the speed governor of hydroelectric power plants through pump-controlled actuators. In this case, each of the hydraulic power plant functions is developed by an exclusively designed actuator. This conception is illustrated in Figure 4. These actuators have a hydrostatic transmission arrangement in which the pump and actuator form a closed loop.

Thus, each actuator is in a closed system, in which the primary conversion unit also performs the function of the limitation and control unit, as illustrated in Figure 5.

In this system, the pump directly controls the actuator providing only the needed flow rate by its variable displacement, rotational speed and direction or both. Therefore, it does not require proportional valves which results in greater efficiency when compared with centralized hydraulic systems. Furthermore, in case of control by the angular velocity of the pump, the energy is used only when the actuator is in operation, decreasing the electricity consumption.

Figure 3 - Simplified centralized hydraulic circuit in hydraulic power plant.

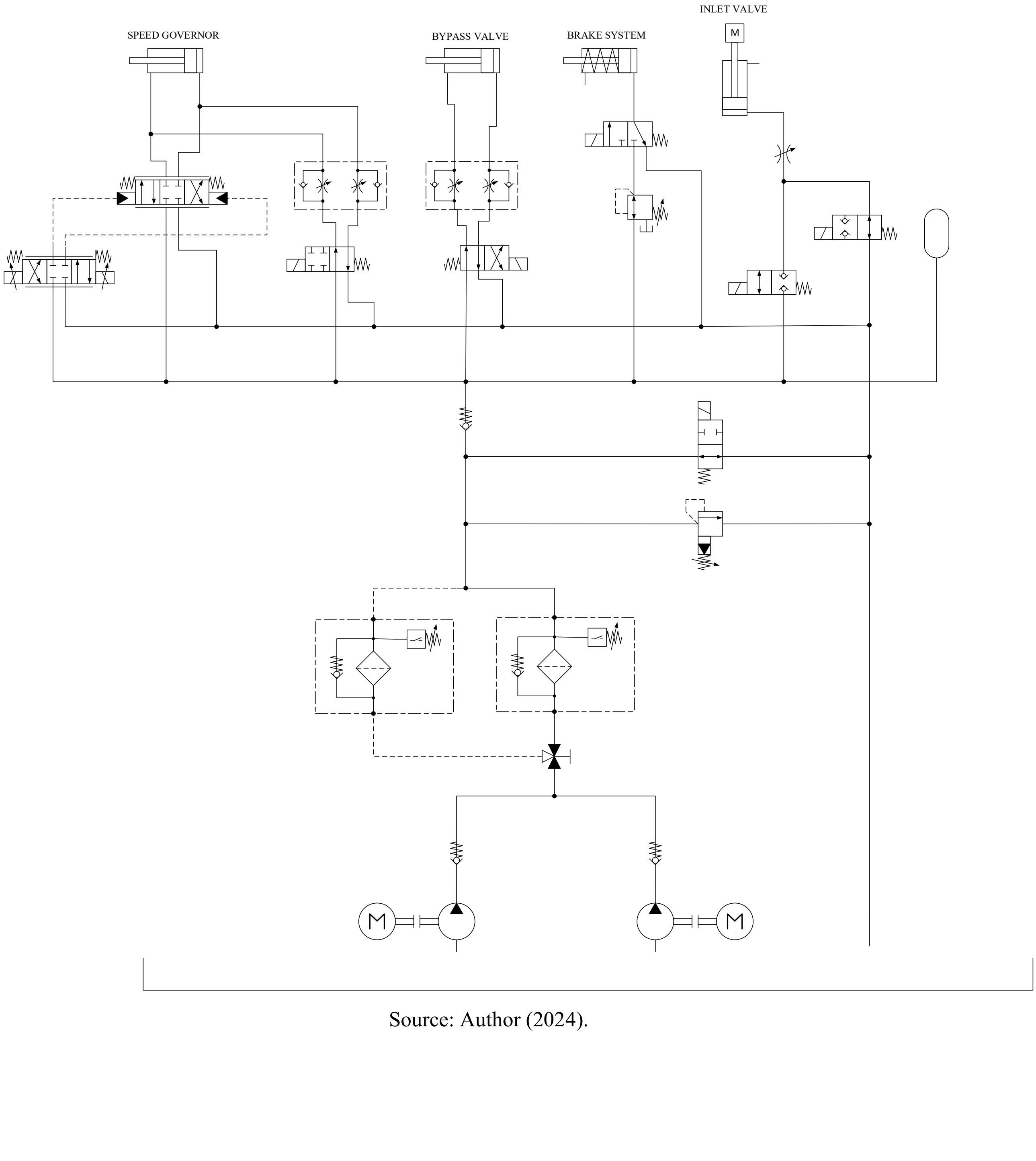

Source: Author (2024).

Figure 4 - Example of a decentralized architecture in hydroelectric power plant.

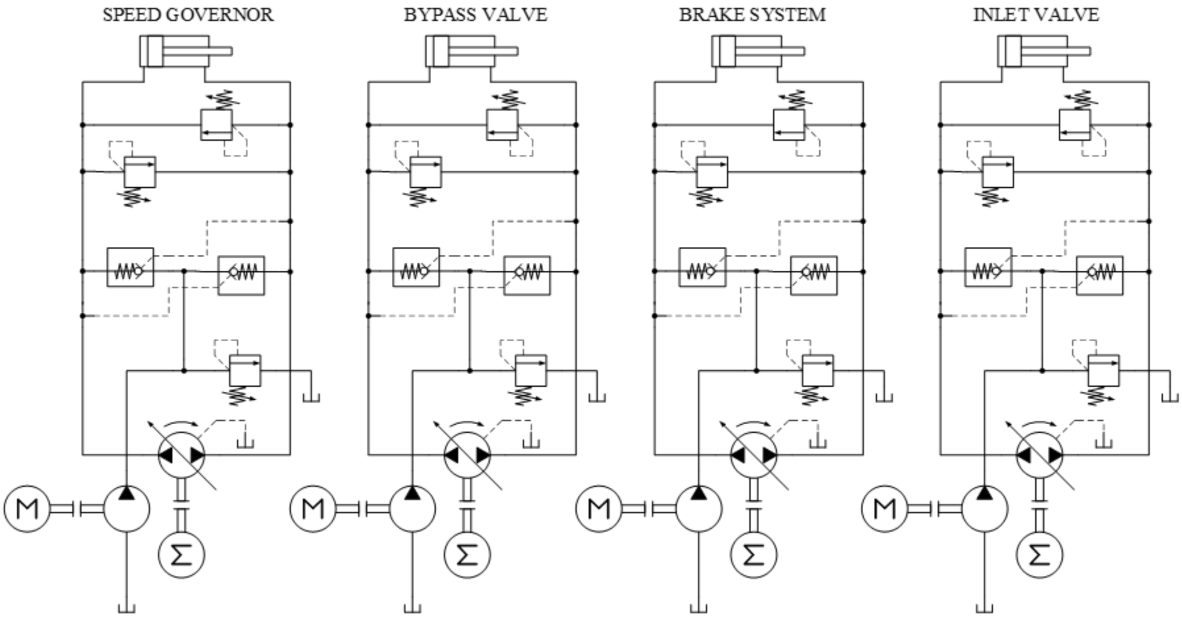

Source: Author (2024).

Figure 5 - Generic electro-hydrostatic actuator.

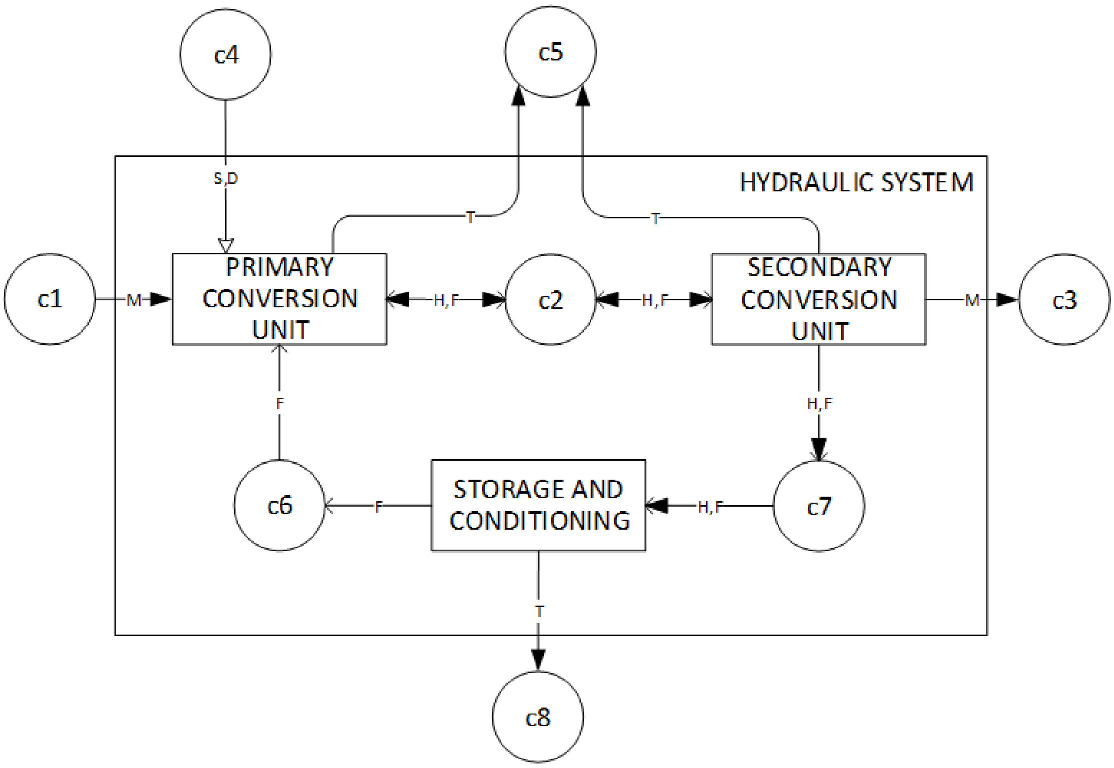

F = Hydraulic Fluid; H = Hydraulic Energy;
M = Mechanical Eergy; T = Thermal Energy;
S, D = Signal and Data.

Source: Author (2022).

Furthermore, a speed governor using a pump-controlled decentralized hydraulics eliminates the need for a distributing valve to control the servomotor (hydraulic actuator which controls the distributor), which facilitates the modernization and maintenance of the generating units. These valves, according to Retzlaff *et al*. (2009), often do not have spare parts since they have an old architecture and have been in operation for decades. In addition, in most cases, they cannot be replaced by components available on the market due to not having the necessary flow rate requirements for good performance of the plant. Also, they are costly since they are manufactured in small batches and even in single units. Another point to be highlighted is the precision requirements for manufacture, that are more precise than the typical specifications for the valves available in the market, in which small variation (micrometers), both in radial clearances and overlap between the spool and the valve sleeve, may cause it not to meet the due performance.

Moreover, decentralized systems require less hydraulic fluid than traditional hydraulics due to their compact architecture, where all components of the hydraulic circuit are close to each other, eliminating the need for long pipes to convey the fluid between the pump, reservoir and actuators. The reduced volume of hydraulic fluid helps to mitigate the environmental issues generated not only by the hydraulic fluid production and disposal but also in cases of leakage failure, where less fluid would leak into the environment. Decentralized systems also have the advantage of the ease of maintenance and safety, as each actuator has its own primary energy conversion source (pump).

Therefore, this master's thesis aims to evaluate the feasibility of replacing speed governor controlled by conventional hydraulic systems by a decentralized system using pump-controlled actuators in hydroelectric power plants. A hydraulic system to control a Francis hydraulic turbine speed governor will be developed, aiming to decrease hydraulic oil consumption. The speed governor is chosen because it plays a key role in the performance of hydraulic turbines.

1.1 AIM AND OBJECTIVES

1.1.1 Aim

The aim of the present master's thesis is to design a hydraulic circuit suitable for speed governor using a pump-controlled actuator applicable to Francis hydraulic turbines employed in hydroelectric power plants. The design comprises the modelling of the hydraulic system and subsequent analysis of its dynamic response to evaluate its opening time, response to transients in the consumption of the generated electrical energy from the power grid as well as to an emergency scenario.

1.1.2 Objectives

The following objectives are defined in order to achieve the aim of this master's thesis:

- To identify the main possible configurations of EHAs, as well as their characteristics through a literature review on the subject;
- To propose a pump-controlled architecture applicable to speed governors;
- To select components for the pump-controlled actuator in order to evaluate its feasibility;
- To model the system through a multi-domain system modelling and analysis software;
- To simulate the modelled system;
- To evaluate the system dynamic response to assess its opening time, response to transients in the consumption of electrical energy from the power grid as well as to an emergency scenario.

2 LITERATURE REVIEW

2.1 HYDROELECTRIC POWER PLANTS

Hydroelectric power plants are structures that harness the potential energy of stored water to generate clean and renewable electricity, in which there are three energy conversions, from potential energy to kinetic, and subsequently to mechanical, and electrical energy (MENDOZA, 2006). Their main elements are illustrated in Figure 6.

Figure 6 - Hydraulic power plant.

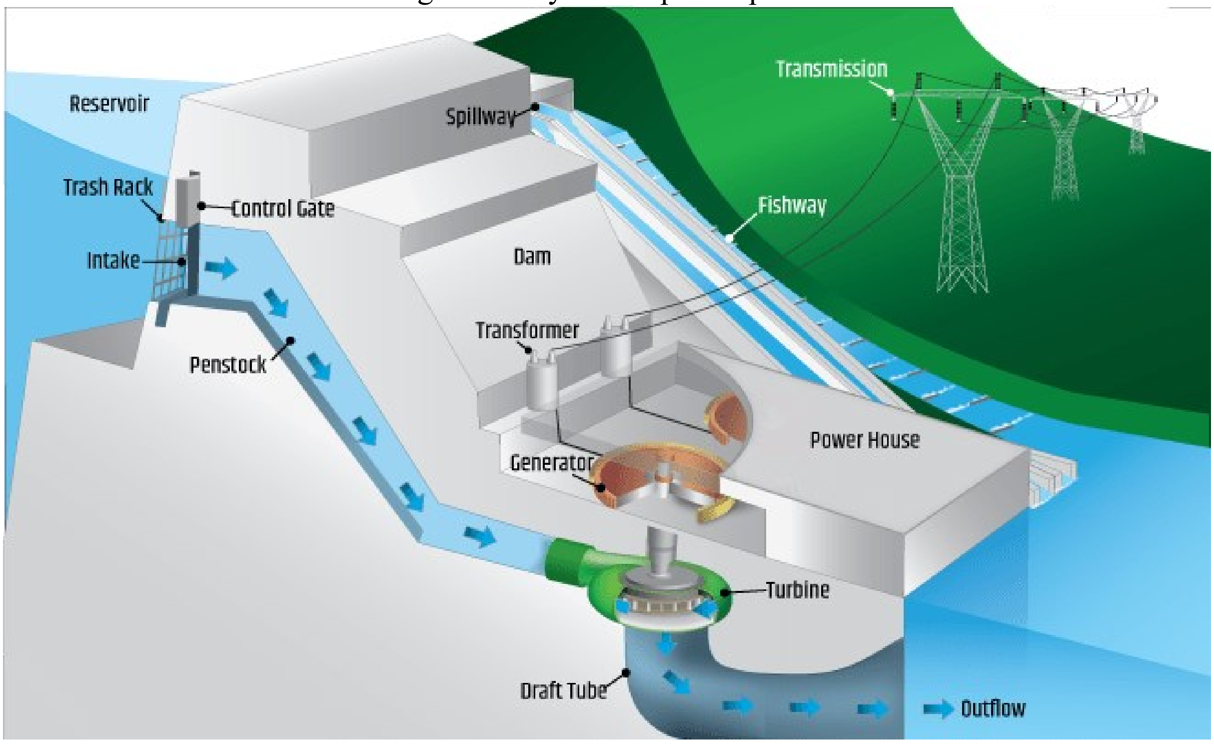

Source: Office of Energy Efficiency & Renewable Energy (2022).

Dams are structures, whose function is to create water reservoirs, thus increasing the water level upstream of a body of water making it possible to provide the flow rate in the penstock. This level difference serves as a source of hydraulic potential energy. Water flows through the water intakes to the penstock converting potential energy into kinetic energy. The penstock is a pipe or conduit made of steel or reinforced concrete that goes from the reservoir to the inlet valve to conduct the stored water and transform its potential energy into kinetic energy. The penstock features a small cylindrical reservoir, whose name is surge chimney, to prevent overpressure caused by sudden load variations (CORÀ *et al.*, 2020). The surge chimney, called a surge chamber when the penstock is a free-flowing channel, also has another purpose, which is to act as a "capacitor" storing water in order to supply sudden surges at the turbine inlet (HENN, 2006).

The load variations mentioned previously are known as a water hammer and are a result of the flow rate changes caused by the opening and closing of the inlet valve or wicket gate. Therefore, a minimum time for closing the wicket gate or inlet valve must be respected, as the overpressure suffered by the system is inversely proportional to it. A wicket gate is a device that regulates the flow rate of water into the turbine, and consequently, the turbine speed. (CORÀ *et al.,* 2020)

The most common types of turbines are Francis, Kaplan and Pelton, whose selection is made according to the available flow rate and hydraulic head of the hydroelectric power plant. These machines are responsible for converting the kinetic energy of the water into mechanical energy, which is later converted into electrical energy by a generator, whose shaft is coupled to the turbine shaft. The transformer converts the electricity into a higher voltage that is transmitted to the power lines. Depending on its power capacity, a hydroelectric power plant may have one or more turbines. (CORÀ *et al*., 2020)

After providing the energy to drive the turbine, the water is discharged into a channel leading to the river when Pelton turbines are used or to a draft tube when reaction turbines are employed (HENN, 2006). The draft tube is located at the discharge of the reaction turbines, and it partially recovers the kinetic energy of the water providing an additional hydraulic head (MACINTYRE, 1983).

In order to prevent the entry of debris and solid objects that could damage the system, there is a trash rack in the water intake. In addition, there are stoplogs in the floodgates to cut off the water supply in the event of an emergency or maintenance (HENN, 2006).

A spillway is a passage designed to control the reservoir level through the release of surplus water beyond the predetermined maximum water level from a dam. These safety structures avoid excess erosion on the dam leading the water over, around or through it. The spillway gates are built from welded sheet metal and can be mechanically or hydraulically operated. Radial gates are predominant in large plants considering that they are easier to move when compared to vertical and flap gates. The latter generally are present in small head and large spilling length power plants or for fine control of the reservoir level where radial gated are employed. (CORÀ *et al*., 2020)

Many fish species need to swim up or down the river to reproduce, so there must be structures that make this possible, they are called fishways. The mechanisms employed in fishways are fish ladders for low height dams, fish passes for medium height dams from 30 m to 46 m, fish elevators for high height dams, and fish locks. Fish ladders are low-slung artificial river sections made along the dam, fish passes are a succession of pools that overflow one another, fish elevators are mechanical lifting tanks, and fish locks are chambers connected by a gallery with a valve that allows the fish to pass. (CORÀ *et al.,* 2020)

The National Agency of Electrical Energy - Agência Nacional de Energia Elétrica - ANEEL (2008) classifies the power plants into three categories according to their capacity; where those with capacity below 1 MW are Mini Hydropower Plant (*Centrais Geradoras Hidrelétricas*), Small Hydropower Plants (*Pequenas Centrais Hidrelétricas*) with capacity between 1.1 MW and 30 MW and, and Large Hydropower Plants (*Usina Hidrelétrica de Energia*) with capacities above 30 MW.

2.1.1 Hydroelectric turbines

Turbines are responsible for converting hydraulic energy into mechanical energy, they superseded the old water wheels that by the 18th century achieved an energy efficiency as high as 60%. Currently, hydraulic turbines have an energy efficiency of over 90%. Besides the increased efficiency, they are smaller than their predecessors as they operate with higher water heads, thus higher pressure, resulting in increased speeds. (BREEZE, 2018)

The three main turbine types found in hydropower plants are Francis, Kaplan and Pelton turbines. According to Schreiber (1977), the first two are classified as reaction turbines and the last one as impulse turbine. ABNT NBR 06445:2016 defines reaction turbines as those that convert kinetic and pressure energy into mechanical energy through their runner, while an impulse turbine uses only the kinetic energy of the water flow rate.

The Pelton turbine, whose inventor is the American engineer Lester Allen Pelton, works similarly to the water wheels. Nevertheless, it utilizes a high-pressure water jet instead of using the natural flow of water of a body of water as a source of kinetic energy (BREEZE, 2018). This is possible via a tall water column that pressurizes the water at its bottom. A nozzle converts the water pressure into velocity creating a water jet which impinges on the spoon-shaped buckets assembled around the runner so that imparting the momentum from the water to the runner. (BEECHER, 1991)

According to Beecher (1991), these machines achieve the highest efficiency when the impinging water speed is twice the peripheral speed of the buckets. Pelton turbines may have one or several nozzles that control the water flow through a needle. In case of the need for an emergency shutdown a deflector redirects the water jet away from the turbine allowing the valve to close at suited rate to avoid the water hammer. The Figure 7 depicts a schematic view of a simple Pelton turbine.

Figure 7 - Schematic of a simple Pelton turbine.

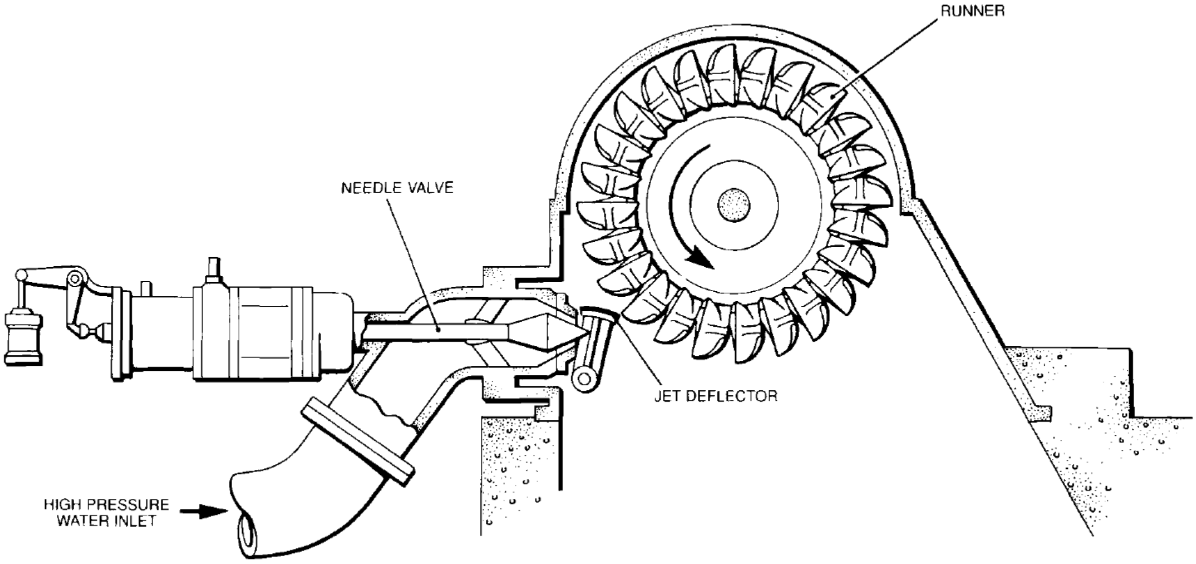

Source: Beecher (1991).

In reaction turbines, the water inlet occurs through a spiral case and the wicket gates rather than through nozzles, allowing an even distribution of water all around the runner (MATAIX, 1975). Besides the wicket gates, Kaplan turbines (Figure 8) also count on blades with an adjustable pitch which favors their application in a greater range of speeds, power output and water heads, maintaining good efficiency (BEECHER, 1991). These turbines, designed by Victor Kaplan, are employed for small water heads and large flow rates (COZ *et al.*, 1995).

Invented in 1838 by Samuel Howd and enhanced by the Englishman James Bicheno Francis (18158-1892), which bears his name (COZ *et al.*, 1995), the Francis turbine (Figure 9), according to Mazzorana (2008), is the most common type of turbine in the country as a result of their features suitable for most part of the national territory. In these turbines, as illustrated in Figure 9, the water intake occurs through the bigger area of the spiral case cross-section, whose function is to distribute the water as uniformly as possible over the wicket gates. For that reason, it has a decreasing cross-section combined with the stay vanes (some systems do not have stay vanes). The water then passes through the wicket gates, which are responsible for optimizing the energy conversion efficiency by varying the flow rate for different load conditions. Finally, the fluid collides with the runner blades, causing it to rotate around its axis, thus converting hydraulic energy into mechanical energy. Mechanical energy, in turn, is transformed into electricity through a generator coupled to the turbine runner shaft. (MAZZORANA, 2008).

Figure 8 – Schematic of a Kaplan turbine.

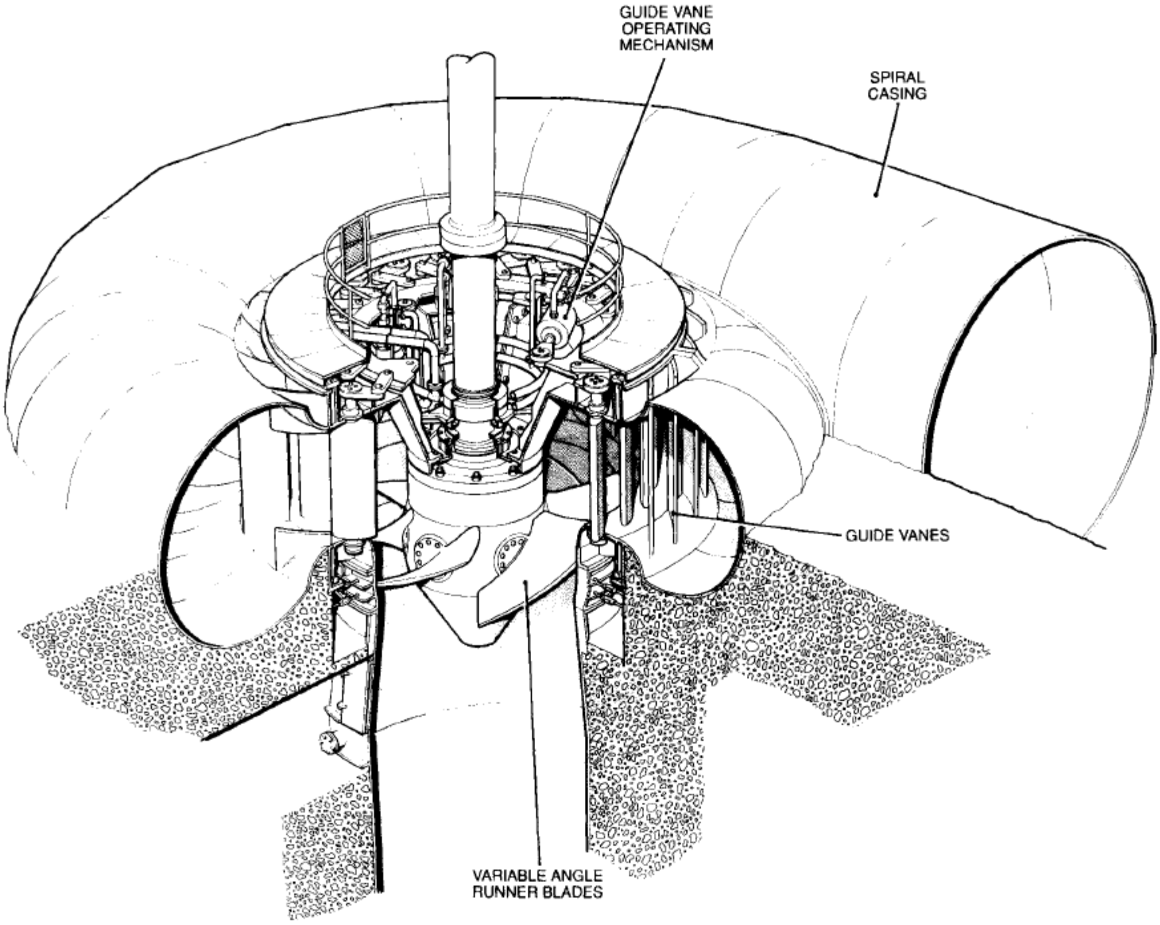

Source: Beecher (1991).

The main characteristics of these turbines are summarized in Table 1, where Pelton turbines are installed with low water flow rates and large hydraulic heads, while Kaplan turbines need large water flow rates and small hydraulic heads. Meanwhile, Francis turbines are more flexible as they work with intermediate water flow rates and hydraulic heads. In addition, Francis turbines have more than twice the power range of other turbines.

Figure 9 - Basic features of a Francis turbine.

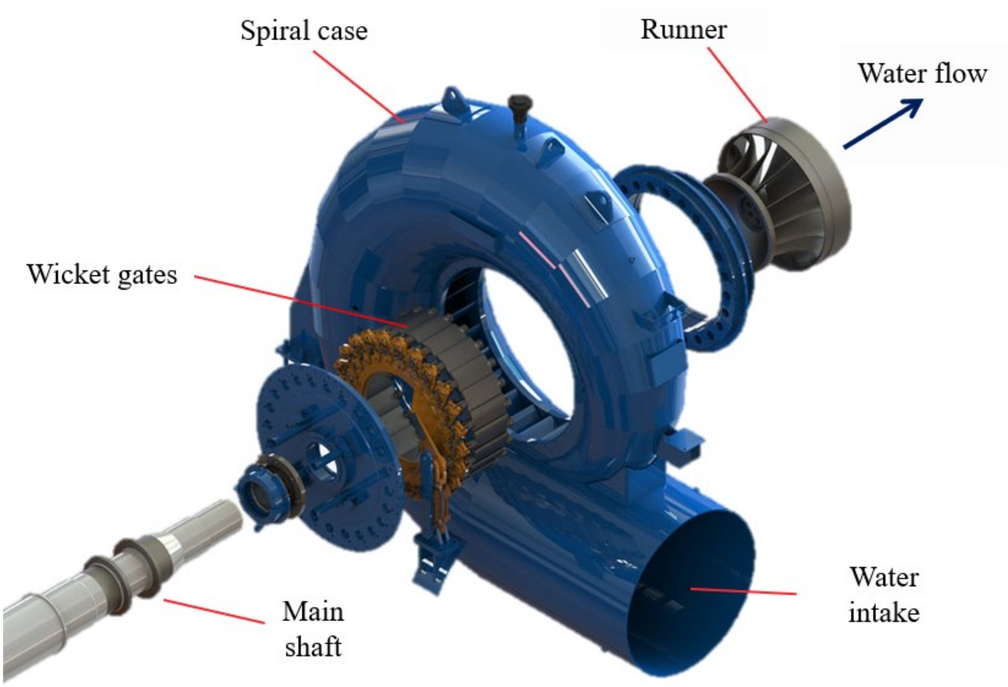

Source: Adapted from Hidroenergia (2021).

Table 1 - Properties of the main hydraulic turbines.

Turbine	Un.	Pelton	Francis	Kaplan
Water flow rate	m^3/s	0,05-50	1-500	1000
Hydraulic head	m	30-1800	2-750	5-80
Power range	kW	2-300000	2-750000	2-200000
Maximum efficiency	%	91	92	93

Source: Based in Coz *et al*. (1995).

Speed governors are used in order to improve the turbines performance. In other words, they must allow the turbines to have smooth speed transitions, maintain a constant runner speed with as little hydraulic losses as possible, and avoid overspeeding due to abrupt load variations.

2.1.2 Speed governors

This section presents the Fink wicket gate speed governor used in reaction turbines, such as Kaplan and Francis turbines. This device, in addition to the functions mentioned above, flow rate control and, consequently, runner speed and power supplied by the turbine, must also promote frequency control and synchronization between the multiple machines and the power distribution system. Another point to be mentioned is that the speed governor is responsible for providing fast, safe, and suitable speed transients for each operation, whether to develop a stable start or a fast closing in response to a power rejection by the transmission line (MENDOZA, 2006; PEREIRA, 2020). An inadequate response of this subsystem to voltage drops or excess water flow in the turbine can cause or maximize incidents for both the transmission line and those involved in the power plant, thus highlighting its importance in hydroelectric power plants (BRAVO *et al*., 2012).

According to Fasol (2002), the first methods used to control both hydraulic turbines and engines were flyball governors (Figure 10), with emphasis on the work of Professor Max Ch. Tolle in 1905, called *Die Regelung der Kraftmaschinen*, which was one of the first textbooks to deal with control with a focus on hydraulic turbines. It is also possible to cite other relevant works and contributions from pioneers in this area, such as Sir George Biddell Airy, James Clerk Maxwell, Iwan Alexejewich Wishnegradski and Aurel B. Stodola, who paved the way for future engineers to develop more accurate systems that gave rise to mechanical governors.

Figure 10 - Flyball governor.

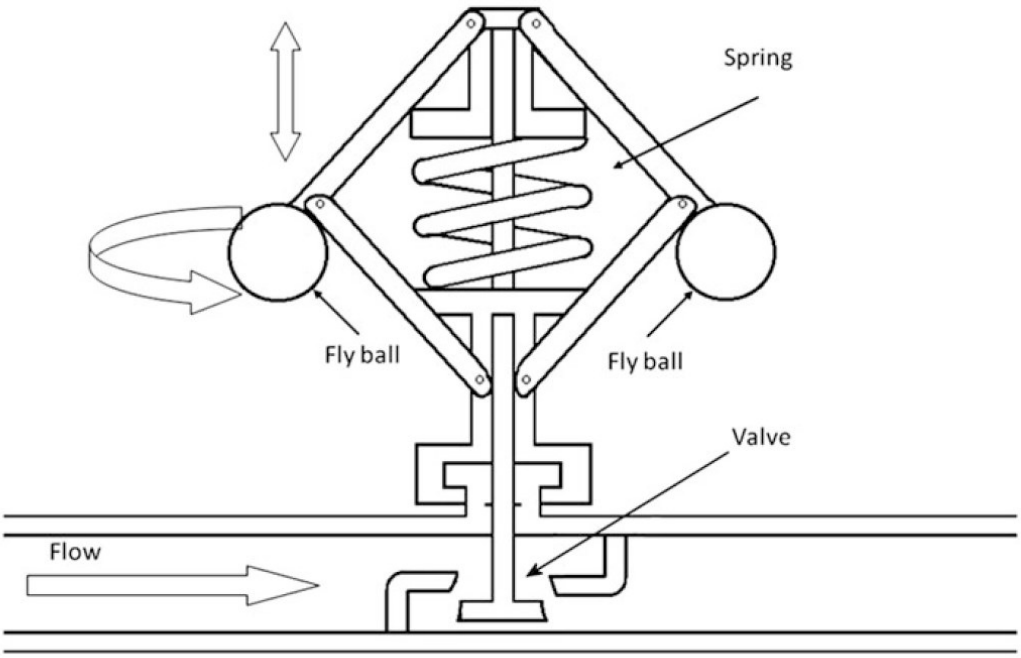

Source: Munoz-Hernandez, Mansoor and Jones (2013).

The first mechanical governors used in hydroelectric power plants are considered direct descendants of the flyball regulator with the addition of the servomotors, which were mechanical actuators such as levers, gears and hydraulic actuators to move the control valves or wicket gate (MUNOZ-HERNANDEZ; MANSOOR; JONES, 2013). Despite having been widely used until the first half of the 20th century, the flyball governors were no longer used as actuators but as speed meters that incorporated electronic and electromagnetic sensors. Thus, the governors went from mechanical governors to analog governors, then to modern digital controllers which, through a programming language, provided greater versatility and flexibility for modifications and adjustments in the control system (FASOL, 2002). A more comprehensive approach to the history of hydropower control is available in Fasol (2002).

The wicket gate is the mechanical component responsible for the speed control in reaction turbines such as Kaplan and Francis. Figure 11 presents its main parts, where the lower ring (1) and the upper ring (3) are responsible for supporting the gates (2), whose function is to act on the fluid to control its direction and flow rate. The levers (4) and the adjustable slotted guides (5) set on the upper ring are responsible for transferring the movement of the operating ring (6) to the gates. Through the operating ring, it is possible to control the angles of all steering blades simultaneously. (MENDOZA, 2006; MAZZORANA, 2008)

Figure 11 - Wicket gate.

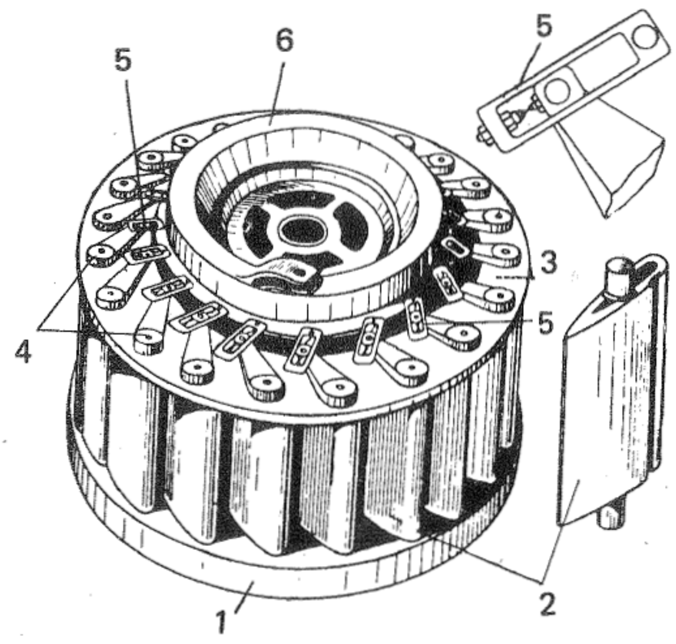

Source: Mataix (1975).

As shown in Figure 12, there are two possible operating ring arrangements, internally or externally to the gates.

Figure 12 - Operating ring arrangements.

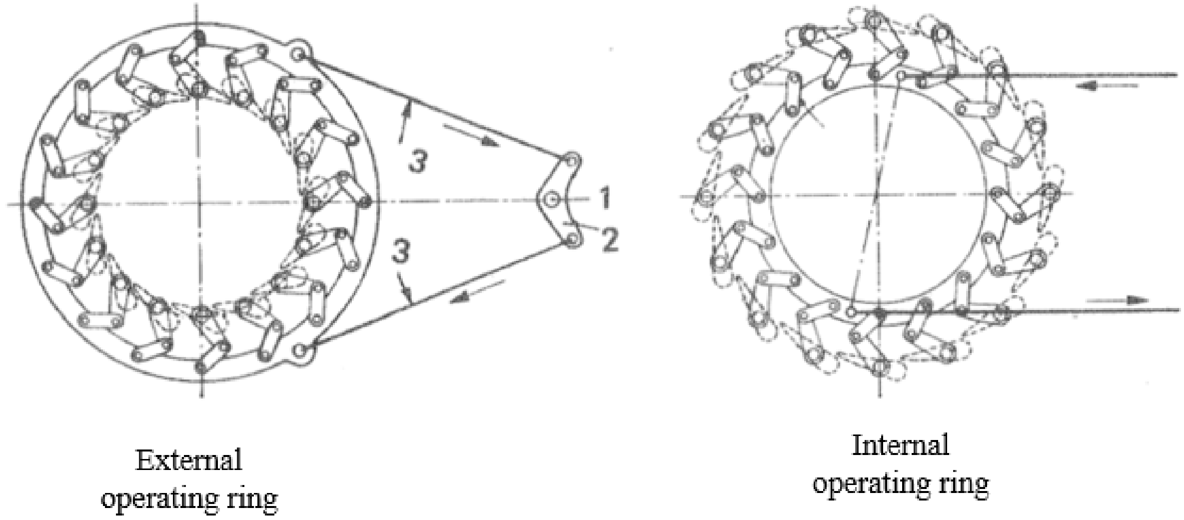

Source: Mataix (1975).

According to Mendonza, De Negri and Soares (2016), depending on the size of the controlled turbine, one or more linear hydraulic actuators, called servomotors, for this application, control the gates. Typically, a servovalve or a proportional valve controls the distributing valve. Consequently, the distributing valve controls the servo motors. Small hydraulic turbines only require a proportional valve or servovalve to operate the servomotor. Figure 13 illustrates the simplified hydraulic circuit conventionally used in speed governors, where the LVDT sensor supplies the servomotor position to the controller, which sends a voltage to the solenoid of the pilot valve 1V1 (proportional directional valve). The solenoid drives the valve spool 1V1, providing flow rate to one of the chambers of the distributing valve 1V2, thus driving its spool directing hydraulic fluid to one of the chambers of the servomotor (hydraulic actuator 1A), causing its position to change. Therefore, the servomotor moves the wicket gate operating ring, which drives its gates to control the speed of the hydraulic turbine. Bravo *et al*. (2012) presents a detailed electro-hydraulic diagram of a speed governor.

According to Souza, Santos and Bortoni (1999), the servomotor load varies depending on its position and moving direction, and its maximum value occurs near its closing position. There are three sources of resistance to the movement of the gates, which are a torque on the gates due to hydraulic pressure, the friction forces on the bearings and pins, and the moment originated by the contact between the gates when fully closed (SOUZA; SANTOS; BORTONI, 1999). As suggested by Vivier (1966 apud MENDOZA, 2006), a practical way to acquire the sum of the loads is to measure the servomotor chamber pressure during its movement. The opening and closing load profiles of the wicket gate are displayed in Figure 14, where the green area above the horizontal axis illustrates the sum of the opening loads on the gates and the red area below the horizontal axis the sum of the closing loads. The middle dashed line represents the hydraulic load. The servomotor design must consider the maximum load during opening and closing of the gates, which occur at points A and B as observed by Souza, Santos and Bortoni (1999) and highlighted by Mendoza (2006).

Figure 13 - Simplified hydraulic circuit conventionally used in speed governors.

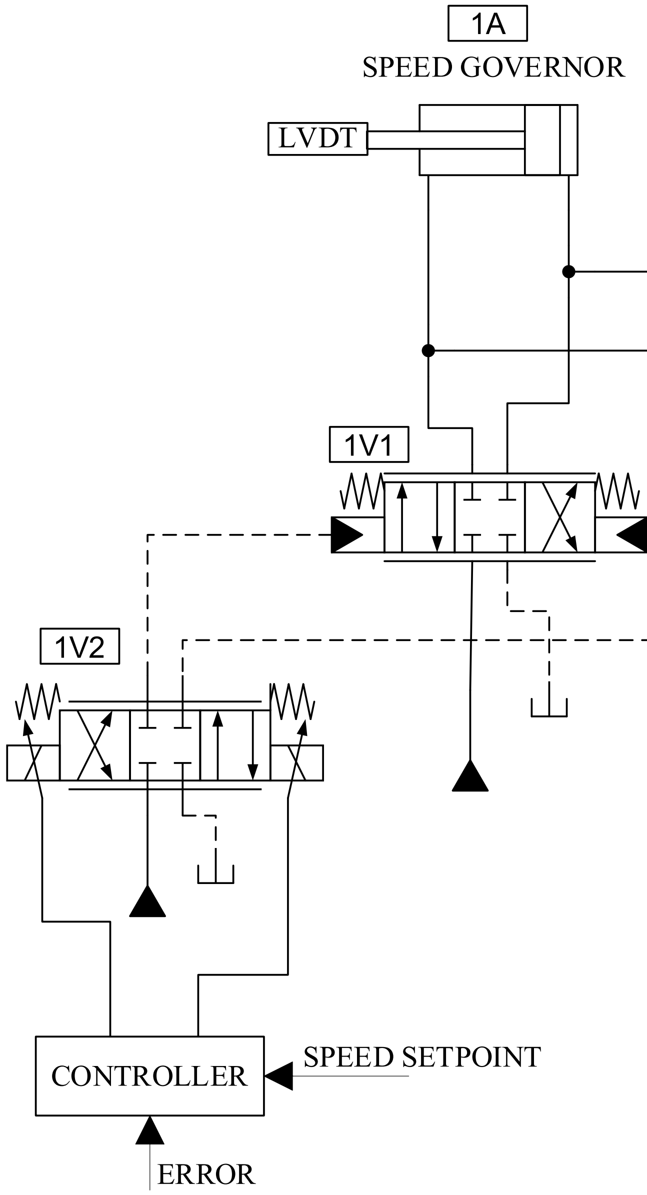

Source: Adapted from Furst (2001).

Figure 14 - Servomotor load profile.

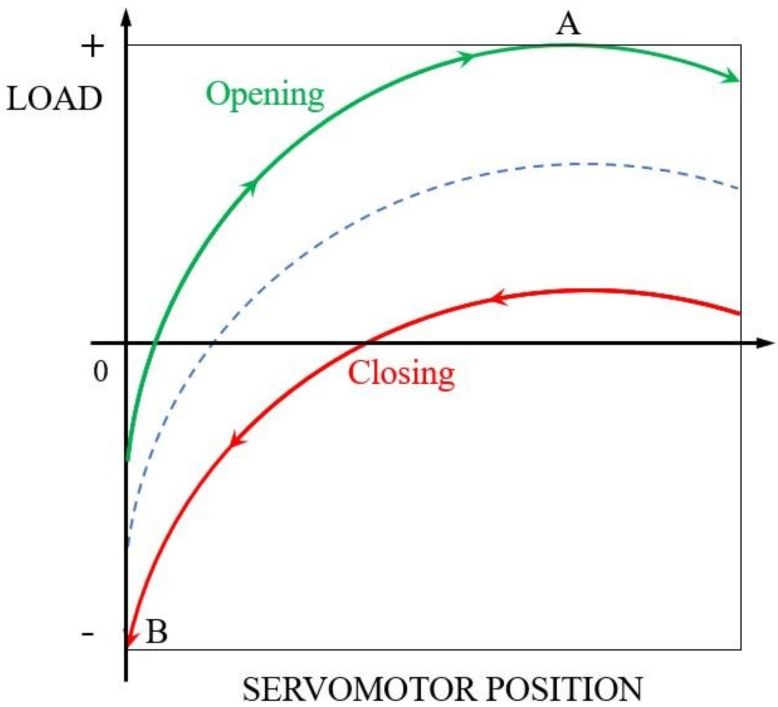

Source: Adapted from Vivier (1966).

As mentioned by Mendoza, De Negri and Soares (2016), the technical standards IEEE 125:2007 and IEC 61362:2012 define the requirements for the proper static and dynamic behavior of speed governors in order to avoid the turbine overspeed or the water hammer in the penstock. Henn (2006) defines a water hammer as the sudden change in pressure resulting from the abrupt interruption of the liquid flow, in which the velocity energy present in the flow rate is transformed into pressure energy. The pressure variation behaves as alternating waves of overpressure and depression along the penstock until the dissipation all its energy through friction on the pipe walls or protection mechanisms such as the balance chimney. In reaction hydraulic turbines, the change in the flow rate by the adduction valve and the wicket gates can induce a water hammer.

2.1.3 Emergency shutdown

According to the International Standard IEC 61362:2012 and IEEE 125:2007, it must be possible to release an emergency shutdown "in case of over-speed, serious faults in the turbine governing system or when the emergency shutdown push-button is activated." This can be accomplished by closing the guide vanes or shutting the main shutoff valve or gate.

IEC 61362:2012 lists four tripping criteria for quick shutdown or emergency shutdown, which are mechanical fault, electrical fault in the unit, serious fault in the governing system, and emergency shutdown push-button pressed. The provisions by which the emergency shutdown may be provided comprises “additional oil volume in the hydraulic energy supply system”, “a separate pressure oil supply”, “closing weight”, “pressure water servomotor (e. g. for the deflector in the case of high hear installations)”, and “closing spring”.

When using an accumulator as a source of hydraulic energy, IEC 61362:2012 recommends that its usable oil volume be at least three times the volume of all servomotors. This is due to the need for the accumulator to supply oil for the servomotor control and its emergency/quick shutdown.

Hydraulic accumulators are pressurized containers whose purpose is to store hydraulic fluid to meet sudden high flow demand, mitigate the impact of pressure spikes and pump pulsation, and serve as leakage compensator and emergency energy source. Due to the low compressibility of the fluid, the accumulator stores hydraulic pressure through three distinct mechanisms that categorize them. Therefore, they are classified into weight or gravity loaded, spring-loaded and gas loaded types. The weight-loaded model provides constant pressure fluid regardless of oil level. On the other hand, the remaining models have a variable pressure supply as they vary their pressure depending on the level of hydraulic fluid in the accumulator due to the pressure exerted on it by a spring or pressurized gas. Figure 15 shows the main types of accumulators. Where “a” is a weight-loaded accumulator, “b” is a spring-loaded accumulator and the other gas-loaded accumulators, without separation between liquid and gas “c”, a piston-type “d” and a diaphragm type "e."(LINSINGEN, 2016; LINSINGEN; DE NEGRI, 2012)

Figure 15 - Hydraulic accumulator types.

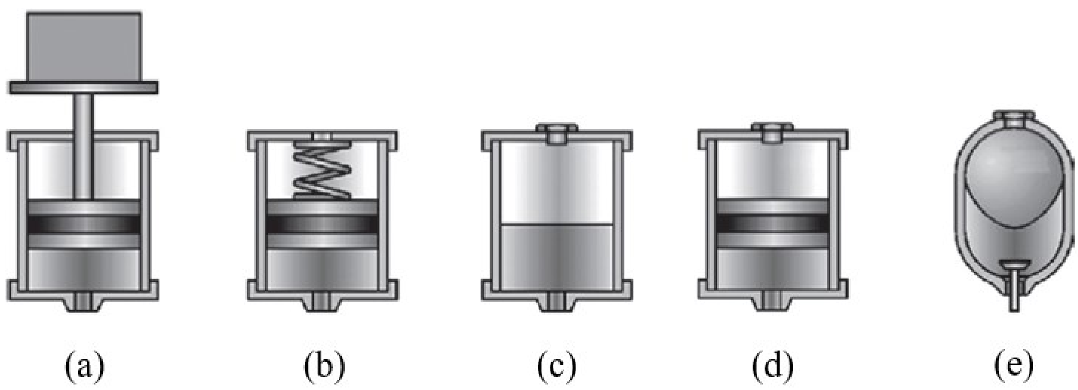

Source: Linsingen (2016).

Other options for energy storage, especially for more electrical systems, are battery storage technologies or even supercapacitor storage technologies in the future as they evolve. When it comes to batteries, three types stand out, lead-acid, nickel-based and lithium-based batteries (HADJIPASCHALIS; POULLIKKAS; EFTHIMIOU, 2009).

Lead-acid batteries are known to have high efficiency with relatively low investment, easy maintenance and installation. These batteries are ideal for long-term storage applications, as their self-discharge is very low, around 2%, compared to other batteries, but with a small cycle life and operational lifetime. Their cycle life is impaired by the depth of discharge as well as high temperatures, although the last may improve their capacity (HADJIPASCHALIS; POULLIKKAS; EFTHIMIOU, 2009; RAHMAN 8., 2020).

Nickel-based batteries are superior to lead-acid batteries regarding their operational life and cycle life. Nevertheless, they face many disadvantages compared to lead-acid ones, such as high cost, lower efficiency and higher self-discharge rate (HADJIPASCHALIS; POULLIKKAS; EFTHIMIOU, 2009).

Maintenance and energy efficiency are some of the areas where lithium-based batteries excel compared to the previously mentioned batteries. However, its life cycle is strongly affected by high temperatures and deep discharges (HADJIPASCHALIS; POULLIKKAS; EFTHIMIOU, 2009; RAHMAN *et al*., 2020).

2.2 SPEED GOVERNOR DECENTRALIZED ARCHITECTURES

Although the International Standard IEC 61362:2012 (2012) suggests the possibility of a decentralized architecture, there are not many applications so far. The Standard presents a concept of a closed-circuit system where the system is characterized "by the fact that the pump flow rate and its direction are both controlled." In other words, a control valve is not necessary since the pump is responsible for producing and distributing hydraulic energy. IEC 61362:2012 also has three recommendations for closed-circuit systems:

- "Both servomotor sides shall be protected by safety valves which should preferably discharge into the opposite servomotor side" (IEC 61362:2012);
- "In order to cover internal leakages and/or to accommodate for servomotor area differences, means of replenishment via check valves shall be provided" (IEC 61362:2012);
- "These systems additionally require a small constant displacement pump to cover the need for pilot oil pressure" (IEC 61362:2012).

The German manufacturer Voith owns a patent under the number JP2018135915A

(TAKESHI *et al.*, 2018) employing a hybrid system for gate and intake valve control. The patent claims three different embodiments, as illustrated in the Figure 16, Figure 17 and Figure 18.

Figure 16 - Voith patent embodiment 1.

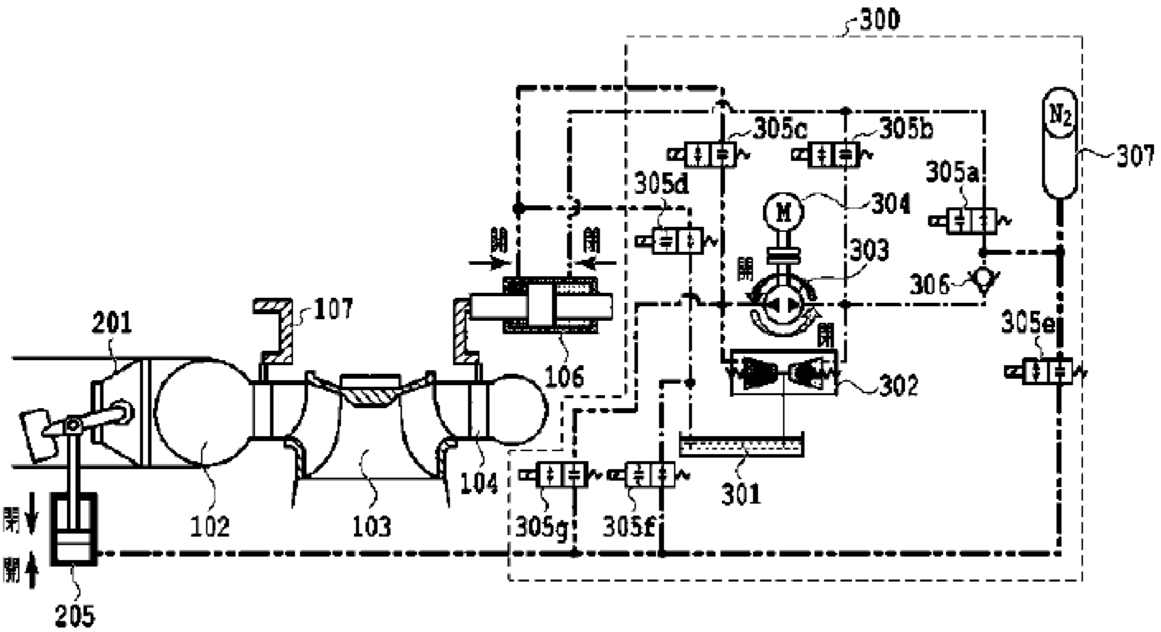

Source: Takeshi *et al.* (2018).

Figure 17 - Voith patent embodiment 2.

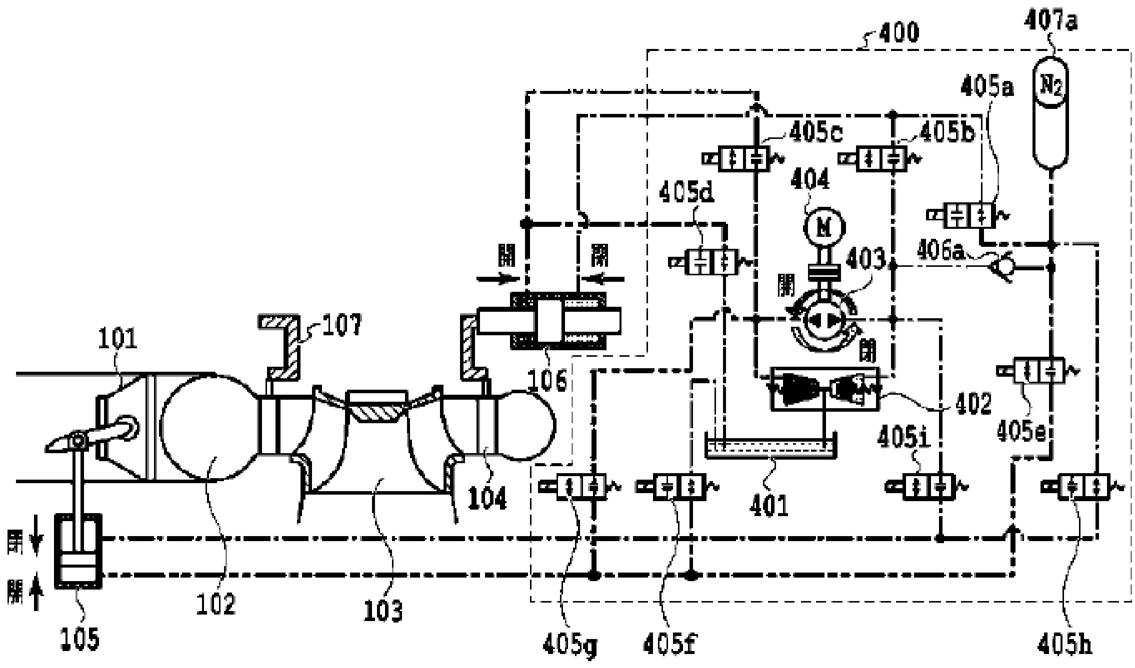

Source: Takeshi *et al*. (2018).

Figure 18 - Voith patent embodiment 3.

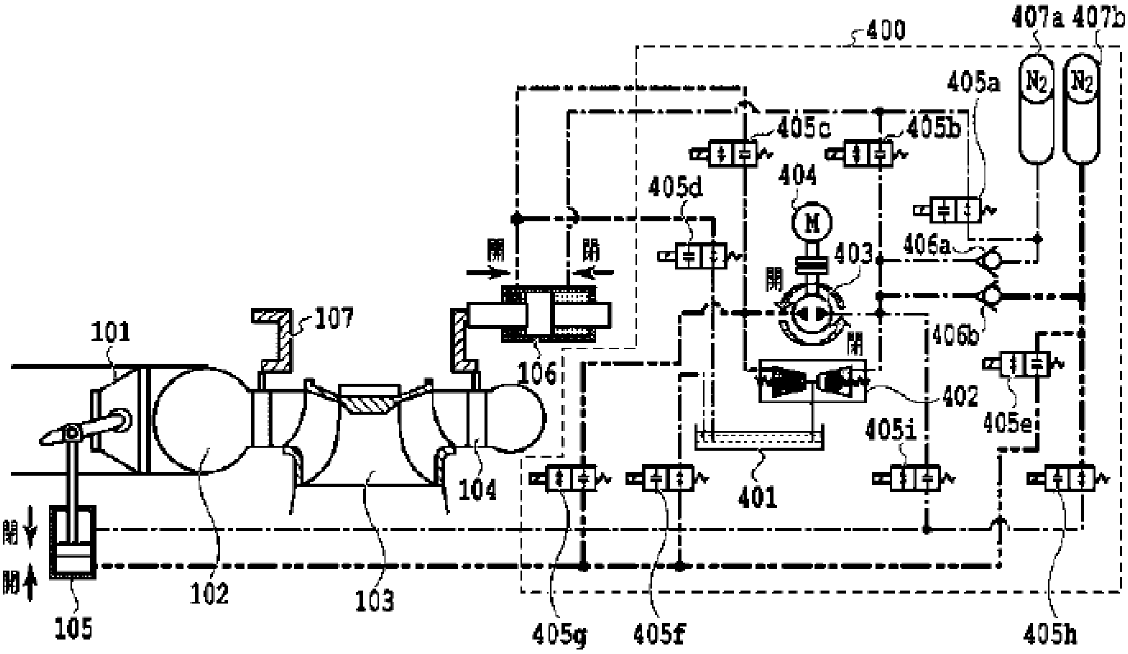

Source: Takeshi *et al.* (2018).

Although in the patent, Voith has presented a solution with a revertible piston pump, it has launched to the market a solution for speed governors employing an inner gear pump under the name HyCon GoHybrid. In order to drive this pump, it uses an AC electric motor with an inverter whose voltage ranges from 209V to 529V. The rated electric current for the largest solution so far is 390 A reaching 450 A at their peak. For this solution, the flow rate is limited to 320 L/min with a maximum volume of oil of 500 L and a rated pressure of 120 bar. By simple math, one can assume that this product is limited to applications up to 64 kW.

2.3 ELECTRO-HYDROSTATIC ACTUATORS

Electro-Hydrostatic Actuators (EHA) are systems that comprise different engineering domains, such as mechanical, hydraulic, electrical and control systems (ALLE *et al.,* 2016). These actuators are robust, compact, have good efficiency and low leakage, making them suitable for aeronautical applications. For example, the Airbus A380 was the first commercial aircraft to adopt this technology for backup functions (BOSSCHE, 2006; MARÉ, 2017). In addition, mobile hydraulics is another area that is harnessing its advantages, as seen in the works of Batista (2019) and Su & Jiang (2010). Batista (2019) proposes the use of EHAs for industrial and mobile machinery, whose design employs a fixed displacement pump and a variable speed electric motor that allowed the use of energy regeneration. Su & Jiang (2010) use the same electric motor and pump arrangement in a servo ship rudder, where they reported an increase in efficiency as well as superior celerity and precision compared to the specifications of the standard ISO 4051:1997.

These systems encompass hydrostatic power transmissions (Figure 19), where, depending on the EHA configuration adopted, the pump speed and/or its displacement variation control the actuator movement. As they decrease throttle losses by eliminating the need for proportional valves for their operation and consume less energy during standby, they offer an increase in the efficiency of the system when compared to conventional hydraulics (ALLE *et al.*, 2016; SOUZA; SANTOS; BORTONI, 1999). For example, Agostini *et al.* (2020) showed a decrease in energy consumption of 46% compared to traditional electro hydraulic systems applied to industrial mobile machinery, and Zimmerman, Busquets and Ivantysynova (2011) presented a reduction of 40% of fuel consumption in a compact excavator.

Figure 19 - Simplified hydrostatic transmission.

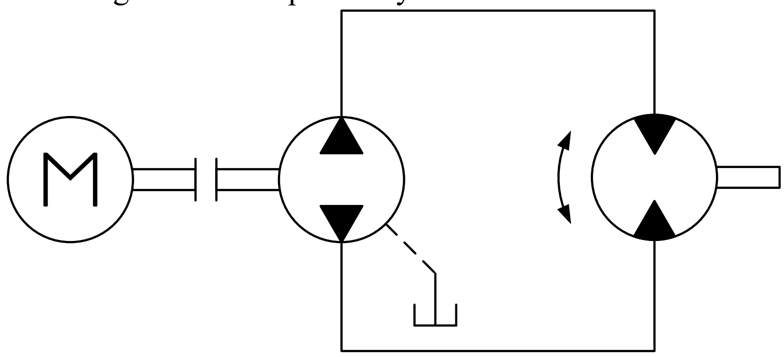

Source: Adapted from Costa and Sepehri (2015).

Moreover, they offer better protection to common failures when compared to centralized hydraulic systems, including maintenance failures, which in the event of a malfunction in a hydraulic line can compromise the entire system, unlike systems with EHAs. Also, decentralized systems are easier to maintain and rearrange, with less risk of leakage since they are available in compact blocks, where all hydraulic elements are in a single component. (BOSSCHE, 2006).

According to Bossche (2006), EHA jamming during service life is extremely unlikely if properly bypassed when compared to electromechanical systems. In addition, its service life is easier to predict since it can be associated with the wear of its parts, mainly pump wear, which decreases the volumetric efficiency of the system.

However, this technology presents some challenges to be overcome in order to be widely used in the market. Those are, as Ketelsen *et al.* (2019) points out, the reduced amount of oil can cause its temperature to rise beyond limits, impairing its performance and reliability. Also, the positioning accuracy and control bandwidths may be negatively affected by the low stiffness inherent to some system architectures. Furthermore, fluid maintenance such as cooling and filtering can be problematic in close-circuit architectures as hydraulic fluid is pumped directly from one cylinder chamber to the other.

An EHA typically comprises an electric motor, hydraulic pump, linear actuator, hydraulic accumulator, and relief and check valves. Nevertheless, there are different configurations based on the application. A summary of the configurations of the different components for an EHA with asymmetrical cylinder is depicted in Figure 20, where a fixed or variable displacement pump supplies the hydraulic fluid to the system, and an electric motor or an internal combustion engine is used to drive the pump. When energy recovery is desirable, a hydraulic machine, i.e. bidirectional pump/motor, replaces the pump, and the electric motor works as a generator. There are two fluid supply options to compensate for different volumes in each cylinder chamber as well as leakage. Those are vented when using a reservoir or sealed when adopting an accumulator. Auxiliary components comprise safety valves such as relief valves, load holding valves, passive or active valves to deal with the uneven flow rate in cylinder chambers, and other elements such as oil filters and coolers.

Figure 20 - Summary of EHA possible configurations.

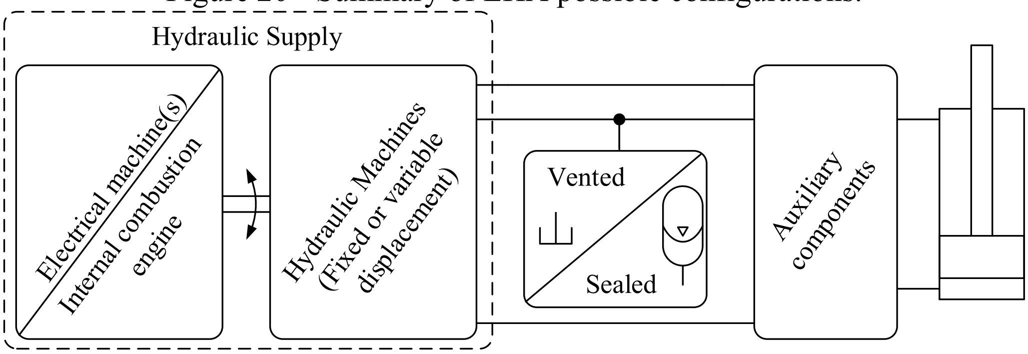

Source: Adapted from Ketelsen *et al*. (2019).

Alle *et al*. (2016) present the three predominant arrangements regarding the drives in EHAs, with fixed displacement pumps/motors and variable speed motor (FPVM) (Figure 21), variable displacement pumps/motors and fixed speed motor (VPFM) (Figure 22) and variable displacement pumps/motors and variable speed motor (VPVP) (Figure 23).

Figure 21 – EHA hydraulic circuit with fixed displacement pump/motor and variable speed motor.

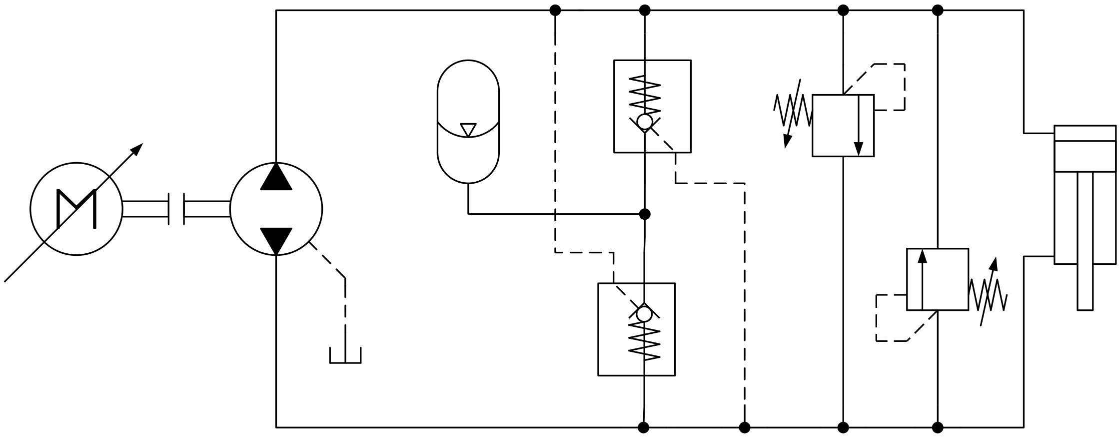

Source: Adapted from Alle *et al*. (2016).

Figure 22 - EHA hydraulic circuit with variable displacement pump/motor and fixed speed motor.

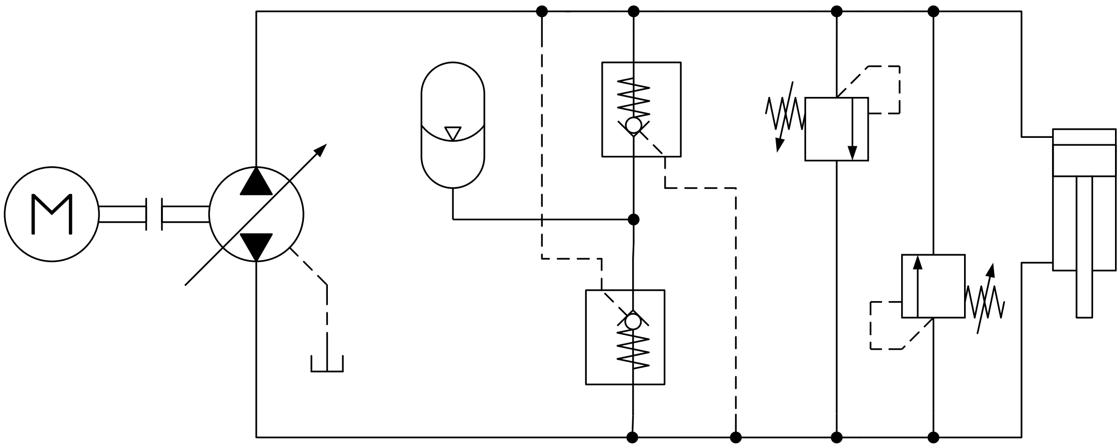

Source: Adapted from Alle *et al.* (2016).

Figure 23 - EHA hydraulic circuit with variable displacement pump/motor and variable speed motor.

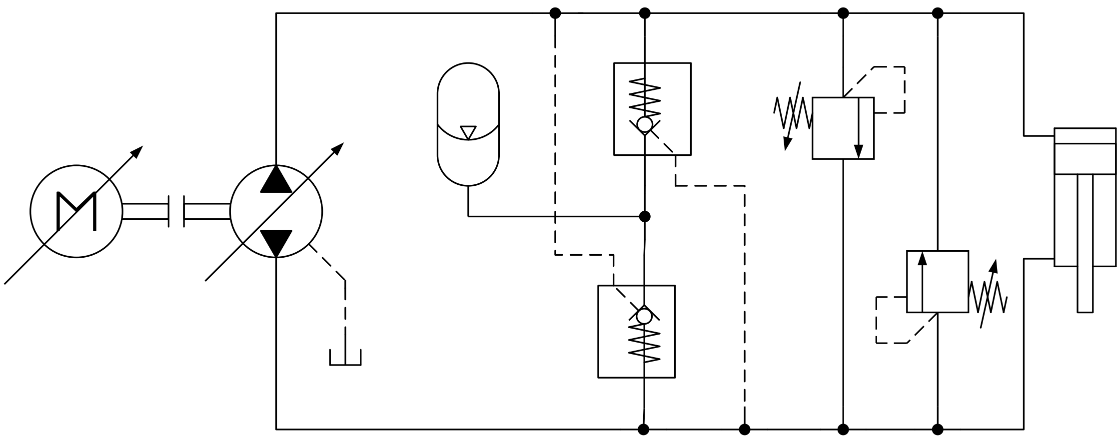

Source: Adapted from Alle *et al.* (2016).

FPVM systems are simpler and more efficient, while VPFM systems offer better dynamic responses. Tašner & Lovrec (2011) compared the three settings where the FPVM was about five times slower than the VPFM and VPVM. However, in Helduser's (1999) comparison, FPVM has proven to be 21.43% more energy efficient than the VPFM. This is mainly due to part-load efficiency and idling mode. In this case, VPVM systems combine the characteristics of both mentioned above. In other words, they combine good energy efficiency with a faster dynamic response compared to FPVM systems, nonetheless, with greater complexity and a higher price than the others (ALLE *et al*., 2016;WANG; GUO; DONG, 2020).

Table 2 - Summary of the predominant arrangements of EHA.

	VPFM	VPVM	FPVM
Characteristics	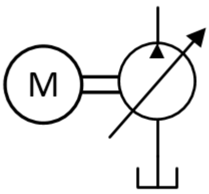	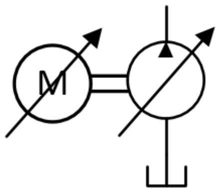	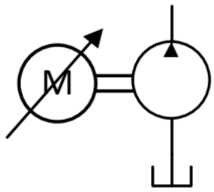
Flow/pressure control means	Pump displacement	Pump displacement and speed control	Speed control
Efficiency at partial load	Low	Better	Better
Idling losses	Yes	Reduced losses (control principle dependent)	Reduced losses

Source: Based on Helduser (1999).

It is important to note that when the hydraulic system is operating at corner power the majority of the time, EHAs with speed control offer little or no advantage regarding energy consumption compared to EHAs with displacement control (HELDUSER, 1999). Therefore, their design should follow the application-specific requirements concerning their duty cycle, idling time and dynamic response. Furthermore, speed controlled EHAs need the pump to handle speeds in both directions which limits the pump choice as there are not many of-the-shelf models (KÄRNELL *et al*., 2021).

All three concepts of electro-hydrostatic actuators have intrinsic characteristics to their constructive principle, which delays their dynamic responses and reduces their rigidity compared to conventional hydraulic systems (ALLE *et al*., 2016). However, it is possible to meet several design demands in multiple applications through these different configurations.

2.3.1 Hydraulic machine operating quadrants

Hydraulic pumps and motors serve as mechanical and hydraulic energy converters. Pumps are responsible for the primary energy conversion in hydraulic circuits, that is, for converting mechanical energy into hydraulic energy. Likewise, motors and linear actuators are responsible for the secondary energy conversion, from hydraulic to mechanical energy (LINSINGEN; DE NEGRI, 2012). Some pumps can also operate as motors depending on their constructive principle, which is convenient for applications with energy regeneration.

Figure 24 illustrates the operating modes of a hydraulic machine. When the flow rate and pressure differential direction are the same, such as in quadrants I and III from the Figure 24, the machine is converting mechanical into hydraulic energy, thus actuating as a pump. Otherwise, when the flow rate and pressure differential are opposite to each other, the machine operates as a motor, that is, converting hydraulic energy into mechanical energy, as shown in quadrants II and IV. (MICHEL; WEBER, 2012; TEIXEIRA, 2015)

Figure 24 - Hydraulic machine operating quadrants.

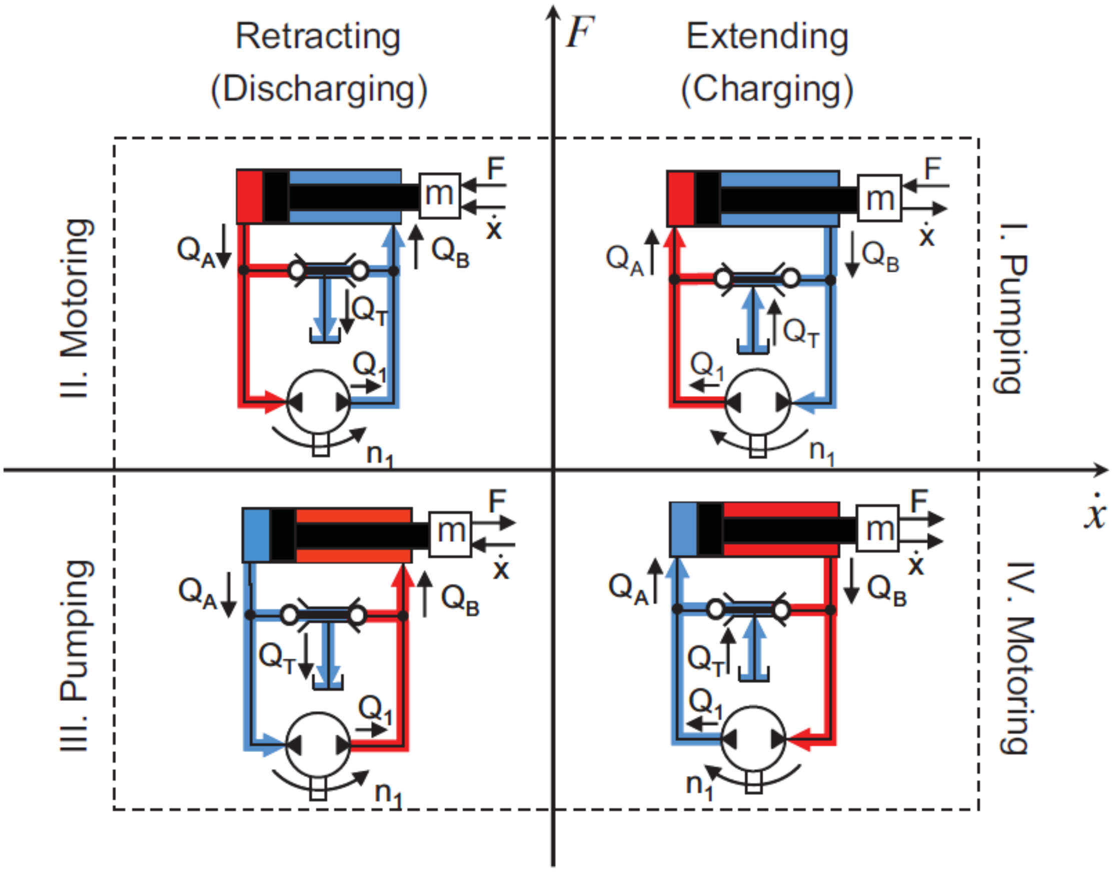

Source: Michel & Weber (2012).

2.3.2 Asymmetrical linear hydraulic actuators compensation methods

Linear actuators or hydraulic cylinders are a means of converting hydraulic energy into linear mechanical energy with constant speed, position control, force control, or only to provide a force to fix something (LINSINGEN; DE NEGRI, 2012). EHAs can employ symmetrical or asymmetrical actuators. Asymmetric cylinders offer a compact solution with a high strength/diameter ratio. Nonetheless, their inlet and outlet flow rates are different as they have unequal chamber areas, which results in a more complex control when compared to symmetric cylinders. However, this difference can be compensated with proper hydraulic circuit arrangements using hydraulic accumulators, check and pressure valves. (AGOSTINI *et al*., 2020b).

The different areas on each side of the asymmetrical cylinder piston may lead to performance issues such as unequal acceleration and speed between extension and retraction actions. Furthermore, it may cause the system to reach critical pressure limits such as overpressure or even fluid depletion during extension action. Therefore, there are several forms to mitigate these problems, where Quan, Z., Quan, L. and Zhang (2014) summarize six different methods in Figure 25.

The systems of Figure 25 (a) and (c) rely on an extra pump, referred to as pump 1, to provide the surplus flow rate during extension. Although, in Figure 25 (c), a single motor drives both pumps coupled to the same shaft. In retraction action, the excess hydraulic fluid drives pump 1, which is now working as a motor and discharges into a reservoir.

The remaining approaches to tackle the unbalanced flow rates in the actuator adopt only one pump/motor, where Figure 25 (e) depicts a solution with two piloted check valves and Figure 25 (f) pictures an arrangement in which the EHA works as a single-acting cylinder, utilizing a hydraulic accumulator.

For a more comprehensive review, see Ketelsen *et al*. (2019). In their approach, they aim to summarize the research and classify the EHA architectures investigated as far as 2019. Even though Ketelsen *et al.,* (2019) propose a high-level classification, i.e. a more general classification not regarding more specific components topology, the number of possible architectures is vast. Therefore, this work will not address them all but rather focus on one of the possible configurations capable of meeting the demands of the studied system.

Kärnell *et al.* (2021) propose a configuration without an accumulator (Figure 26) in order to reach a simpler solution, but still considering a high efficiency. In their approach, they replace the hydraulic accumulator with a pressure source. This choice is based on intrinsic issues found in closed circuits with accumulators. These are troublesome filtration and cooling, and difficult maintenance, servicing and air-bleeding.

Figure 25 - Compensation methods for asymmetrical cylinders.

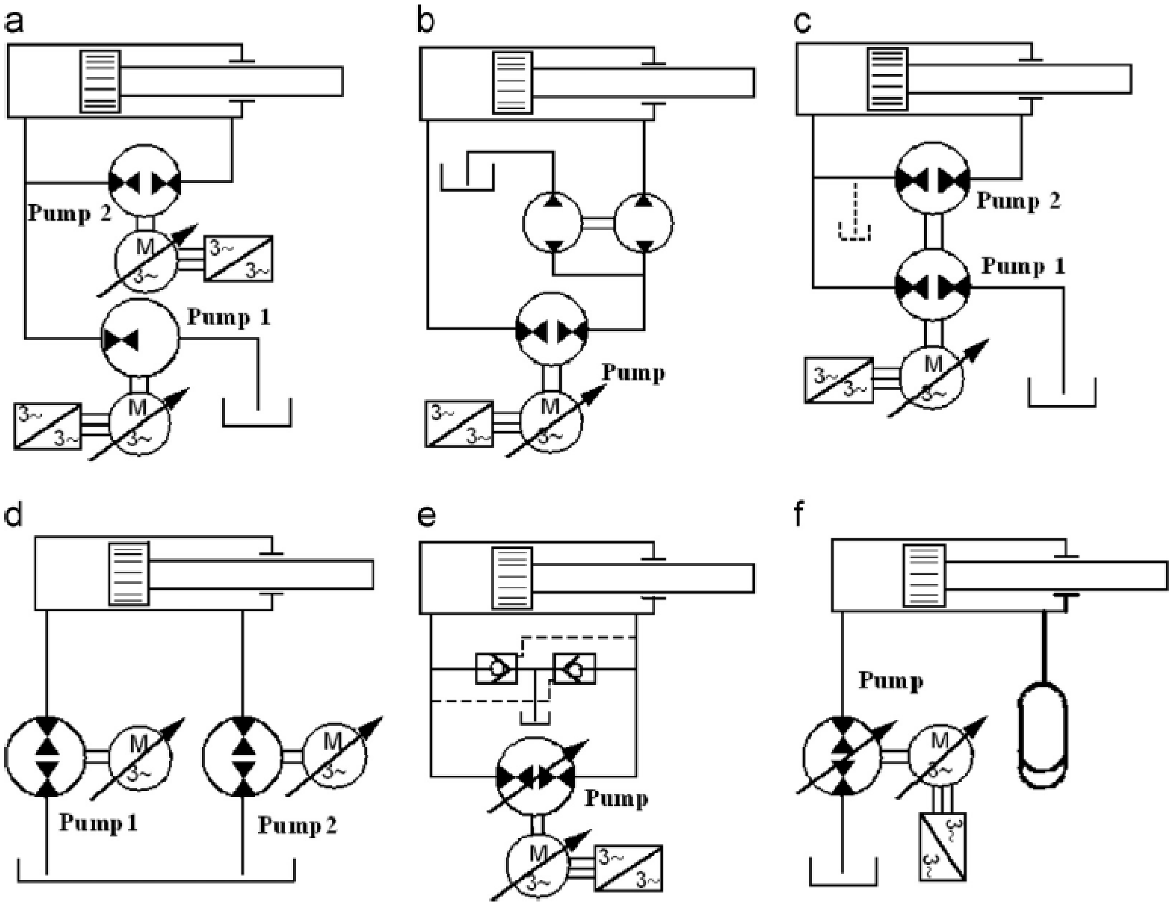

Source: Quan, Quan and Zhang (2014).

In Figure 25 (b), the author balances the flow rate in the cylinder chamber through the use of a hydraulic transformer or two coaxial-driven pumps. In Figure 25 (d), the author addresses the problem using two independent pumps/motors, each controlling one chamber of the cylinder.

Kärnell *et al*. (2021) also conclude in their paper that a state-of-the-art accumulator-based architecture would be more efficient, nonetheless, it would add complexity as mentioned earlier. Furthermore, concerning the pressure supply, they observe that an internal pressure supply is more efficient than an external one. But the former requires a size match between the cylinder ratio and the charge pump in case of a differential cylinder, which is an additional problem as the charge pump must be able to compensate for the system leakage that depends on the rated system pressure.

Figure 26 - Generalised pump-controlled concept without an accumulator.

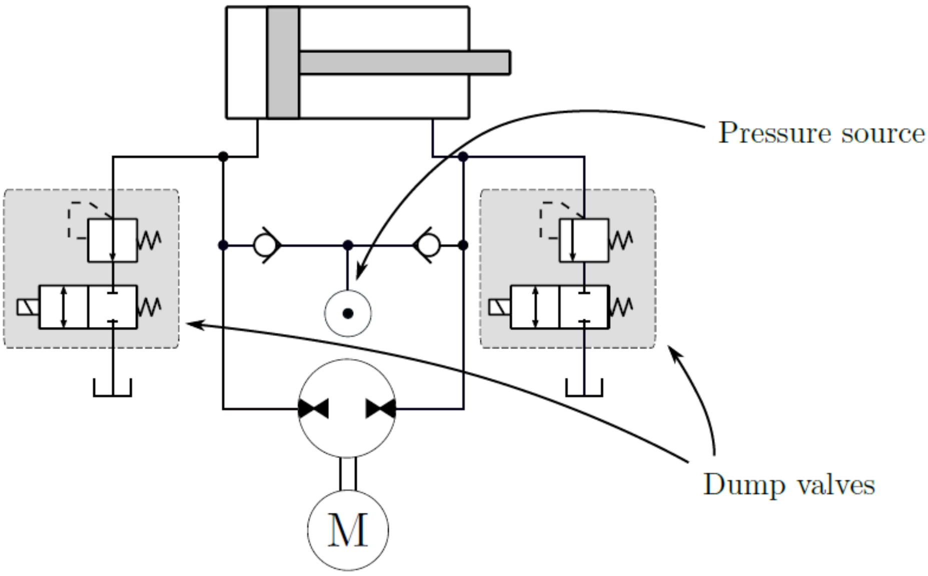

Source: Kärnell *et al.* (2021).

2.3.3 Electrical Motors

The choice of electrical motor is a key factor in the performance of pump-controlled systems with a fixed displacement pump and variable speed motor as it is the component responsible for the system control. Elbuluk & Kankam (1995) state that a drive selection depends on "power rating, operating speed range, operating environment, fault tolerance, reliability, performance requirements, thermal capability, cost and other criteria." Cao *et al.* (2012), Bostanci *et al.* (2017), and Elbuluk & Kankam (1995) overviewed the main motors used for either propulsion or more electrified aircraft, although this comparison applies to the subject of this thesis as they have similar requirements. They point out that so far, the motors with the greatest potential for these applications are Induction Machines (IM), Switched Reluctance Machines (SRM), and Permanent Magnet Machines (PM).

Induction machines, particularly the squirrel cage type, are widely available in industry and traditional workshops due to their simplicity, low cost, and well-known ruggedness. However, their efficiency is limited because of their intrinsic characteristics, e.g. magnetic coupling. Furthermore, when dynamic performance is a major concern and over a wide speed range, their drive becomes expensive and their control difficult to implement. (CAO *et al.,* 2012; ELBULUK; KANKAM, 1995)

According to Elbuluk & Kankam (1995), Switched Reluctance Motors (SRM) have a simple construction and low inertia that leads to faster system responses in servo applications. In addition, due to the independent phase windings present in these machines, they are considered fault tolerant, as they can operate with partial torque in the event of a short circuit in one of their phases (CAO *et al*., 2012).

Although switched reluctance motors have been proposed as a possible solution for variable speed applications since 1969 (KRISHNAN, 2001), they still need further development to mitigate some drawbacks (BOSTANCI *et al*., 2017). Those are “high torque ripple and the need to have an absolute position sensor to help the controller establish the phase current pulses” (ELBULUK; KANKAM, 1995, p. 513).

Permanent Magnet Synchronous Motors (PMSM) stand out for having high torque/inertia, torque/electric current and torque/volume ratios. Furthermore, they feature high efficiency, reliability and service life, which, combined with a low noise and operating temperature, and a wide speed range and the ability to withstand shocks and vibrations, make them an interesting choice for low power applications as well as industrial automation and aerospace applications (CAO *et al*., 2012; OBED; KADHIM, 2018; PATEL; HIRVANIYA; RATHOD, 2014).

However, they need a shaft positioning system such as Hall sensors, position revolver and absolute position sensors (ELBULUK; KANKAM, 1995; PATEL; HIRVANIYA; RATHOD, 2014). Other disadvantages are the limited operating temperature range, since the magnets present in the motor cannot withstand high temperatures (JACK; MECROW; HAYLOCK, 1996), and the price and availability of rare earth to manufacture these magnets (YANG *et al*., 2015).

These machines can be powered with different waveforms of supply, making them brushless DC or brushless AC machines, depending on the waveform they are supplied. In other words, brushless AC and brushless DC motors are the same in hardware (CAO *et al*., 2012).

3 MODELING DESCRIPTION

In this section, a detailed description of the hydraulic model will be presented. The aim is to provide a general understanding of the hydraulic system and its main components. The model of a hydroelectric power plant and its speed governor are outside the scope of this thesis and will not be discussed.

3.1 DESIGN REQUIREMENTS

A set of design requirements for the speed governor is listed by analyzing the major applicable standards along with manufacturers' data. IEEE 125:2007 (2007) states that an automatic shutdown shall be provided under the following conditions: Failure of the governor controller's main CPU, failure of all power supplies, failure of all speed signals, failure of main control actuator (gate or deflector) position transducer, oil temperature critical high, sump oil level critical low, oil pressure critical low, accumulator oil level critical high, accumulator oil level critical low, overspeed, and electrical and mechanical protection systems external to the governor.

For the dynamics of the servomotor, IEC 61362 (2012) suggests a time constant between 0.1 s and 0.25 s for its servo-positioner, thus resulting in a maximum settling time of approximately 0.75 s. However, for large installations, the integrity of the external components, such as ducts, may be taken into account, leading to longer response times. "The opening and closing travel times should be specified and are normally dictated by the permissible water-hammer effect in the water conduit and the permissible overspeed following load rejection." (IEEE 125:2007, 2007).

As analyzing the dynamics and structural integrity of an entire hydropower plant would be time-consuming and beyond the scope of this thesis, a partner company has provided data collection from an existing plant where they performed the commissioning. The Table 3 gives a general overview of the plant.

Table 3 - Analyzed hydraulic power plant data.

Hydroelectric power plant parameters		
Power	MW	190
Nominal Pressure	bar	31
Total oil volume	L	10869
Oil volume inside the tubulation	L	848
Accumulator oil volume	L	4054
Number of servomotors	-	2
Piston diameter	mm	770
Rod diameter	mm	250
Stroke	mm	700
Opening time	s	13.7
Closing time 100% to 10%	s	12.3

Source: Provided by an undisclosed company (2024).

3.2 PROPOSED ARCHITECTURE

The following architecture (Figure 27) is proposed by analyzing the system requirements in the Section 3.1. It comprises a pair of hydraulic cylinders, 1A1 and 1A2 connected directly to the wicket gates, which are differential actuators that work together to provide the required force to control the opening and closing of the gates in order to limit the flow of water to the turbine, consequently, controlling its speed. Since they are mechanically connected to the operating ring, when one is extending the other is retracting proportionally as if they were a single symmetrical actuator.

The main pump, 1P1, is responsible for controlling the cylinders' position. To accomplish this, it has to be a closed-circuit variable displacement pump capable of reversing its flow rate direction. This set is chosen because it offers better dynamics than the motor-controlled set since the motor dynamics would greatly limit the system response time for large machines like the one studied in this work. For further details on this subject see APPENDIX A. The hydraulic accumulator 3Z1 is responsible for storing hydraulic energy for later use in an emergency shutdown.

A smaller replenishing circuit is coupled to the primary circuit to supply internal and external leakage of the components, avoiding pump cavitation and maintaining a minimum pressure in the suction line. As the main circuit pump is reversible, the piloted check valves 2V3 and 2V4 are necessary to maintain high pressure on one side of the primary circuit and avoid pressures higher than that defined as the low-pressure side. In summary, it comprises a fixed displacement pump, 2P1, two check valves, 2V3 and 2V4, and its auxiliary valves, 2V5 and 2V6. The function of these auxiliary valves is to keep the check valves from opening in undesired moments.

Figure 27 - Simplified hydraulic circuit of the speed governor.

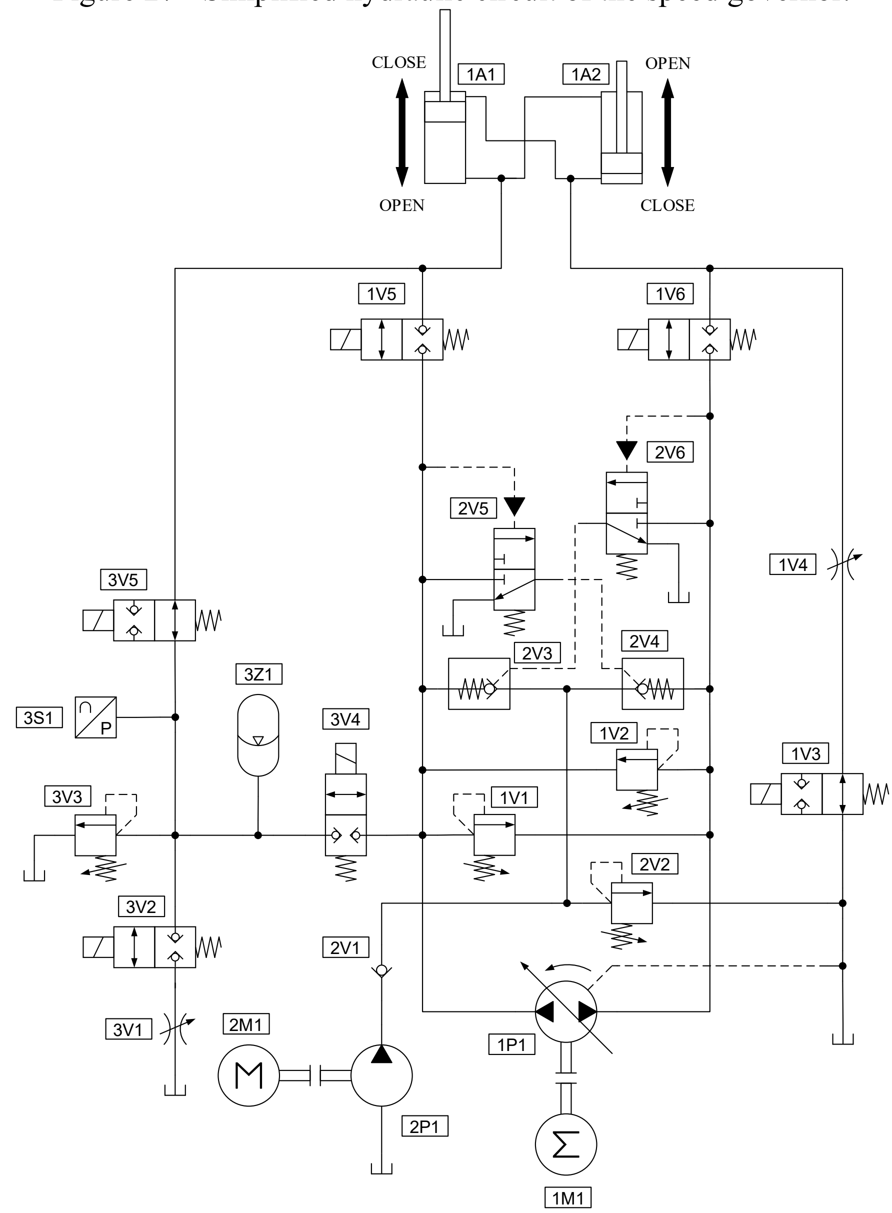

Source: Author (2024).

This new arrangement has three operating modes: starting mode, control mode and emergency mode. Starting mode occurs before the speed governor comes into operation. At this stage the hydraulic accumulator is filled with hydraulic fluid so that it can provide pressure and flow rate in an emergency. Its operation consists of actuating the valves 3V4 and 3V5, starting the motor 2M1 which drives pump 2P1. At the same time, the motor 1M1 comes into operation driving the variable displacement pump 1P1 where the displacement of the pump 1P1 is adjusted to provide a flow rate to the accumulator line slightly below the flow rate of the fixed displacement pump 2P1 to avoid cavitation. The system remains in this mode until the accumulator is completely filled. The Figure 28 depicts the circuit during starting mode, where the red lines represent the high-pressure lines and the yellow line represent the low-pressure line.

Figure 28 - Hydraulic circuit while in starting mode.

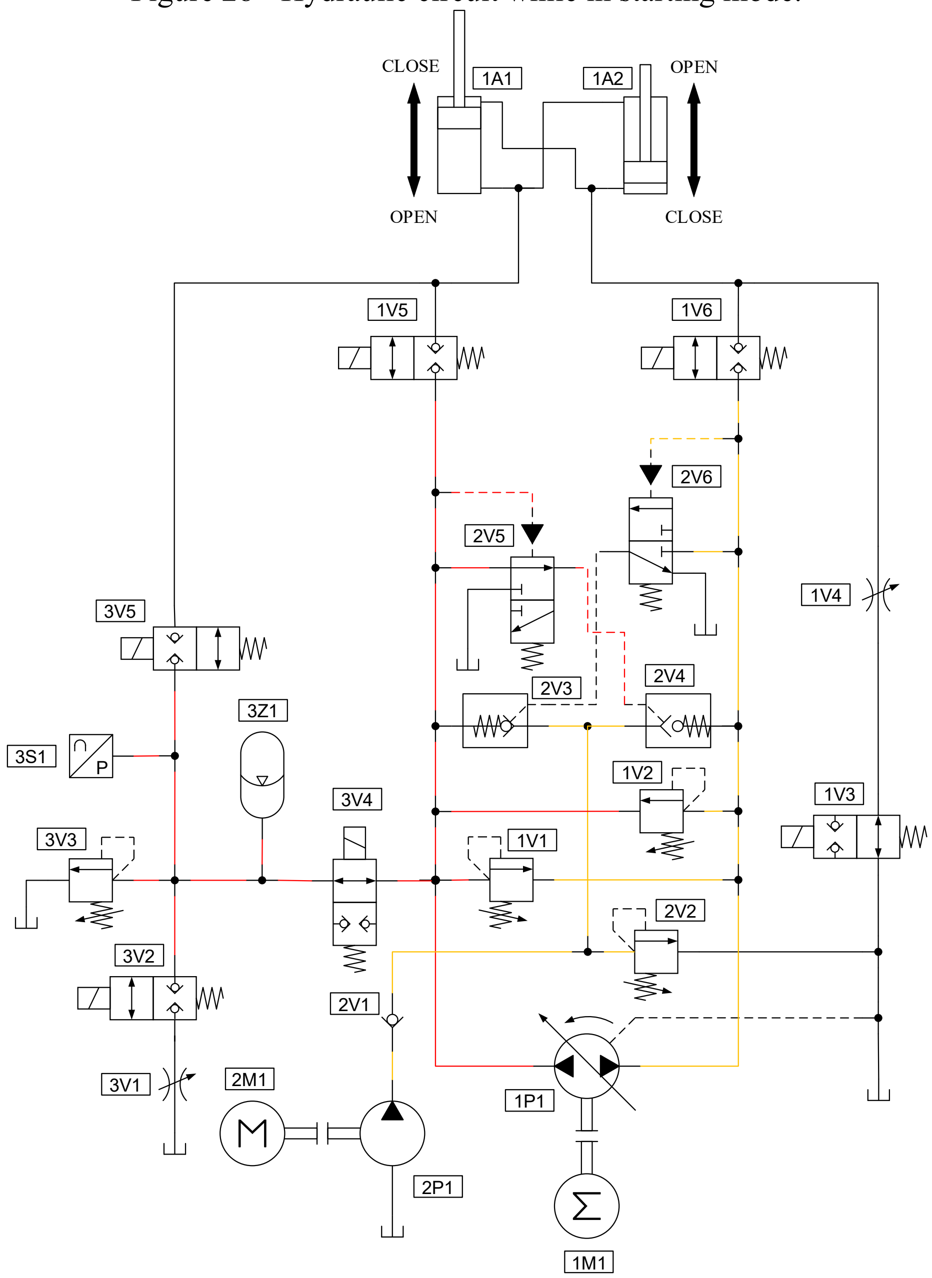

Source: Author (2024).

After the accumulator reaches the maximum pressure set in the system, the signal to solenoid valve 3V4 ceases, leaving it in its original position, confining the high-pressure oil inside the accumulator 3Z1. Now the control mode is enabled. In this mode, the signal to the valve 3V5 is maintained so that it remains in its closed position. Likewise, the motors 1M1 and 2M1 remain running. In addition, valve 1V3 is actuated so that it moves to its closed position. The valves 1V5 and 1V6 are set to their open position. Therefore, the position of the servomotors is completely controlled by the displacement of pump 1P1. Figure 29 shows the hydraulic circuit while in control mode.

Figure 29 - Hydraulic circuit while in controlling mode.

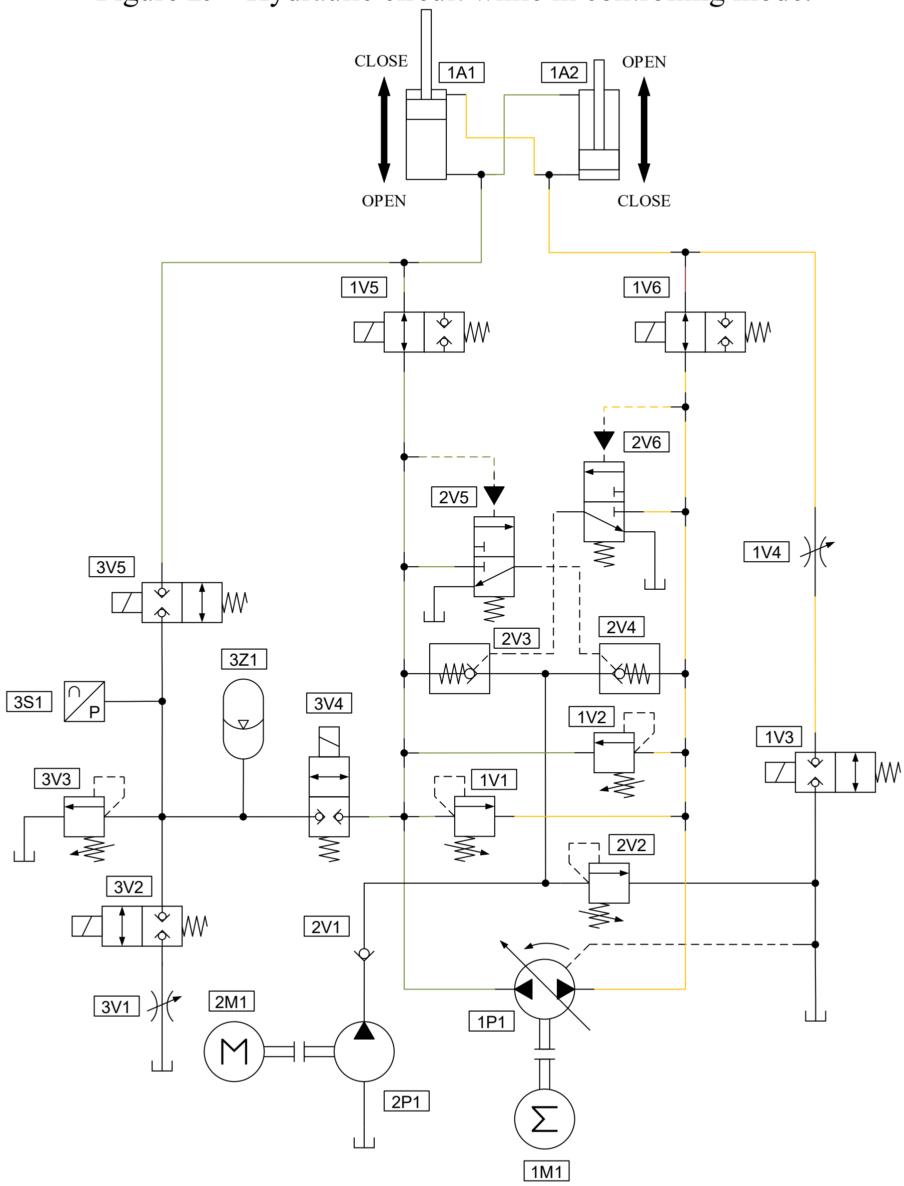

Source: Author (2024).

Emergency mode consists of the system ability to close the wicket gates in a controlled manner in the event of failure of a critical component of the generating unit. In this mode, no electrical power is required, only the stored hydraulic energy is sufficient to shut down the machine. For example, in a power failure, all valves would move to their resting position, allowing pressurized oil from the 3Z1 accumulator to flow into one of each of the hydraulic cylinder chambers. At the same time, the opposite chambers of the hydraulic cylinders are opened towards the reservoir, which allows them to close the gates. To control their closing speed, a flow control valve, 1V4, is placed between the cylinders and the reservoir. Figure 30 depicts the hydraulic circuit while in emergency mode. The red lines are the high-pressure hydraulic lines while the blue lines are reservoir-pressure hydraulic lines.

Figure 30 - Hydraulic circuit while in emergency mode.

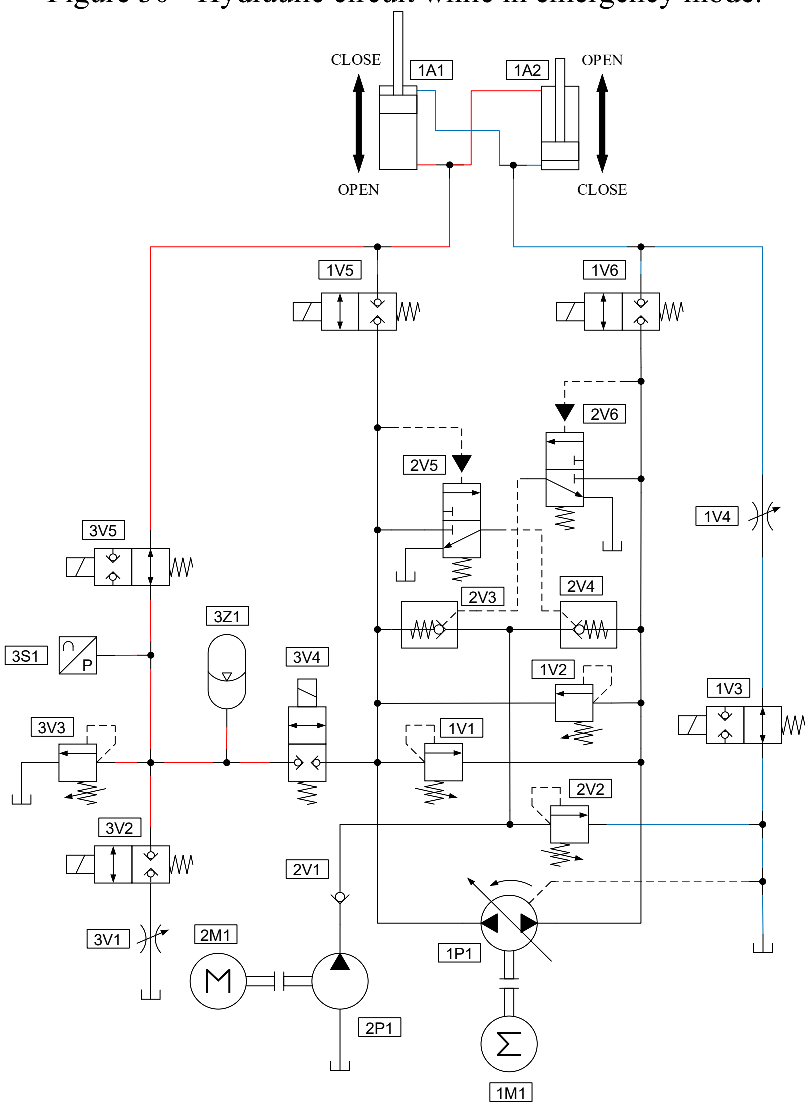

Source: Author (2024).

In the following sections each of the main components of the circuit are studied in further detail as well as their models. Each component of the hydraulic system is modeled through Hopsan. Hopsan is an open-source multi-domain system simulation tool which uses the Transmission Line Modeling (TLM) technique. The control was developed using Matlab Simulink. During the simulations a fixed simulation step time of 1×10^{-4} s is used.

3.3 SERVOMOTOR

This section presents the cylinder sizing and its mathematical model. As the architecture proposed in this master's thesis does not need a pressurized reservoir as the hydroelectric power plant analyzed, the pressure can be increased without worrying about the air/oil mixing. Through the data in Table 3 and the Equation 3.1 one can determine the combined force of the servomotors. This is the equivalent force of the original system, whose data is available in Table 3, where its nominal pressure and the actuator dimensions are used to compute its maximum load force through Equation 3.1. The rod side force of the retracting actuator plus the piston force of the extending actuator results in 2682.9 kN. By keeping the force constant and varying the load pressure it is possible to find the new cylinder combined area, the piston area plus the ring area on the piston rod side, that is depicted in Figure 31.

Figure 31 – Variation of the cylinders' total equivalent area as a function of the load pressure.

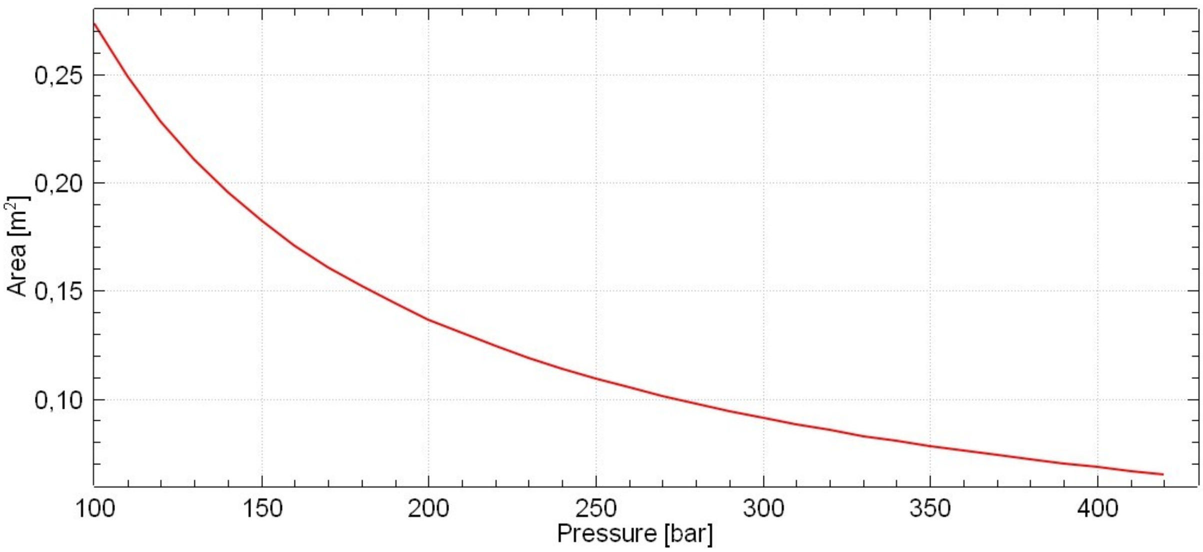

Source: Author (2024).

$$p_L = \frac{F_L}{A_e}, \qquad 3.1$$

where:

p_L = Load pressure [Pa];

F_L = Load force [N];

A_e = Equivalent area [m^2].

Due to the limitation of the shelf products the adopted maximum system pressure is 3.5×10^7 Pa (350 bar). Since that the servomotor will be controlled directly by a pump, it is assumed that the pressure in the opposite cylinder chamber will be near zero. Consequently, the load pressure is assumed to be equal to the maximum system pressure and the combined area of the two cylinders results on 0.07814 m^2. Therefore, the adoption of the cylinder is directed by the minimum area to be able to move the wicket gates and its maximum buckling force, resulting in the cylinder described in Table 4. Depending on the slenderness ratio the Buckling calculation is defined by Euler theory or Tetmajer theory as suggested by Bosch Rexroth (2022).

Table 4 - Servomotor parameters.

Servomotor parameters		
Piston diameter	m	0.25
Rod diameter	m	0.14
Stroke	m	0.7

Source: Author (2024).

The procedure for selecting the commercial hydraulic cylinder for correct use is described below. To choose the most suitable hydraulic cylinder, firstly one has to calculate its slenderness ratio using the Equation 3.2. for the free buckling length, l_k, see ANNEX A.

$$\lambda = \frac{4 \cdot l_k}{d}, \qquad 3.2$$

where:

λ = Slenderness ratio [1];

l_k = Free buckling length [mm];

d = Piston rod diameter [mm].

If the cylinder slenderness ratio is greater than the slenderness ratio limit given by Equation 3.3, the Euler equation (Equation 3.4) should be used to define the critical load of the component, otherwise the critical force should be calculated by the Tetmajer equation (Equation 3.5). For the full calculation see APPENDIX B.

$$\lambda_0 = \sqrt{\frac{\pi^2 \cdot E}{0.8 \cdot R_e}}, \tag{3.3}$$

where:

λ_0 = Slenderness ratio limit [1];

E = Module of elasticity [N/mm^2];

R_e = Yield strength of the piston rod material [N/mm^2].

$$F_{cr} = \frac{\pi^2 \cdot E \cdot I}{4 \cdot \nu}, \tag{3.4}$$

where:

F_{cr} = Critical buckling force [N];

E = Module of elasticity [N/mm^2];

I = Geometrical moment of inertia [mm^2];

ν = Safety factor [1].

$$F_{cr} = \frac{d^2 \cdot \pi (335 - 0.62 \cdot \lambda)}{4 \cdot \nu}, \tag{3.5}$$

where:

F_{cr} = Critical buckling force [N];

d = Piston rod diameter [mm];

λ = Slenderness ratio [1];

ν = Safety factor [1].

For simulation purposes, a symmetrical hydraulic cylinder can be used since their behavior is similar as they are mechanically linked to each other. This combination is possible because the piston area of 1A1 plus the rod side area of 1A2 is the same as the piston area of 1A2 plus the rod side area of 1A1.

Figure 32 presents the Hopsan "C type Symmetric Piston" model. According to the Hopsan documentation, this model considers the dead volume of the chambers, viscous friction and internal leakage. It does not consider the end stops. The software advises the user to handle it via an adjacent component as a mass for example.

Figure 32 - Hopsan C type Symmetric Piston icon.

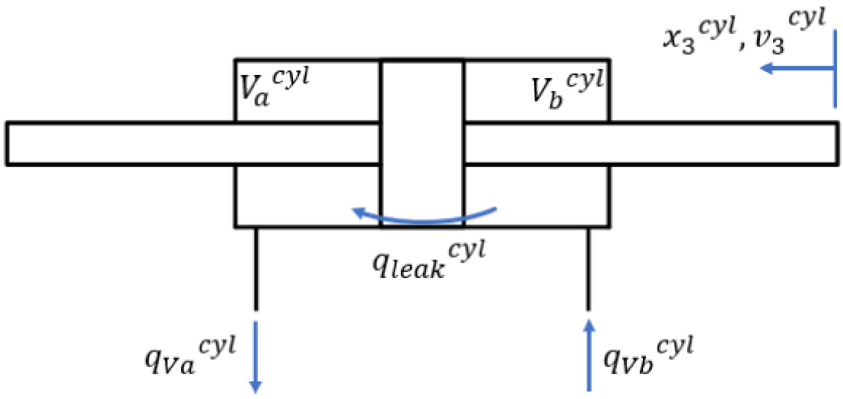

Source: Author (2024).

The model uses the continuity equation (Equation 3.6) to compute the pressure in each of the cylinder chambers as it is modelled as two variable volumes. The leakage flow rate is neglected in this study since it is too small to interfere with the behavior of the system as a whole, nevertheless, it can be implemented through this same model as a laminar flow described by Equation 3.7.

$$\begin{cases} q_{Va}{}^{cyl} = q_{leak}{}^{cyl} + A_a{}^{cyl} \cdot v_3{}^{cyl} - \frac{V_a{}^{cyl}}{\beta_e}\frac{dp_a{}^{cyl}}{dt} \\ q_{Vb}{}^{cyl} = -q_{leak}{}^{cyl} + A_b{}^{cyl} \cdot v_3{}^{cyl} + \frac{V_b{}^{cyl}}{\beta_e}\frac{dp_b{}^{cyl}}{dt}, \end{cases} \quad 3.6$$

where:

$q_{Va}{}^{cyl}$ = Cylinder chamber A flow rate [m³/s];

$q_{Vb}{}^{cyl}$ = Cylinder chamber B flow rate [m³/s];

$A_a{}^{cyl}$ = Cylinder chamber A piston area [m²];

$A_b{}^{cyl}$ = Cylinder chamber B piston area [m²];

$v_3{}^{cyl}$ = Piston speed [m/s];

$V_a{}^{cyl}$ = Cylinder chamber A volume [m³];

$V_b{}^{cyl}$ = Cylinder chamber B volume [m³];

$p_a{}^{cyl}$ = Cylinder chamber A pressure [Pa];

$p_b{}^{cyl}$ = Cylinder chamber B pressure [Pa];

β_e = Fluid bulk modulus [Pa].

$$q_{leak}{}^{cyl} = (p_a - p_b)k_{leak}{}^{cyl} \ , \qquad 3.7$$

where:

q_{leak} = Leakage flow rate [m³/s];

$p_a{}^{cyl}$ = Cylinder chamber A pressure [Pa];

$p_b{}^{cyl}$ = Cylinder chamber B pressure [Pa];

$k_{leak}{}^{cyl}$ = Leakage coefficient [m³/(s·Pa)].

3.4 FRICTION MODEL

According to Valdiero (2005), friction is a nonlinear phenomenon consisting of static and kinect effects, sometimes desired or undesired. They are present in all machines with relative motion between their parts, whether necessary to manipulate a component providing the essential grip or being the source of power losses, track errors and delays. The literature presents a myriad of nonlinear defects caused by friction, among those cited by Canudas De Wit *et al*. (1995) are stick-slip, hunting, standstill and quadrature glitch (Figure 33).

As depicted in Figure 33 (a), "stick-slip" is the intermittent motion between sliding and rest. "Hunting", Figure 33 (b), when there is an oscillation around the desired signal and it is present only is systems with position feedback. The loss of movement that happens while the system crosses near the zero speed is called "standstill", (Figure 33 (c)). Finally, the quadrant glitch, Figure 33 (d), is the track error associated with multiple axes.

Besides the error generation, friction alone is responsible for a significant power loss in hydraulic cylinders. Therefore, it is essential to have an accurate mathematical model to represent its effects whenever simulating a hydraulic system. Furthermore, authors such Perondi (2002) and Valdiero (2005) highlight the importance of the models in the design of friction compensators.

As mentioned before, friction comprises both static and kinect effects and are dependent on factors beyond the relative velocity as many of the classical friction models suggested. Among those factors are the materials in contact, constancy of lubrication, temperature of operation and the state of wear (ARMSTRONG-HÉLOUVRY; DUPONT; DE WIT, 1994).

Figure 33 - Examples of tracking defects caused by friction.

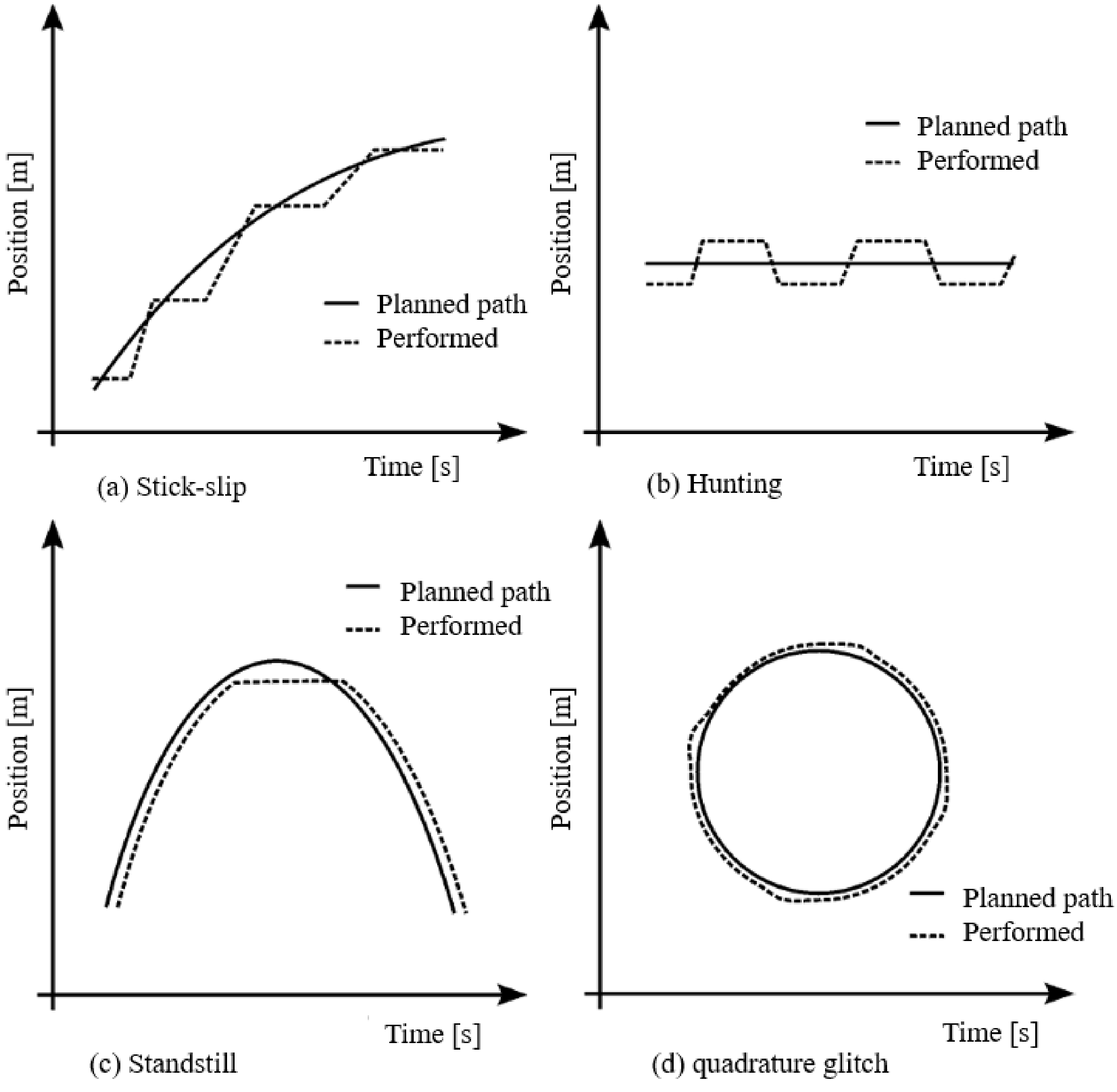

Source: Adapted from Valdiero (2005).

Moreover, since friction has its kinect parcel of effect, those models that adopt only the friction map, usually velocity dependent, are not enough to represent the dynamics of the model because they would not be able to describe an instantaneous change in speed. Aiming to consider this effect many models were proposed, including the model suggested by Dahl (CANUDAS DE WIT *et al*., 1995), which later led to the LuGre model that was modified by many authors such as in Swevers *et al*. (2000) and in Dupont, Armstrong and Hayward, (2000).

The Dahl model introduces the idea of a spring-like behavior during stiction. It "is essentially Coulomb friction with a lag in the change of friction force when the direction of motion is changed" (CANUDAS DE WIT *et al*., 1995). Canudas De Wit *et al*. (1995) then extended the Dahl model creating the LuGre model which considers the Stricbeck effect. Later on, other features such as the hysteresis model, frictional memory, and pressure dependency were introduced by other authors up to this day (VALDIERO, 2005).

The present work adopts the LuGre model to characterize friction. As observed in Canudas De Wit *et al*. (1995), this model describes the Stribeck effect, stick-slip effect and pre-sliding behavior, and is, therefore, well-suited for the application. In order to model the pre-sliding, Canudas De Wit *et al.* (1995) considers the surfaces in contact as two rigid bodies that make contact with each other through bristles. When a tangential force is applied to one of these bodies, it causes the bristles to deflect, generating a rise opposite force. If the force magnitude is large enough the bristles deflect in a way that the bodies slip. This behavior is represented in Figure 34.

Figure 34 - LuGre friction interface between two surfaces.

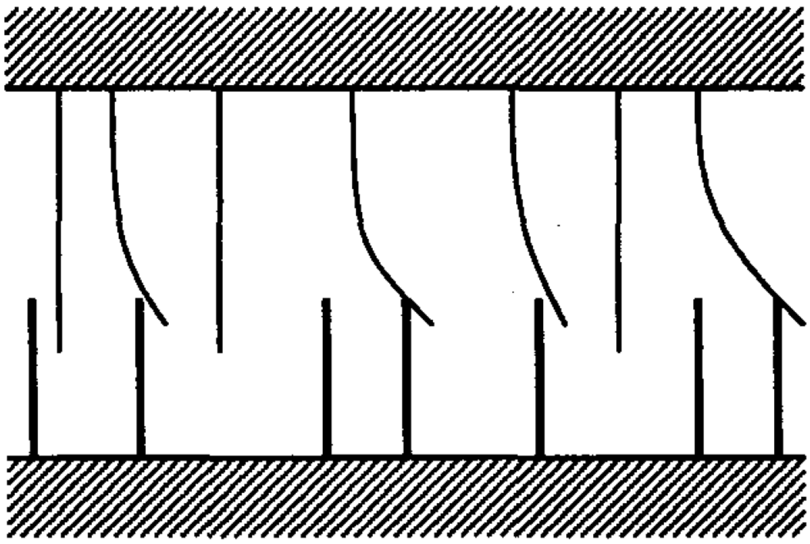

Source: Canudas De Wit *et al.* (1995).

This friction is described by Equation 3.8 for a hydraulic cylinder. The first two terms relate to the created reaction caused by the bristle's deflection and the third term to the viscous friction.

$$F_{fr} = \sigma_0 \cdot z + \sigma_1 \cdot \dot{z} + \sigma_2 \cdot {v_3}^{cyl} \,, \qquad 3.8$$

where:

F_{fr} = Friction force [N];

σ_0 = Stiffness of the bristles [N/m];

z = The average deflection of the bristles [m];

σ_1 = Damping coefficient [N·s/m];

σ_2 = Viscous friction damping coefficient [N·s/m];

${v_3}^{cyl}$ = Piston speed [m/s].

The variable z is the average deflection of the bristles and is obtained by Equation 3.9, where, $g({v_3}^{cyl})$ is a positive function that depends on material properties, lubrication, temperature and other specific factors. This function is computed by Equation 3.10.

$$\frac{dz}{dt} = {v_3}^{cyl} - \sigma_0 \frac{|{v_3}^{cyl}|}{g({v_3}^{cyl})} z \,, \qquad 3.9$$

where:

z = The average deflection of the bristles [m];

${v_3}^{cyl}$ = Piston speed [m/s];

σ_0 = Stiffness of the bristles [N/m];

$g({v_3}^{cyl})$ = Function that characterizes the contact condition [N].

$$g({v_3}^{cyl}) = \frac{F_C + (F_S - F_C) e^{-\left(\frac{{v_3}^{cyl}}{{v_S}^{cyl}}\right)^{\alpha}}}{\sigma_0} \,, \qquad 3.10$$

where:

$g({v_3}^{cyl})$ = Function that characterizes the contact condition [N];

F_C = Coulomb friction force [N];

F_S = Stiction force [N];

${v_3}^{cyl}$ = Piston speed [m/s];

${v_S}^{cyl}$ = Stribeck velocity [m/s];

α = Stribeck curve coefficient [1];

σ_0 = Stiffness of the bristles [N/m].

In the steady-state the friction force (Equation 3.8) becomes Equation 3.11.

$$ {F_{fr}}^{SS} = \sigma_0 \cdot g({v_3}^{cyl}) \cdot sgn({v_3}^{cyl}) + \sigma_2 \cdot {v_3}^{cyl} \, , \qquad 3.11 $$

where:

${F_{fr}}^{SS}$ = Friction force in steady-state [N];

σ_0 = Stiffness of the bristles [N/m];

σ_2 = Viscous friction damping coefficient [N·s/m];

$g({v_3}^{cyl})$ = Function that characterizes the contact condition [N];

${v_3}^{cyl}$ = Piston speed [m/s].

By combining Equation 3.10 and Equation 3.11 one has the equation that describes the steady-state friction force (Equation 3.12).

$$ {F_{fr}}^{SS} = F_C + (F_S - F_C)e^{-\left(\frac{{v_3}^{cyl}}{{v_S}^{cyl}}\right)^{\alpha}} + \sigma_2 \cdot {v_3}^{cyl} \, , \qquad 3.12 $$

where:

${F_{fr}}^{SS}$ = Friction force in steady-state [N];

$g({v_3}^{cyl})$ = Function that characterizes the contact condition [N];

F_C = Coulomb friction force [N];

F_S = Stiction force [N];

${v_3}^{cyl}$ = Piston speed [m/s];

α = Stribeck curve coefficient [1];

${v_S}^{cyl}$ = Stribeck velocity [m/s];

σ_2 = Viscous friction damping coefficient [N·s/m].

The classical friction map as a function of relative velocity between the surfaces comprises the stiction, Coulomb friction and viscous friction as depicted in Figure 35.

Typically, the static parameters (F_C, F_S, ${v_S}^{cyl}$ and σ_2) are identified by means of an experimental curve called friction map. This curve is plotted by varying the piston speed and measuring the friction force indirectly by the pressure difference between the cylinder chambers. Therefore, using a numerical method such as the nonlinear least squares used in Teixeira (2015) it is possible to identify the static parameters. The dynamic parameters are estimated by experiments and appropriate numerical methods. For more details on this topic, see Perondi (2002), Valdiero (2005) and Teixeira (2015).

Due to limited resources, this study relies solely on theoretical analysis and simulations. As a result, it was not possible to obtain the friction map and experimental parameters. Instead, the friction map was generated using the steady-state friction force Equation 3.12. The parameters used in this equation are adapted from the Valdiero (2005) and Teixeira (2015) case study, being adjusted to more accurately represent a real physical system. Stiction was set to one-hundredth of the maximum force produced by the actuator, with Coulomb friction set to one-third of that value. Where the damping coefficient follows the data from Perondi (2002), Valdiero (2005) and Teixeira (2015), and the stiffness of the bristles computed through 3.13 considering the hypothesis of critically damped dynamic behavior (ζ=1) as suggested by Perondi (2002).

Figure 35 - Friction map as a function of velocity.

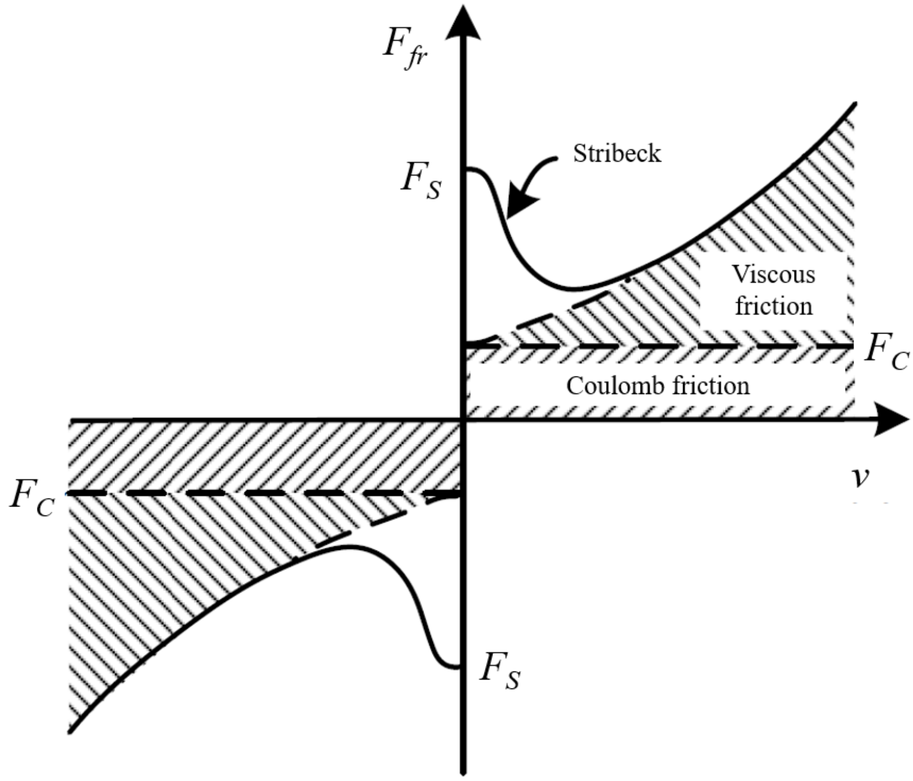

Source: Valdiero (2005).

$$\sigma_1 = 2\zeta\sqrt{\sigma_0 \cdot m} - \sigma_2 \, , \qquad 3.13$$

where:

σ_1 = Damping coefficient [N·s/m];

ζ = Damping ratio [1];

σ_0 = Stiffness of the bristles [N/m];

m = Displaced mass [kg];

σ_2 = Viscous friction damping coefficient [N·s/m].

Figure 36 presents the steady-state friction map as a function of velocity, generated using 3.12 and the parameters listed in Table 5. It is possible to observe that it has the same characteristic curve as the one in Figure 35. For the purposes of this study, the map was assumed to be symmetrical for both positive and negative speeds; however, the behavior could differ depending on the direction. The block diagram for the LuGre friction is available on APPENDIX C.

Figure 36 - Hydraulic cylinder friction map.

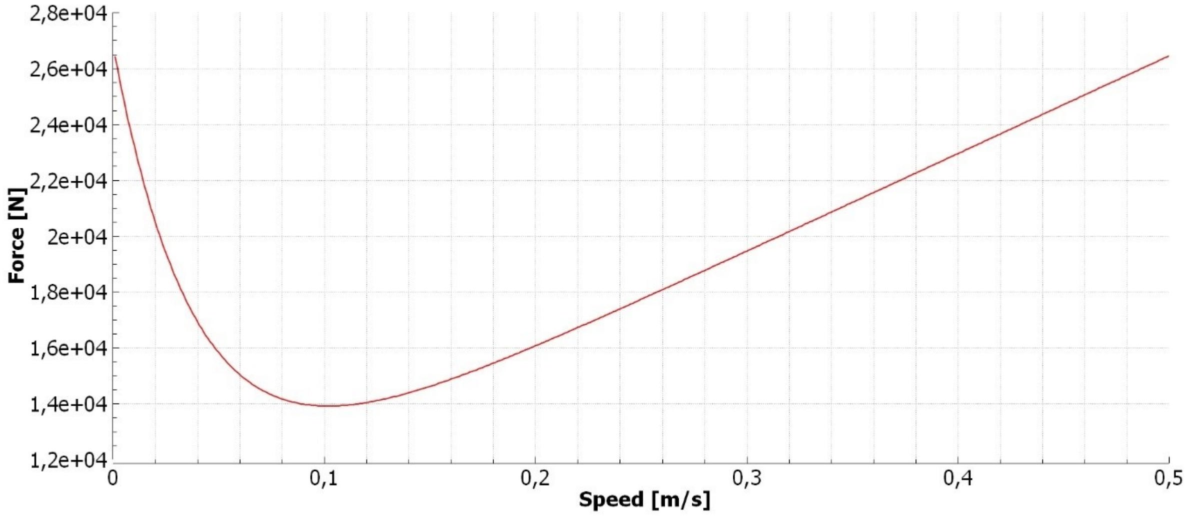

Source: Author (2024).

Table 5 – Friction parameters of the studied hydraulic cylinder.

Friction map parameters		
Stiction force	N	26829.7
Coulomb friction force	N	8943.2
Stribeck velocity	m/s	0.04
Viscous friction damping coefficient	N·s/m	35000
Stribeck curve coefficient	1	1
Stiffness of the bristles	N/m	306251
Damping coefficient	N·s/m	0.1

Source: Author (2024).

3.5 LOAD PROFILE

The load on the servomotor changes with its position, producing a load profile similar to that shown in Figure 14. A series of points were established along the profile to represent this load, with the maximum force set at approximately 80% of the servomotor's capacity. The external force as a function of servomotor position, described by Equation 3.14, was obtained using a Polynomial Curve Fit. Figure 37 illustrates the load profile resulting from Equation 3.14. For the block diagram see APPENDIX D.

$$F_L = -47352000x^4 + 8291500x^3 - 61540000x^2 + 23750000x - 1786600\ , \tag{3.14}$$

where:

F_L = External load [N];

x = Servomotor position [N].

Figure 37 - Servomotor external load.

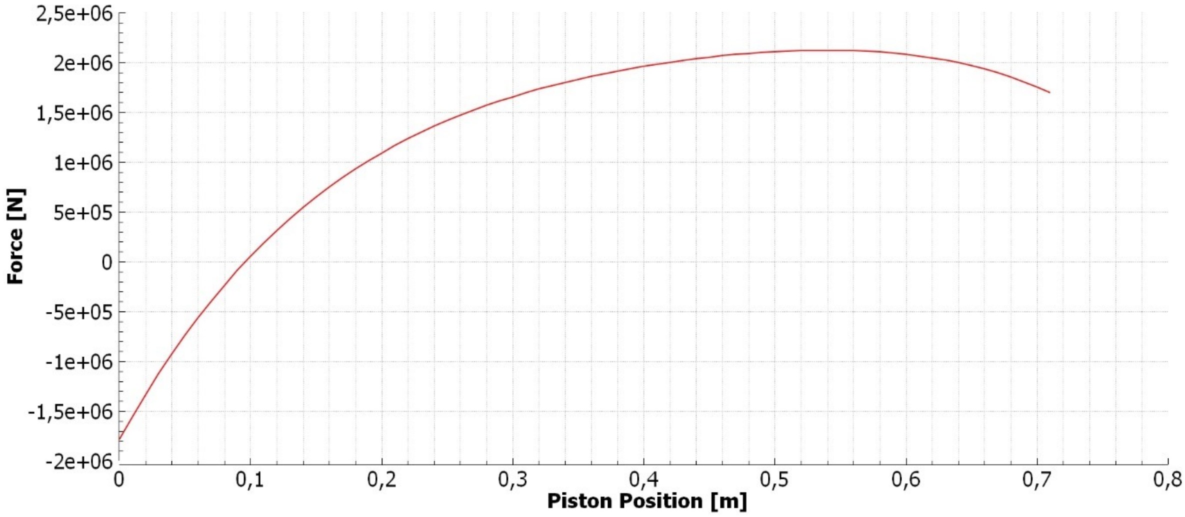

Source: Author (2024).

3.6 VARIABLE DISPLACEMENT PUMP

As mentioned in Section 3.2, the variable displacement pump, 1P1, is responsible for controlling the position and speed of the hydraulic cylinder. The most common variable displacement pumps available on the market are vane and axial piston pumps. The latter are offered in larger sizes, which is why this model was used in this work. These machines vary their flow rate by changing the angle of the swash plate and, consequently, varying the stroke of their internal pistons, causing the volume displaced in each shaft revolution to vary continuously.

De Negri, Ramos Filho and Souza (2008) suggest a method for designing a hydraulic position system that later was updated originating the paper (MURARO; TEIXEIRA; DE NEGRI, 2013). This work follows the first part of the "System and Actuator Characterization" presented in their paper. Therefore, pump sizing begins by calculating the undamped natural frequency required by the system using Equation 3.15. This equation comes from the settling time equation using the 2% criterion described in Gene *et al* (2013). The settling time for the 2% criterion is the time it takes the system to reach the desired position within a 2% error of its input.

$$\omega_n{}^{SYS} = \frac{4}{\zeta^{SYS} . t_s{}^{SYS}} , \qquad 3.15$$

where:

$\omega_n{}^{SYS}$ = System natural frequency [rad/s];
ζ^{SYS} = System damping ratio [1];
$t_s{}^{SYS}$ = System settling time [s].

The system damping ratio characterizes its overshoot. If overshoot is undesirable or impossible in the studied system, its damping ratio should be 1. Otherwise, if overshoot is not a problem, 0.7 is the fastest possible response. Note that the closer it is to 1, the smaller the overshoot. In this work, the settling time is a system requirement provided by an undisclosed company.

The second step is to calculate the maximum velocity of the actuator. For damping ratios smaller than 1, the maximum velocity occurs at the time described by Equation 3.16 and is calculated by Equation 3.18.

$$t_{v\_M}{}^{SYS} = \frac{1}{\omega_d{}^{SYS}} \cdot tan^{-1}\left(\frac{\sqrt{1-\zeta^{SYS^2}}}{\zeta^{SYS}}\right), \qquad 3.16$$

where:

$t_{v\_M}{}^{SYS}$ = Time of the piston's maximum speed [s];

$\omega_d{}^{SYS}$ = Damped natural frequency [rad/s];

ζ^{SYS} = System damping ratio [1].

The damped natural frequency is computed by Equation 3.17.

$$\omega_d{}^{SYS} = \omega_n{}^{SYS} \cdot \sqrt{1 - \zeta^{SYS^2}} \,, \qquad 3.17$$

where:

$\omega_d{}^{SYS}$ = Damped natural frequency [rad/s];

$\omega_n{}^{SYS}$ = System natural frequency [rad/s];

ζ^{SYS} = System damping ratio [1].

$$v_M = x_d \cdot \omega_n{}^{SYS} \cdot e^{-\zeta^{SYS} \cdot \omega_n{}^{SYS} \cdot t_{v\_M}{}^{SYS}} \,, \qquad 3.18$$

where:

v_M = Piston maximum speed [m/s];

x_d = Desired step output [m];

ζ^{SYS} = System damping ratio [1];

$\omega_n{}^{SYS}$ = System natural frequency [rad/s];

$t_{v\_M}{}^{SYS}$ = Time of the piston's maximum speed [s].

With the piston's maximum speed, it is possible to compute the system's maximum speed using the Equation 3.19. As can be seen in Figure 27, the hydraulic circuit has two actuators that work together, since they are mechanically connected to each other, they can be considered as a symmetrical cylinder for analysis purposes. Therefore, the area used in Equation 3.19 is the sum of the piston area and the annulus area of the rod side.

$$q_{Vmax}{}^{C} = A^C \cdot v_M \,, \qquad 3.19$$

where:

$q_{Vmax}{}^{C}$ = Hydraulic cylinder's maximum flow [m³/s];

A^C = Piston area [m²];

v_M = Piston maximum speed [m/s].

Then, the pump's required displacement is computed through Equation 3.20.

$$q_{Vmax}{}^{C} = D \cdot \omega^P \ , \tag{3.20}$$

where:

$q_{Vmax}{}^{C}$ = Hydraulic cylinder's maximum flow [m³/s];

D = Pump's volumetric displacement [m³/s];

ω^P = Angular pumps speed [rev/s].

Finally, response of the swash plate should have a frequency at least 3 times the undamped natural frequency of the system.

Two different scenarios are considered for the characterization of the system and actuator: the wicket gate opening (from 0% to 80% of the cylinder stroke) and the control scenario (displacement of 5% of the cylinder stroke). Note that the pump has to be able to meet the worst-case scenario. The results of the system characterization are available in Table 6. As one can see, the worst-case scenario is during the opening of the wicket gates, which requires a flow rate of 5.93×10^{-3} m³/s (356 L/min) while the speed control requires only 4.70×10^{-3} m³/s (282 L/min).

Table 6 - System characterization.

Parameter	Unit	Wicket gate opening	Step of 5%
$\omega_n{}^{SYS}$	rad/s	0.32441	4.12
ζ^{SYS}	1	0.9	0.9
$t_s{}^{SYS}$	s	13.7	1.08
x_d	m	0.56	0.035
$t_{v\_M}{}^{SYS}$	s	3.19	0.25
$\omega_d{}^{SYS}$	rad/s	0.14141	1.79379
A^C	m²	0.0828	0.0828
v_M	m/s	0.07159	0.05676
$q_{Vmax}{}^{C}$	m³/s	5.93×10^{-3}	4.70×10^{-3}

Source: Author (2024).

After the determination of the system parameters, it is necessary to evaluate whether the cylinder with the total coupled load is capable of respond in the given settling time. In order to accomplish this, Muraro, Teixeira and De Negri (2013) asserts that the cylinder with the coupled load should have natural frequency of at least three times the system natural frequency. For symmetrical double acting cylinder, the minimum undamped natural frequency is computed by Equation 3.21.

$$\omega_{n\_min}{}^{C} = \left(\frac{4 \cdot \beta_e \cdot A^{C^2}}{M_t \cdot V_t{}^{C}}\right)^{1/2}, \quad 3.21$$

where:

$\omega_{n\_min}{}^{C}$ = Minimum undamped natural frequency [rad/s];

β_e = Fluid bulk modulus [Pa].

A^C = Piston area [m²];

M_t = Total moveable mass [s];

$V_t{}^{C}$ = Total volume of the cylinder chambers [m³].

The parameters and results of the cylinder with the coupled load analysis is available in Table 7.

Table 7 - Cylinder minimum undamped natural frequency analysis.

Cylinder with coupled load parameters		
$\omega_{n\_min}{}^{C}$	rad/s	687.6
β_e	Pa	1×10^9
A^C	m²	0.0828
M_t	kg	1000
$V_t{}^{C}$	m³	0.058

Source: Author (2024).

Muraro, Teixeira and De Negri (2013) assert in their paper that for the valve selection, its flow coefficient and consequently its maximum flow rate should be between half and two times the hydraulic cylinder's maximum flow rate. Therefore, the chosen pump should be able to provide a flow rate, when fully open, between 2.965×10^{-3} m³/s and 11.86×10^{-3} m³/s.

This data allows the selection of the most appropriate pump for the system. The Bosch Rexroth A4VSG 125 model is chosen by researching the closed-loop models available on the market. This choice is based on the fact that this model fits the pump requirements and there is sufficient data available in its datasheet to complete the analysis, however, other models from other manufacturers could also be chosen. Its characteristics are summarized from Bosch Rexroth (2018) and Bosch Rexroth (2021) in Table 8. The adopted rotational speed is 1750 RPM, although the Pump maximum rotational speed is 2600 RPM. This is due to a four-pole induction electric motor powered by a 60Hz power source which has a nominal rotational speed of 1800 RPM. Therefore, considering the slip present in these machines, the considered rotational speed is 1750 RPM.

Table 8 - Summary of the Bosch Rexroth' pump A4VSG 125 main parameters.

Bosch Rexroth A4VSG 125 main parameters		
Maximum displacement per revolution	cm^3/rot	125
Maximum rotational speed	RPM	2600
Nominal pressure	bar	350
Maximum pressure	bar	400
Minimum pressure	bar	15
Approximate swash plate settling time 0 % to 100 %	s	0.1

Source: Bosch Rexroth (2018, 2021).

The next step is to evaluate the selected pump regarding it dynamic response. The pump flow rate direction and intensity are determined by its swash plate. Correlating with the design method for positioning systems presented by Muraro, Teixeira and De Negri (2013), the swash plate natural frequency could be compared with the proportional valve natural frequency. In their paper, Muraro, Teixeira and De Negri (2013) conclude that the valve natural frequency should be at least three times the system natural frequency in order to yield an acceptable system response. The swash plate natural frequency is calculated by Equation 3.22 and the parameters and result are shown in Table 9. While the system natural frequency is 4.12 rad/s, considering the settling time presented in Table 8, the swash plate natural frequency is 40 rad/s. Therefore, the chosen pump is suitable for the application since its swash plate natural frequency is 9.7 times the system natural frequency.

Table 9 – Natural frequency of the pump swash plate.

Natural frequency	rad/s	40
Damping ratio	1	0.7
Settling time	s	0.1

Source: Author (2024).

$$\omega_n{}^{SP} = \frac{4}{\zeta^{SP} \cdot t_s{}^{SP}}\,, \qquad 3.22$$

where:

$\omega_n{}^{SP}$ = Swash plate natural frequency [rad/s];

ζ^{SP} = Swash plate damping ratio [1];

$t_s{}^{SP}$ = Swash plate settling time [s].

Figure 38 shows the pump's deadband. Deadband is a nonlinearity commonly found in mechanical systems that can be understood as a static input-output relationship in which there is no output for a range of inputs. Note that manufacturer presents the input on the vertical axis and the output on the horizontal axis. A deadband can be the source of errors and poor dynamics so that it is frequently considered a defect and should be dealt with. (VALDIERO, 2005)

Figure 38 - Bosch Rexroth A4VSG 125 deadband.

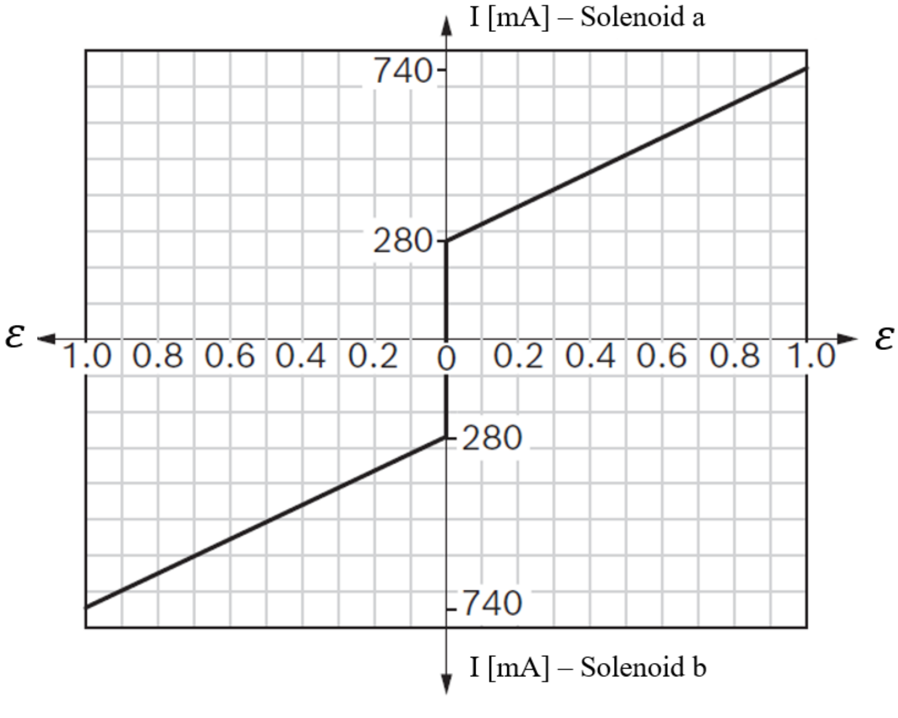

Source: Adapted from Bosch Rexroth (2021).

One deadband compensation method is to develop its parametric inverse function as highlighted by Tao & Kokotovic (1996 *apud* VALDIERO, 2005). Nevertheless, its exact inverse cannot be implemented since its parameters are not precisely known. To overcome this, a smooth deadband inverse function is used in order to avoid discontinuities in the input's origin.

Figure 39 depicts the fixed deadband inverse linearly smoothed in its origin. Where "u_d" is the wished input signal, "u_{czm}" is the compensator output, " lc " is the linear smoothing region, " md" is the right side deadband inclination, " me" is the left side deadband inclination, "zmd" is right side deadband, and "zme" is the left side deadband. Equation 3.23 describes this compensation method, and its block diagram for unitary and equal " md" and " me" is shown in Figure 40.

Figure 39 - Graphical representation of the inverse of the deadband nonlinearity incorporating linear smoothing around the origin.

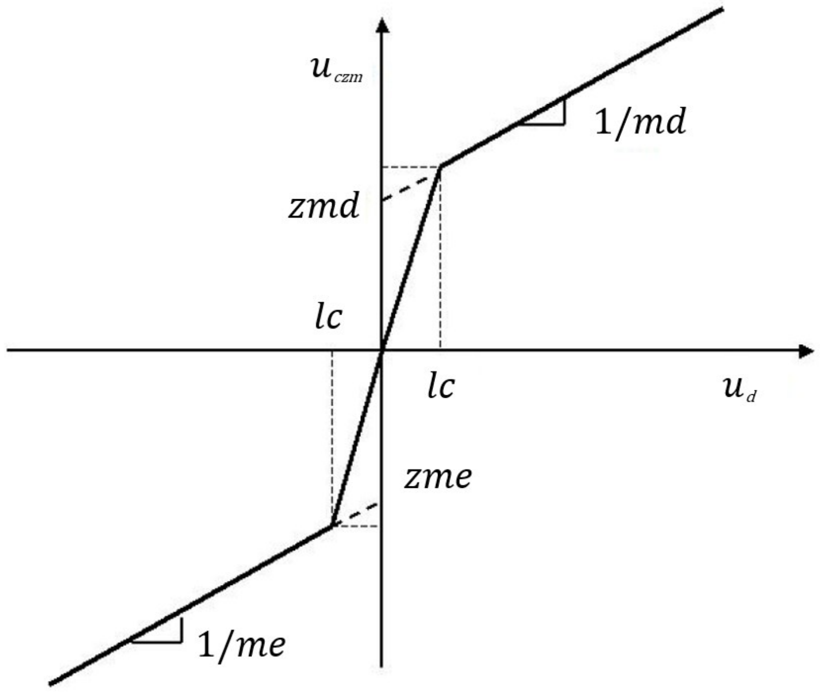

Source: Valdiero (2005).

$$u_{czm}(t) = \begin{cases} \frac{u_d(t)}{md} + zmd, \ u_d(t) \geq lc \\ \frac{u_d(t)}{me} - |zme|, \ u_d(t) < -|lc| \\ \left(\frac{zmd + {}^{lc}/_{md}}{lc}\right) u_d(t), \ 0 \leq u_d(t) < lc \\ \left(\frac{|zme| + {}^{|lc|}/_{me}}{|lc|}\right) u_d(t), \ -|lc| \leq u_d(t) < 0 \end{cases}, \quad 3.23$$

where:

u_{czm} = Compensator output [m];

u_d = Input signal [m];

md = Right side deadband inclination [1];

me = Left side deadband inclination [1];

zmd = Right side deadband [%];

zme = Left side deadband [%];

lc = linear smoothing region [1].

Figure 40 - Deadband compensation block diagram.

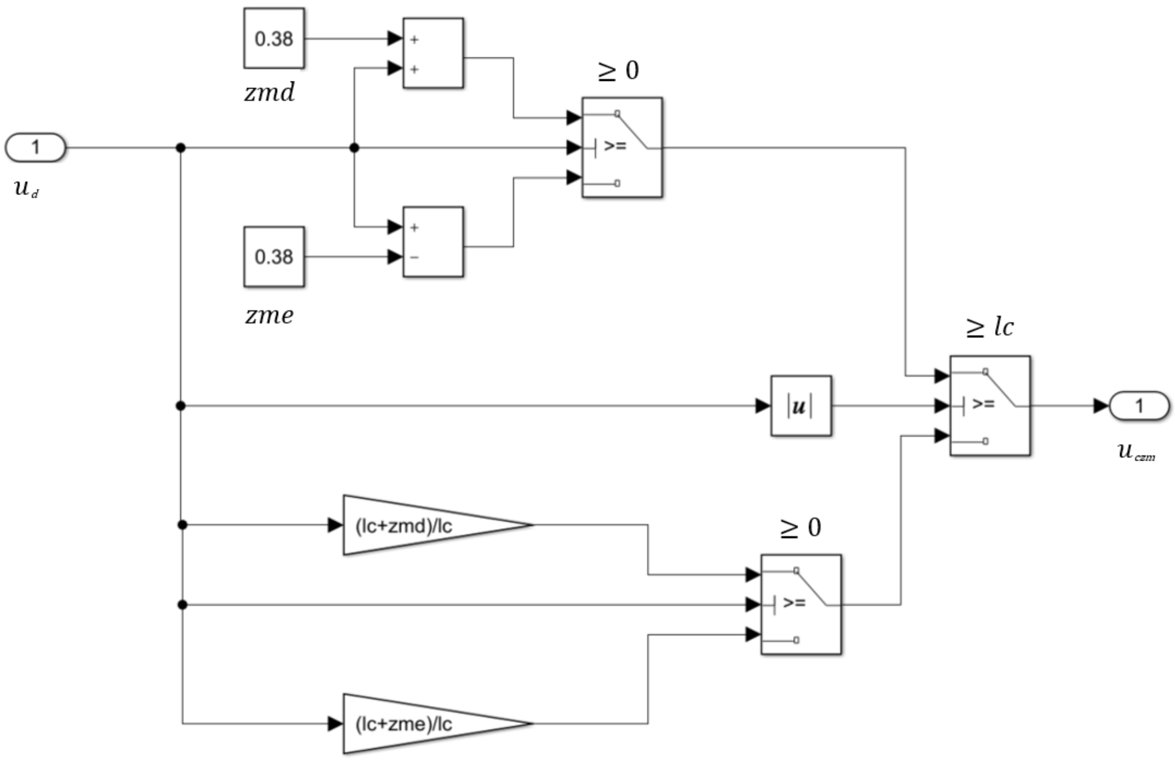

Source: Adapted from Valdiero (2005).

The parameters used in the model are available in Table 10. The right side and left side deadband are expressed as the percentage of the displacement setting.

Table 10 - Deadband compensation parameters.

Parameters		
Right side deadband	%	0.38
Left side deadband	%	0.38
Linear smoothing region	1	0.5

Source: Author (2024).

The Hopsan model adopted for the variable displacement pump is represented by Equation 3.24. In this equation "ε" can assume values from -1 to 1 since the pump is an inversible variable displacement pump.

$$\begin{cases} {q_2}^P = \frac{\varepsilon \cdot D}{2\pi} \cdot \omega^P - {q_{leak}}^P \\ {q_2}^P = -{q_1}^P \end{cases}, \quad 3.24$$

where:

${q_1}^P$ = Pump's input flow rate [m³/s];

${q_2}^P$ = Pump's output flow rate [m³/s];

D = Pump's volumetric displacement [m³/rot];

ω^P = Angular pumps speed [rad/s];

ε = Displacement setting [%];

${q_{leak}}^P$ = Pump's leakage flow rate [m³/s].

The pump's internal leakage is computed by Equation 3.25.

$${q_{leak}}^P = ({p_1}^P - {p_2}^P) \cdot {k_{leak}}^P, \quad 3.25$$

where:

${q_{leak}}^P$ = Pump's leakage flow rate [m³/s];

${p_1}^P$ = Pump's input pressure [Pa];

${p_2}^P$ = Pump's output pressure [Pa];

${k_{leak}}^P$ = Leakage coefficient [m³/(s·Pa)].

A laminar flow rate orifice between each side of the pump and the reservoir models the system external leakage. The leakage flow rate is given by Equation 3.26.

$$\begin{cases} {q_2}^{EL} = ({p_1}^{EL} - {p_2}^{EL}) \cdot {k_{leak}}^{EL} \\ {q_2}^P = -{q_1}^P \end{cases}, \quad 3.26$$

where:

${q_2}^{EL}$ = Orifice output leakage [m³/s];

$p_1{}^{EL}$ = Orifice’s input pressure [Pa];

$p_2{}^{EL}$ = Orifice’s output pressure [Pa];

$k_{leak}{}^{EL}$ = Leakage coefficient [m³/(s·Pa)].

The pump’s swash plate dynamics are included with a second order transfer function where the result can be seen in Figure 41, where the zero position means neutral position and one means fully open to one side.

Figure 41 - Pump's swash plate dynamics.

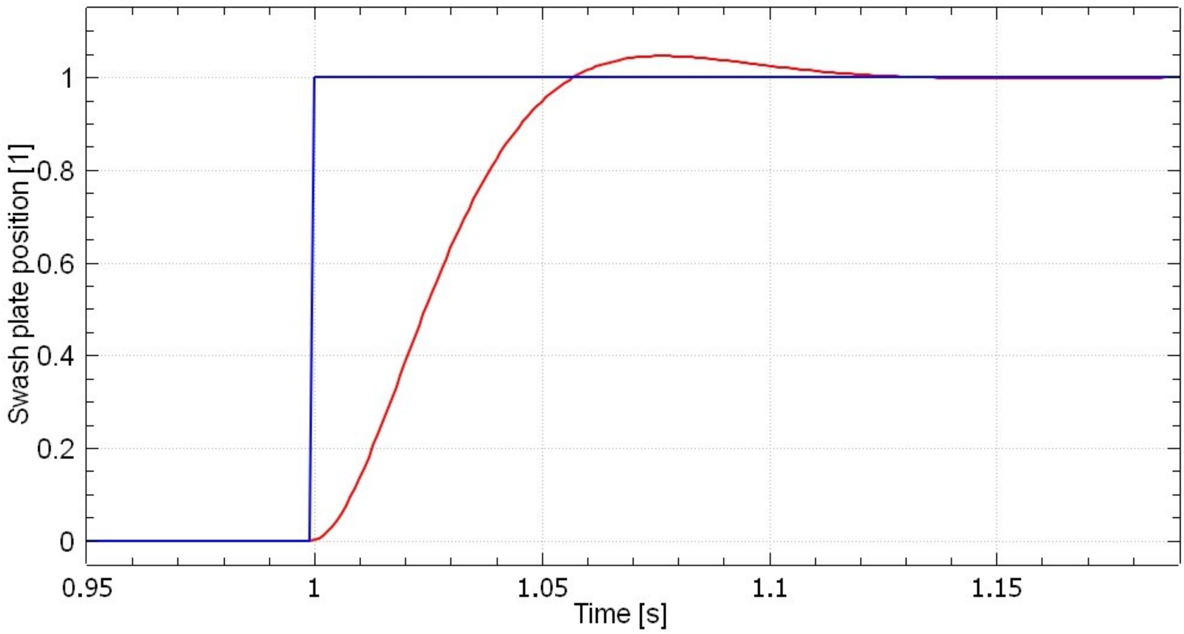

Source: Author (2024).

3.7 PILOT OPERATED CHECK VALVE

On both cylinder chambers there are pilot-operated check valves, 2V3 and 2V4, whose function is to prevent overpressure or residual pressure in the return line (low-pressure hydraulic line). These valves allow flow rate from the inlet port to the outlet port, however block flow rate from the opposite direction unless there is pressure in the pilot port. Equation 3.27 describes their flow rate in Hopsan. In order to avoid singularity and to have a better control of the opening of the piloted check valves a piloted 3/2 directional valve, 2V5 and 2V6, is added to set a pressure interval to the valves. Theses valves are set to open whenever their pilot pressure exceeds a pressure slightly superior to the low pressure. In this case the valves 2V5 and 2V6 are set to open at 15×10^5 Pa (15 bar) while the circuit low pressure is set at 1×10^5 Pa (10 bar).

$$q_2{}^{CV} = \begin{cases} (p_1{}^{CV} - p_2{}^{CV}) \cdot k_S{}^{CV}, & p_1{}^{CV} + p_3{}^{CV} \cdot \varphi - p_2{}^{CV} > p_f{}^{CV} \\ 0, & p_1{}^{CV} + p_3{}^{CV} \cdot \varphi - p_2{}^{CV} \leq p_f{}^{CV} \end{cases}, \quad 3.27$$

where:

$q_2{}^{CV}$ = Valve's output leakage [m³/s];

$p_1{}^{EL}$ = Valve's input pressure [Pa];

$p_2{}^{EL}$ = Valve's output pressure [Pa];

$k_S{}^{CV}$ = Valve's flow rate coefficient [m³/(s·Pa)];

φ = Pilot ratio [1];

$p_f{}^{CV}$ = Valve's cracking pressure [Pa].

3.8 ACCUMULATOR

The Hopsan accumulator model comprises the ideal gas equation and the movement equation. For calculation purposes, the model sets its stroke to 1 and defines the piston area by Equation 3.28. This virtual element is used to simulate the boundary in the accumulator port. A viscous friction (Equation 3.29) on this this element characterizes the inlet/outlet flow rate of the accumulator.

$$A^{ACK} = \frac{V_0{}^{ACK}}{S^{ACK}}, \quad 3.28$$

where:

A^{ACK} = Accumulator's piston area [m²];

$V_0{}^{ACK}$ = Accumulator volume [m³];

S^{ACK} = Accumulator unitary stroke [m].

$$B^{ACK} = \frac{A^{ACK^2}}{K_C{}^{ACK}}, \quad 3.29$$

where:

B^{ACK} = Accumulator friction coefficient [N·s/m];

A^{ACK} = Accumulator's piston area [m²];

${K_C}^{ACK}$ = Accumulator inlet coefficient [m³/(s·Pa)].

The applied force on this virtual piston is computed by Equation 3.30.

$$F^{ACK} = A^{ACK} \cdot {p_1}^{ACK} - A^{ACK} \cdot {p_A}^{ACK} , \quad 3.30$$

where:

F^{ACK} = Force applied on the fake piston [N];

A^{ACK} = Accumulator's piston area [m²];

${p_1}^{ACK}$ = Pressure outside of the accumulator [Pa];

${p_A}^{ACK}$ = Accumulator oil pressure [Pa].

Therefore, the piston speed is obtained by Equation 3.31.

$$F^{ACK} = B^{ACK} \frac{dx^{ACK}}{dt} , \quad 3.31$$

where:

F^{ACK} = Force applied on the fake piston [N];

B^{ACK} = Accumulator friction coefficient [N·s/m];

x^{ACK} = Position of the accumulator's piston [m].

Finally, the accumulator flow rate is calculated through Equation 3.32.

$$ {q_1}^{ACK} = -A^{ACK} \frac{dx^{ACK}}{dt} , \quad 3.32$$

where:

${q_1}^{ACK}$ = Accumulator flow rate [m³/s];

A^{ACK} = Accumulator's piston area [m²];

x^{ACK} = Position of the accumulator's piston [m].

Boyle's law for gas can be used to compute the oil pressure inside the accumulator since the basic pressure volume relationship (Equation 3.33) can be used to define the air/nitrogen gas' pressure and volume.

$$p_1 \cdot {V_1}^n = p_2 \cdot {V_2}^n = cte\ , \qquad 3.33$$

where:

p_1 = Initial pressure [Pa];

p_2 = Final pressure [Pa];

V_1 = Initial volume [m³];

V_2 = Final volume [m³];

n = Ratio of specific heats at constant pressure and constant volume [1].

For isothermal processes, where the volume change occurs slowly, n should be equal to 1 for nitrogen or air. However, for adiabatic processes, where a rapid volume change occurs, n should be equal to 1.4. This thesis uses an intermediate value for n, adopting n equal to 1.2. Adapting it for the accumulator the Equation 3.34 is obtained.

$$p_A{}^{ACK} \cdot V_A{}^{ACK^n} = p_0{}^{ACK} \cdot V_0{}^{ACK^n}, \qquad 3.34$$

where:

$p_A{}^{ACK}$ = Accumulator oil pressure [Pa];

$V_A{}^{ACK}$ = Accumulator oil volume [m³];

$p_0{}^{ACK}$ = Accumulator preload pressure [Pa];

$V_0{}^{ACK}$ = Accumulator volume [m³].

The accumulator oil volume is obtained by Equation 3.35.

$$V_A{}^{ACK} = (S^{ACK} - x^{ACK}) \cdot A^{ACK}, \qquad 3.35$$

where:

$V_A{}^{ACK}$ = Accumulator oil volume [m³];

S^{ACK} = Accumulator unitary stroke [m];

x^{ACK} = Position of the accumulator's piston [m];

A^{ACK} = Accumulator's piston area [m²].

The correct sizing of the accumulator depends on its application. Linsingen (2016) explains and exemplifies its main applications and proposes different methods for its sizing. Its operation involves three distinct phases. First, the accumulator is charged with a gas, usually nitrogen, up to the minimum working pressure of the system.

In a second phase, the accumulator is charged with hydraulic oil, partially replacing the volume occupied by the gas. At this point, the system reaches its maximum pressure, storing the energy for later use. Finally, in the third phase, the system uses the stored energy. During this phase, the pressure of the gas decreases as its volume increases. Equation 3.36 determines the volume of the accumulator to function as an auxiliary power source.

$$V_0{}^{ACK} = \frac{V_A{}^{ACK} \cdot \left(p_3{}^{ACK}/p_0{}^{ACK}\right)^{\frac{1}{n}}}{1-\left(p_3{}^{ACK}/p_0{}^{ACK}\right)^{\frac{1}{n}}}, \quad 3.36$$

where:

$V_0{}^{ACK}$ = Accumulator volume [m³];

$V_A{}^{ACK}$ = Accumulator oil volume [m³];

$p_3{}^{ACK}$ = System minimum pressure [Pa];

$p_0{}^{ACK}$ = Accumulator preload pressure [Pa];

n = Ratio of specific heats at constant pressure and constant volume [1].

The accumulator oil volume is 1.5 times the oil consumed by the actuators, that is 0.087 m³ (87 L). The preload as well as the minimum system pressure are 3×10^7 Pa (300 bar). The maximum system pressure is 3.6×10^7 (360 bar). Therefore, an accumulator of 0.617 m³ (617 L) is set for the circuit.

3.9 DETAILED ARCHITECTURE

In this section, the hydraulic circuit in Figure 27 is further detailed using off-the-shelf components. The result can be seen in Figure 42. The components list of the hydraulic circuit employing off-the-shelf components is available in Table 13.

The motor was sized to match the necessary torque and power for driving the pump. According to Linsingen & De Negri (2012), the minimum torque required in the pump driven shaft is computed by Equation 3.37. The parameters can be observed at Table 11, which results in 773.7 N·m.

$$T_e = \frac{D \cdot \Delta p}{{\eta^P}_m}, \qquad 3.37$$

where:

T_e = Effective torque [N·m];

D = Pump volumetric displacement [m³/rad];

Δp = Pressure difference between the pump's inlet and outlet ports [Pa];

${\eta^P}_m$= Pump mechanical efficiency [1].

Table 11 - Effective torque required in the pump driven shaft.

Parameters		
Effective torque	N·m	773.7
Pump volumetric displacement	m³/rad	125×10^{-6}
Pressure difference between the pump's inlet and outlet ports	Pa	3.5×10^{7}
Mechanical efficiency	1	0.92

Source: Author (2024).

The maximum effective power required to drive the hydraulic pump is given by Equation 3.38, resulting in 143851.9 W (195.6 cv). The remaining parameter adopted are available at Table 12. (LINSINGEN; DE NEGRI, 2012)

$$P_e = \frac{{q_2}^P \cdot \Delta p}{{\eta^P}_m \cdot {\eta^M}_m}, \qquad 3.38$$

where:

P_e = Effective power required at the pump's driven shaft [W];

${q_2}^P$ = Pump's output flow rate [m³/s];

Δp = Pressure difference between the pump's inlet and outlet ports [Pa];

${\eta^P}_m$= Pump mechanical efficiency [1];

$\eta^{M}{}_{m}$ = Electric motor mechanical efficiency [1].

Table 12 - Effective power required at the pump's driven shaft.

Parameters		
Effective power required at the pump's shaft	W	143851.9
Pump's output flow rate	m³/s	3.63×10^{-3}
Pressure difference between the pump's inlet and outlet ports	Pa	3.5×10^{7}
Pump mechanical efficiency	1	0.92
Electric motor mechanical efficiency	1	0.96

Source: Author (2024).

Figure 42 - Hydraulic circuit employing off-the-shelf components.

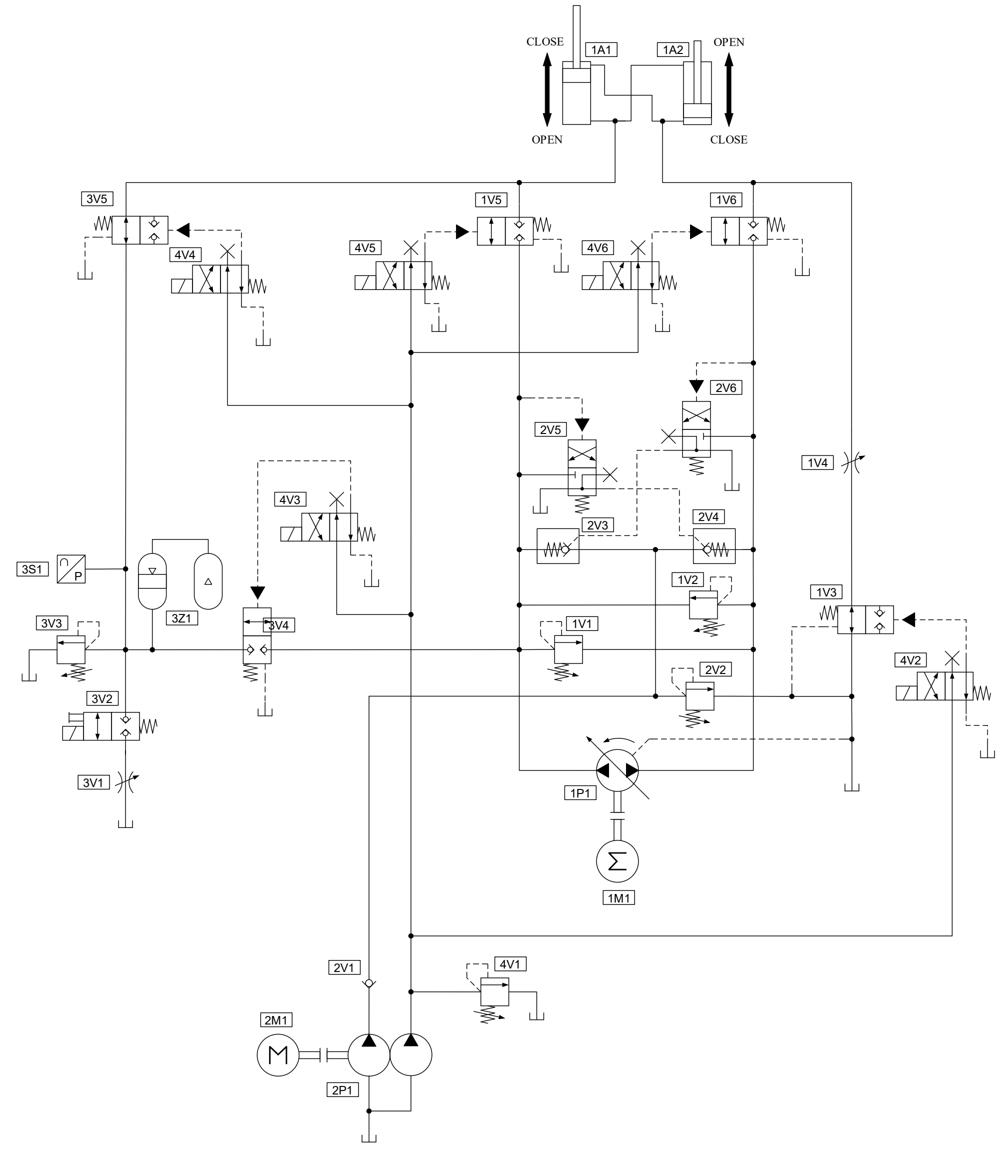

Source: Author (2024).

Table 13 – Components list of the hydraulic circuit employing off-the-shelf components.

ID	MODEL	DESCRIPTION	MANUFACTURER
1M1	W22 IR3 Premium 200 cv 4P 315S/M 3F 220/380 V 60 Hz IC411 - TFVE - B35D	Three Phase Induction Motor - Squirrel Cage	WEG
1P1	A4VSG125EP/30RPPB10K334F	Variable displacement pump	Rexroth
1V1	RPICLAN	Relief valve	Sun Hydraulics
1V2	RPICLAN	Relief valve	Sun Hydraulics
1V3	DOJSXHN	Logic element - NO	Sun Hydraulics
1V4	NFEDLHN	Fully adjustable needle valve	Sun Hydraulics
1V5	DKJSXHN	Logic element - NC	Sun Hydraulics
1V6	DKJSXHN	Logic element - NC	Sun Hydraulics
2M1	W22 IR3 Premium 1 cv 4P 80 3F 220/380 V 60 Hz IC411 - TFVE - B35D	Three Phase Induction Motor - Squirrel Cage	WEG
2P1	AZPFF-12-014/004RAB0101MB-S0052	External gear pump 14/4 cm³/rev	Rexroth
2V1	CXCDXCN	Check valve	Sun Hydraulics
2V2	RDBALAN	Direct-acting relief valve	Sun Hydraulics
2V3	CKIBXCN	Pilot-to-open check valve	Sun Hydraulics
2V4	CKIBXCN	Pilot-to-open check valve	Sun Hydraulics
2V5	DSC3-SA3/12N	Directional valve	Duplomatic
2V6	DSC3-SA3/12N	Directional valve	Duplomatic
3Z1	UAK 90-55-18	Piston accumulator	Roth
3S1	PN-400-SER14-MFRKG/US/ /V	Pressure sensor with display	IFM
3V1	NFCCLCN	Fully adjustable needle valve	Sun Hydraulics
3V2	DTDFMCN	Directional valve	Sun Hydraulics
3V3	RPICLAN	Relief valve	Sun Hydraulics
3V4	DKJSXHN	Logic element - NC	Sun Hydraulics
3V5	DOJSXHN	Logic element - NO	Sun Hydraulics
4V1	RDBALAN	Direct-acting relief valve	Sun Hydraulics
4V2	DS3-TA/11ND24K	Directional valve	Duplomatic
4V3	DS3-TA/11ND24K	Directional valve	Duplomatic
4V4	DS3-TA/11ND24K	Directional valve	Duplomatic
4V5	DS3-TA/11ND24K	Directional valve	Duplomatic
4V6	DS3-TA/11ND24K	Directional valve	Duplomatic

Source: Author (2024).

4 SIMULATION RESULTS

This chapter presents the simulation results for the model discussed in Chapter 3. The results include the assessment of opening time, the system response to oscillations in electrical power consumption, and the closing time in emergency mode. The findings are compared with experimental data from an operating power plant provided by a partner company. Additionally, the pressure within the accumulator is examined during both its charging phase and in emergency situations.

4.1 PERFORMANCE ANALYSIS OF THE CIRCUIT IN CONTROLLING MODE WITH EXTERNAL LOAD

In this section, the system behavior is evaluated considering the external load, whose implementation follows the model described in Section 3.5, whose hydraulic circuit is shown in Figure 29. The typical procedure for evaluating the online response of the servomotor is performed. First of all, the piston is positioned at mid-stroke by an input signal and, subsequently, an input of 5% of the hydraulic cylinder stroke is added, see Figure 43. The complete Hopsan model for the servomotor's position control can be found in APPENDIX E. Similarly, the complete Simulink model for control tests is available at APPENDIX F.

Figure 43 - System position response to a step input of 5% of the cylinder stroke after positioning it at its mid-stroke.

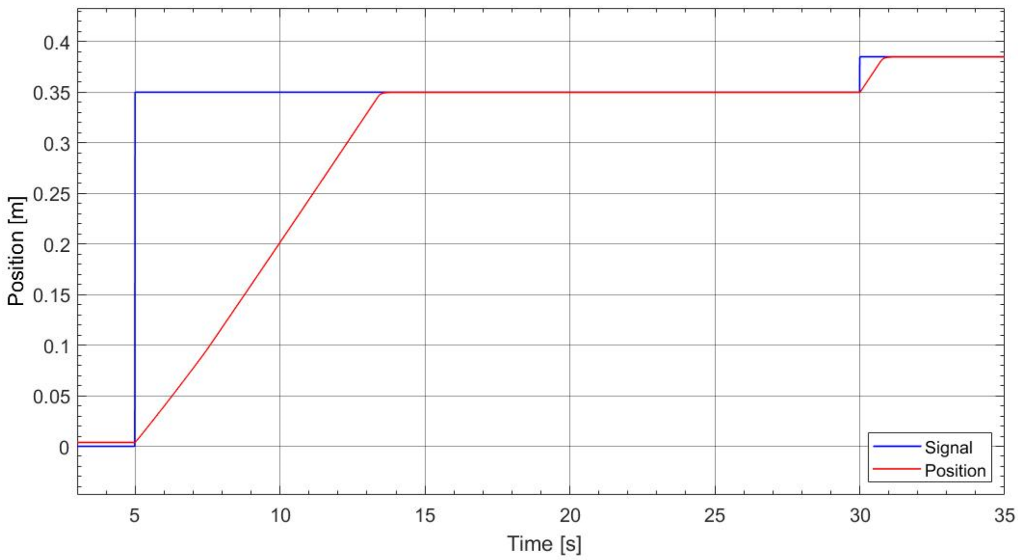

Source: Author (2024).

For clarity, the Figure 44 highlights the position step input of 5% of the cylinder's stroke.

Figure 44 - Highlighted system position response to a step input of 5% of the cylinder stroke after positioning it at its mid-stroke.

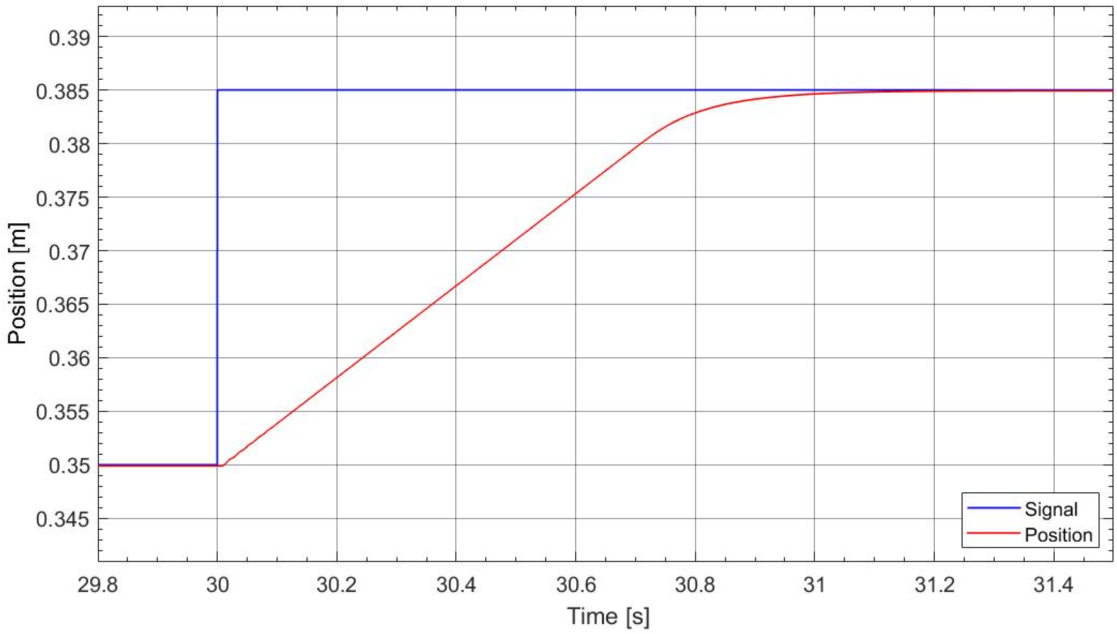

Source: Author (2024).

The system rise time, which is the time for the piston to travel from 10% of the input signal to 90% of the input signal, is 0.66 s. The settling time is 0.92 s within a 2% margin of the input signal considering the position step of 5% of the total stroke. The steady-state error is 6.3×10^{-5} m (6.3×10^{-2} mm), which corresponds to 0.18% of the step input. The position error for the simulation above (system position response to a step input of 5% of the cylinder stroke at the its mid-stroke) is show in Figure 45.

The pump flow rate is presented in Figure 46. It is possible to observe that the pump provides its maximum flow rate for some periods of time in order to attend the system required settling time. After the actuator reaches the desired position the flow rate reduces to a minimum required to maintain the position. This can be observed in the swash plate position (Figure 47). As shown in Figure 47, after the cylinder stops at the desired position it is still necessary to supply enough fluid to compensate for the system leakage. Up to 5 s of the simulation the swash plate position is negative since the higher pressure is at cylinder chamber B due to the external force that tries to pull the piston to the position where the external force generated by the water load is neutral. After approximately 14 s the swash plate remains at a steady small position in order to supply for the leakage in the components connected to the hydraulic line linked to cylinder Chamber A. The reason for that it that around 7.5 s the piston crosses the load neutral force changing its direction (Figure 48).

Figure 45 - Position error for the system position response to a step input of 5% of the cylinder stroke after positioning it at its mid-stroke.

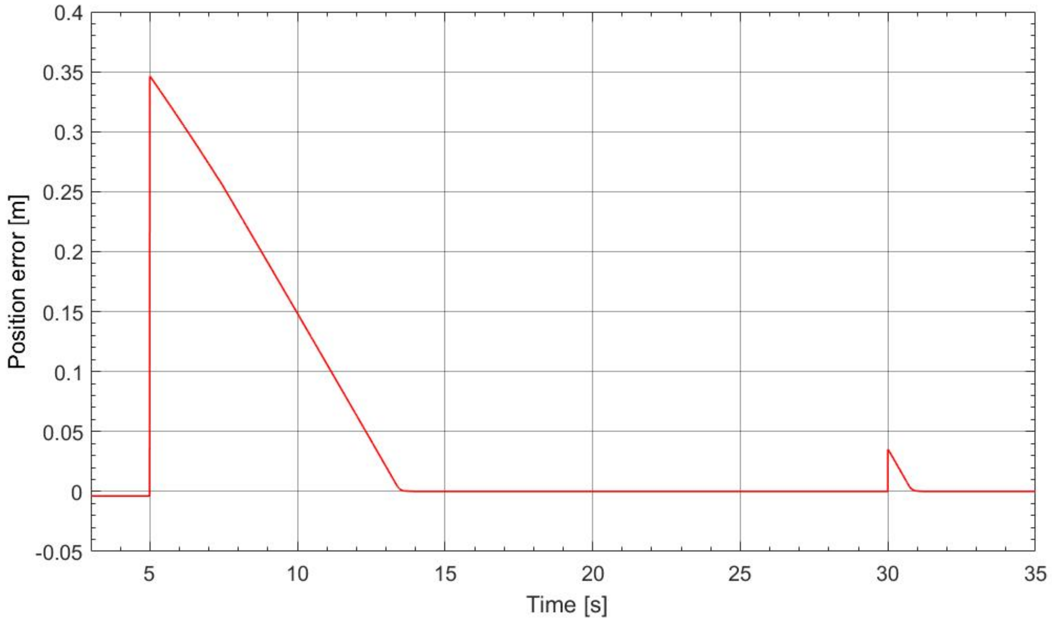

Source: Author (2024).

Figure 46 - Pump flow rate for the system position response to a step input of 5% of the cylinder stroke after positioning it at its mid-stroke.

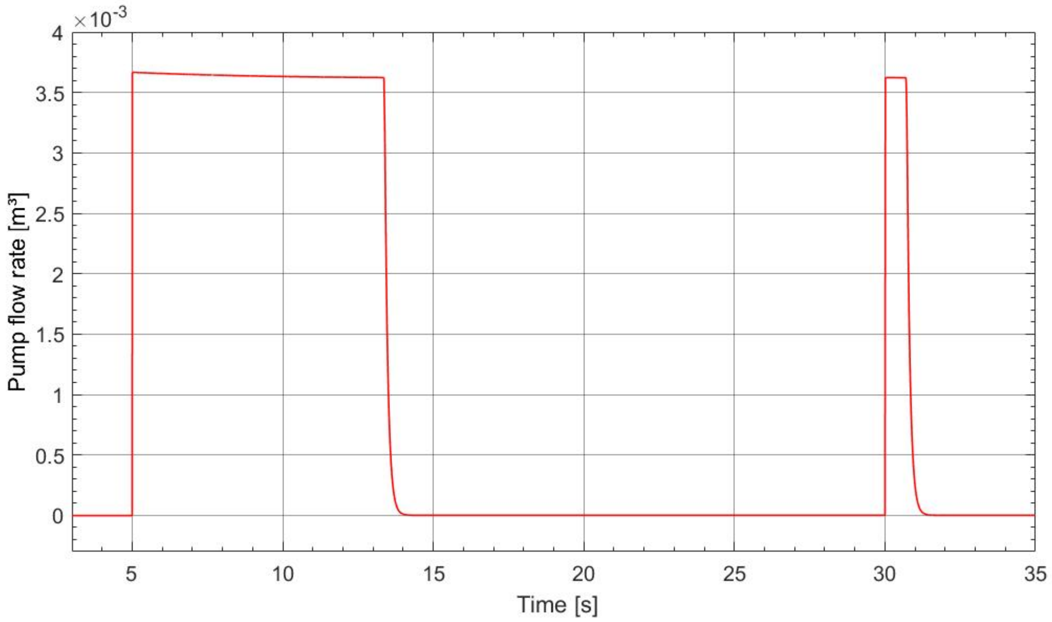

Source: Author (2024).

Figure 47 - Swash plate position for the system position response to a step input of 5% of the cylinder stroke after positioning it at its mid-stroke.

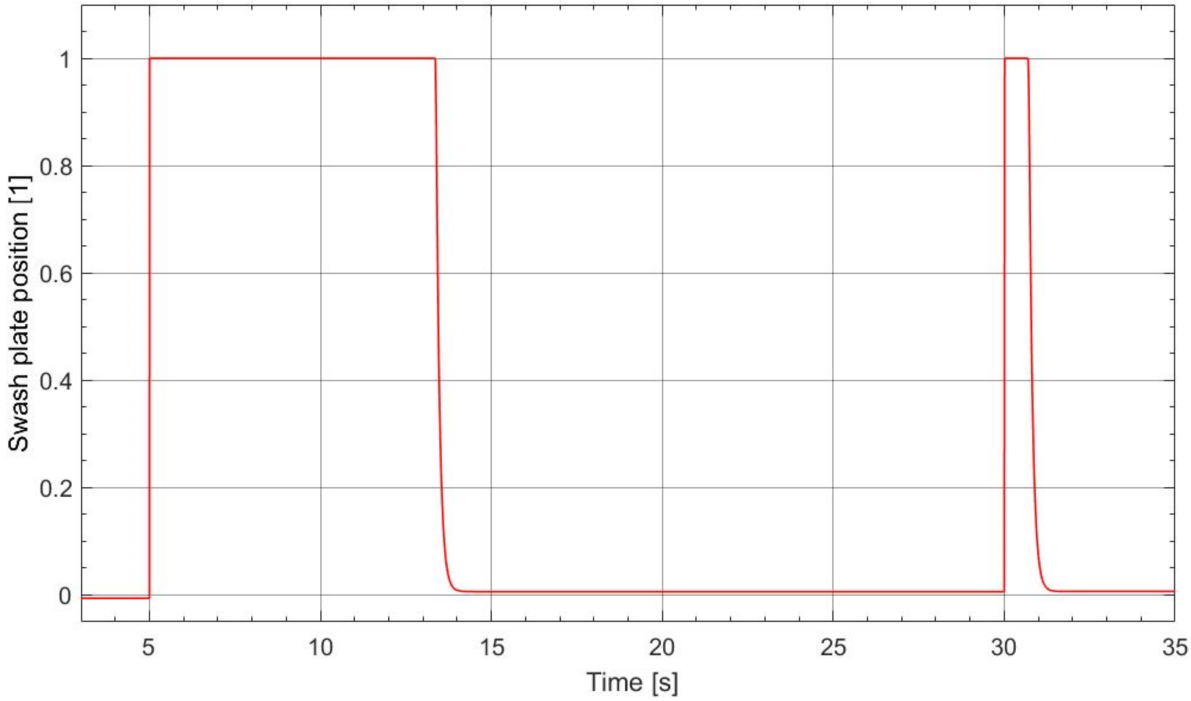

Source: Author (2024).

Figure 48 - External load profile during the simulation of the system position response to a step input of 5% of the cylinder stroke after positioning it at its mid-stroke.

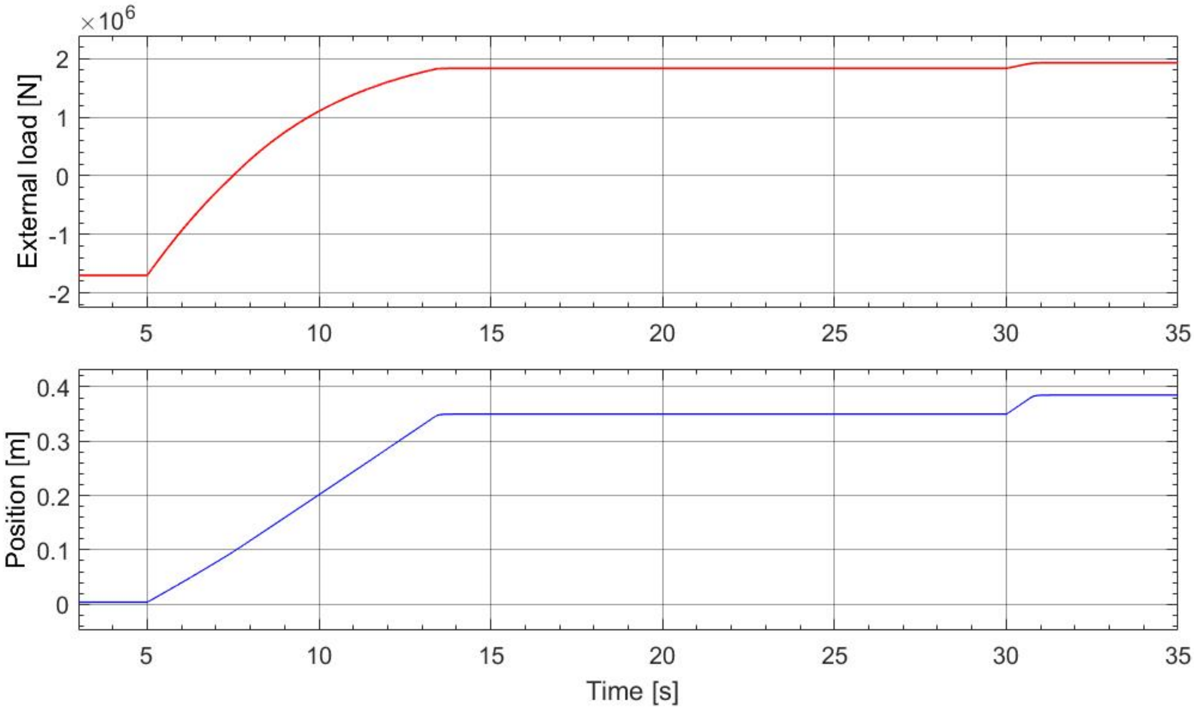

Source: Author (2024).

In a hydraulic system, it is important to verify whether the conditions for cavitation are present in the pump suction port. Cavitation is the formation and collapse of voids in the fluid caused by the liquid/vapor/liquid phase change. Considering this phenomenon for a pump, when the pressure momentarily drops below the vapor pressure at the pump inlet (vapor pressure of mineral oil at 40°C is approximately 6×10^{-7} Pa), small bubbles form in the fluid, which subsequently condense rapidly, accelerating the particles against the system walls. As a consequence, corrosion of the pump walls and rotors occurs, besides the presence of high levels of noise and pressure pulses. In addition, since it consists of an adiabatic compression process, it causes an excessive increase in the temperature of the fluid, leading to its oxidation and deterioration. (LINSINGEN, 2016)

Since the pump model used lacks a cavitation module, the occurrence of cavitation can be identified by examining whether the pressures at the pump ports fall below the mineral oil vapor pressure.

It can be concluded from Figure 49 that cavitation does not occur in the pump as the pressure does not drop below 6×10^{-7} Pa at any point. The pressure is higher in chamber B up to approximately 0.1 m (100 mm) due to the load profile that tries to pull the cylinder to this position. After this position, the pressure inside chamber A begins to rise, and the pressure in chamber B is maintained at 1 MPa (10 bar) by the supercharging circuit (Figure 49).

Figure 49 - System pressures during the simulation of a step input of 5% of the cylinder stroke after positioning it at the its mid-stroke.

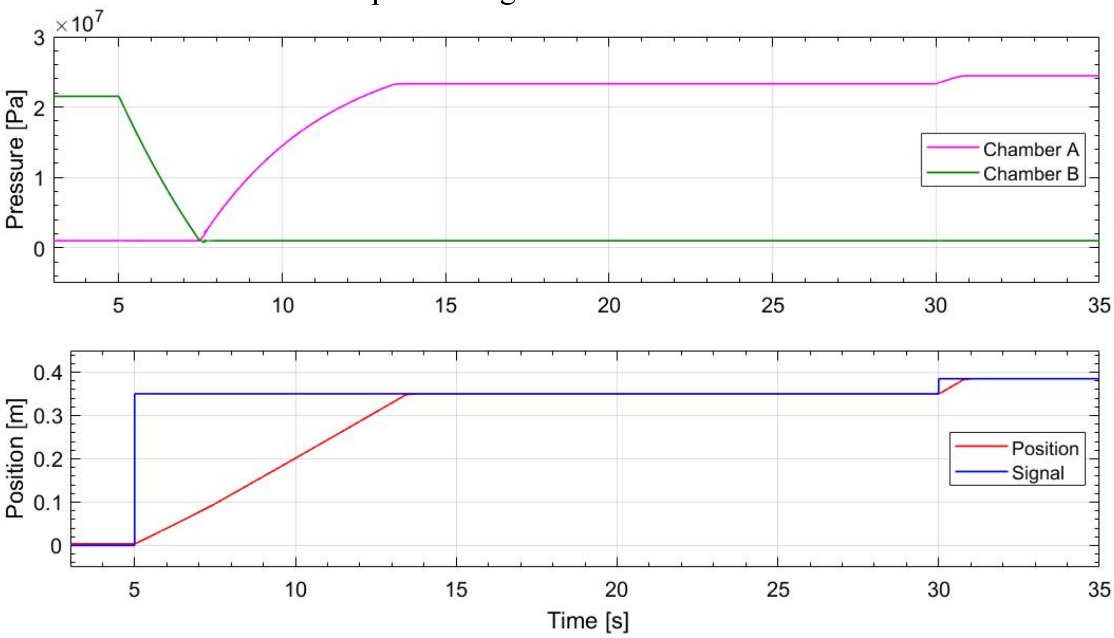

Source: Author (2024).

4.2 WICKET GATE OPENING ANALYSIS

Regarding the opening time, the servomotor reached 80% of its stroke in 13.3 seconds, as shown in Figure 50. In the analysis, a position step input signal corresponding to 80% of the actuator stroke, or 0.56 m (560 mm), was applied at 355 s, and the piston was capable of reaching it at 368.3 s. Comparing this to the experimental data of the existing system, which has an opening time of 13.7 s, it can be concluded that the proposed design meets this requirement.

Figure 50 - Servomotor opening time.

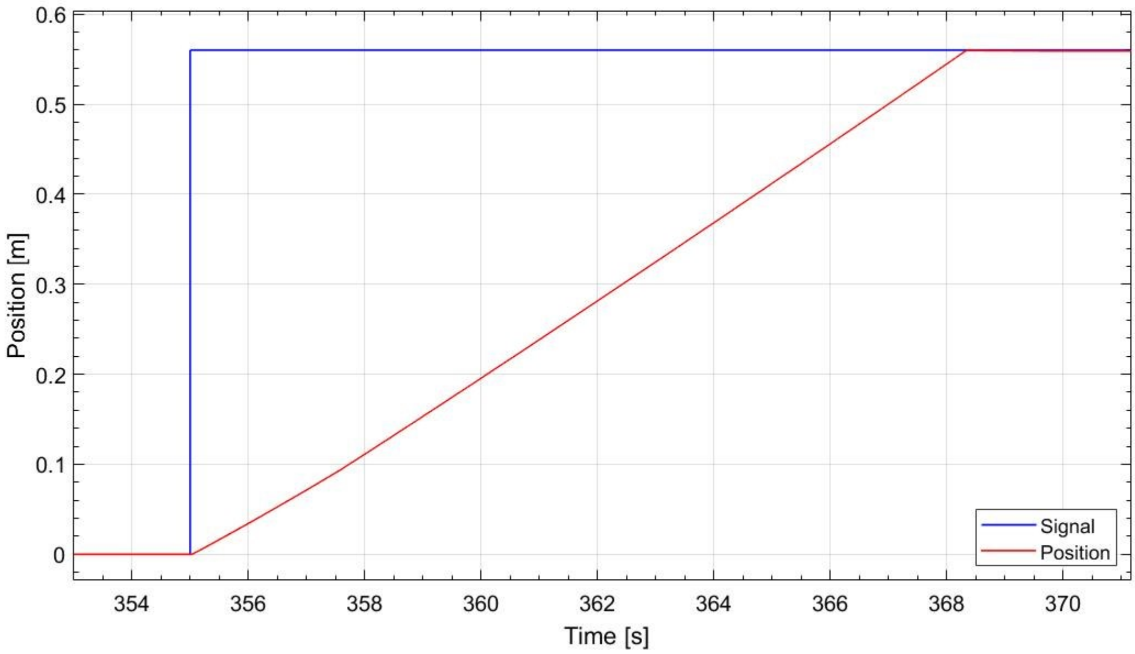

Source: Author (2024).

4.3 PERFORMANCE ANALYSIS OF THE CIRCUIT IN EMERGENCY MODE

The machine is now evaluated during emergency mode. The Hopsan model is available in APPENDIX G and the Simulink model in APPENDIX H. For that, a sequency of events from startup to emergency is simulated. Initially, the hydraulic circuit is configured as shown in Figure 28 during initialization to fill up the accumulator. Shortly after that, the system enters the control mode described in Figure 29, and a slight variation in the speed governor input signal is added. While in normal conditions, a power failure is simulated, consequently triggering the system to switch to the emergency mode (Figure 30) described in Section 3.2.

The simulation results concerning the servomotor position are presented in Figure 51. The pressure inside the accumulator was monitored during the simulation and is available in Figure 52. At the beginning the pressure is the accumulator pre-charge set, and the final pressure is higher than the pre-charge pressure due to the exceeding accumulator's oil volume as it is sized for supplying one and a half the hydraulic cylinders' volume.

Figure 51 - Servomotor position during start-up and emergency mode.

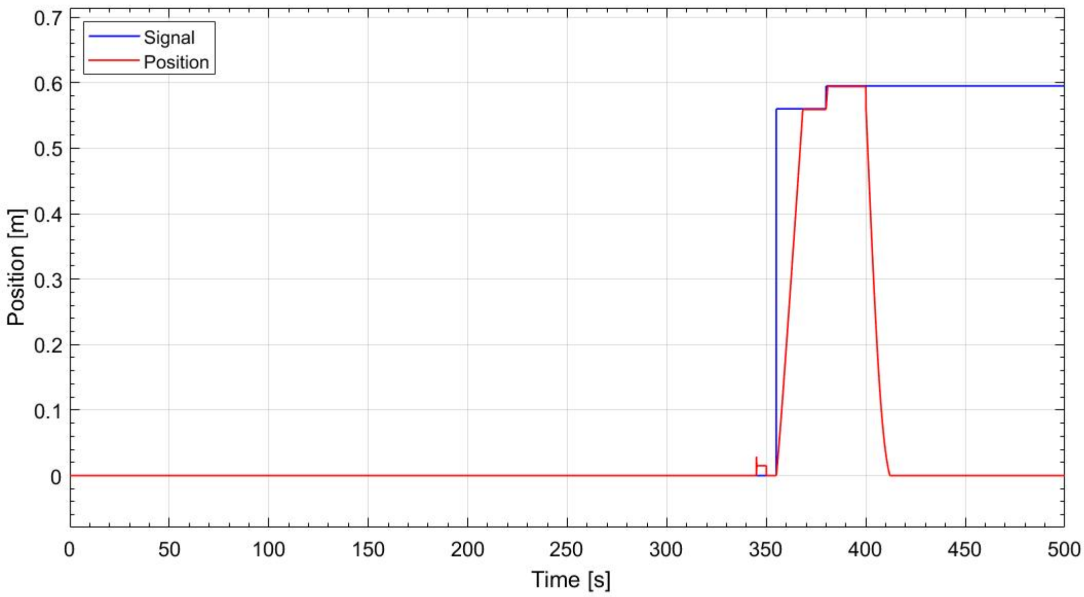

Source: Author (2024).

Figure 52 - Accumulator pressure during start-up and emergency mode.

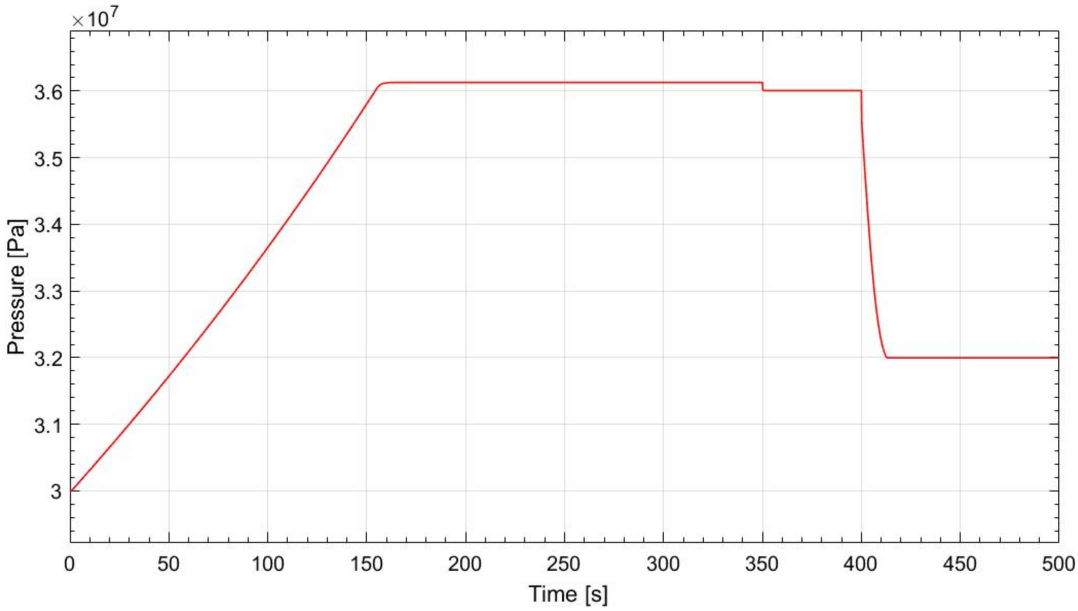

Source: Author (2024).

4.4 PERFORMANCE ANALYSIS IN STILL WATER

Generally, a set of tests is conducted in still water, or standing water, to evaluate a hydraulic power plant. The procedure consists of positioning the actuator at its half stroke and applying a step input to assess its response. Three step amplitudes are adopted for the still water tests: ten percent, five percent, and three percent of the actuator's stroke. In this Section, the simulation results of the system in still water are presented and, compared with data provides from a partner company in order to evaluate the applicability of the proposed system.

Assuming the accumulator is already charged at its working pressure, the directional valves 3V4 and 3V5 are set to their closed positions, according to Figure 29. Additionally, circuit 2 (pump 2P1 and additional components), which handles the supercharging of the main circuit and maintains a low pressure at approximately 1 MPa (10 bar), is treated as a pressure source in the model. The complete Hopsan model for the servomotor's position control can be found in APPENDIX E. Similarly, the complete Simulink model for control tests in still water is available at APPENDIX I.

4.4.1 System response analysis to a step of 10% of the actuator stroke

The first analysis comprises the system response to a step of 10% of the actuator stroke. Figure 53 presents the piston's response to an input signal regarding its position with no external load, e.g., in still water, also called dead water. After setting an input signal to position the piston at mid-stroke, a step of 10% of the total stroke is added to the input signal. For clarity, Figure 54 focuses on this 10% step input. The rise time is 1.27 s. The settling time, or the time for the piston to reach a position error within 0.5% of the total stroke, is 1.53 s.

As expected, the pump remains most of the time at its maximum displacement (Figure 55) since in the pump sizing the smallest pump capable of attending the settling time was chosen. As a consequence, the pump provides its maximum flow rate during most of the time it is performing the controlling of the actuator (Figure 56).

The simulation rendered a steady-state error of 4.11×10^{-4} m (0.411 mm), which is equivalent to 0.59% of the 10% step input. The position error for the simulation is shown in Figure 57. At 5 s the position error is at its maximum and is equivalent to the actuator 50% stroke. Further in 30 s, the position error rises again indicating the addition of the step input of 10% of the cylinder stroke.

Figure 53 - System position response to a step input of 10% of the cylinder stroke after positioning it at the its mid-stroke in dead water.

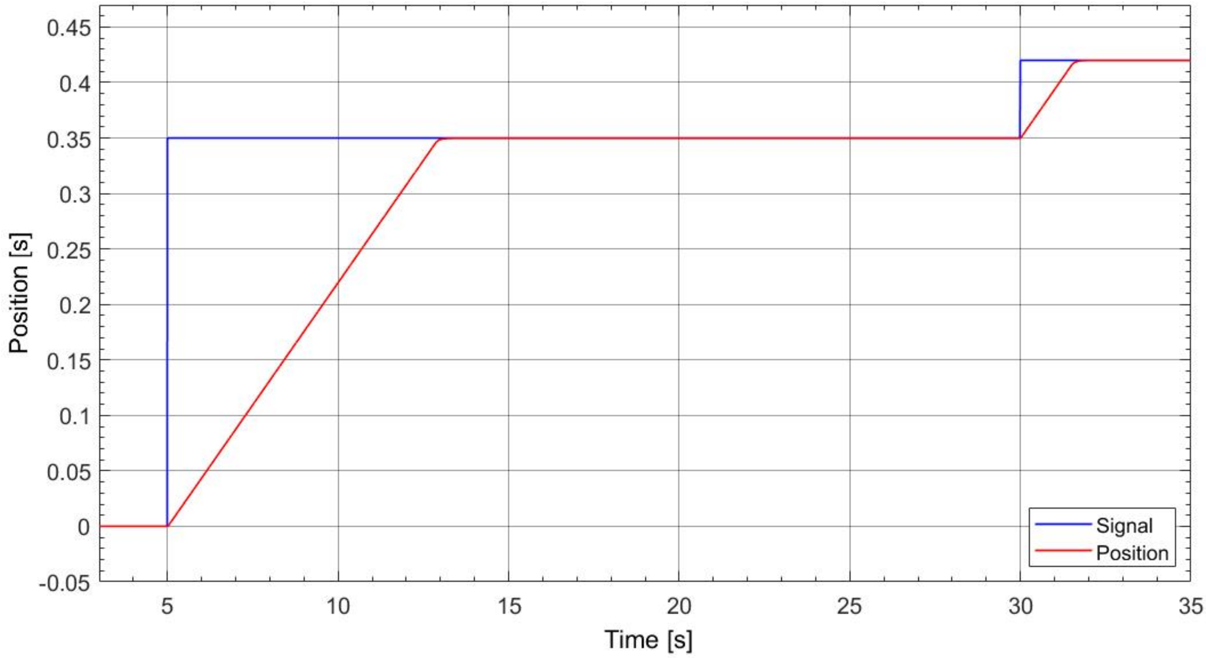

Source: Author (2024).

Figure 54 - Highlighted system position response to a step input of 10% of the cylinder stroke after positioning it at the its mid-stroke in dead water.

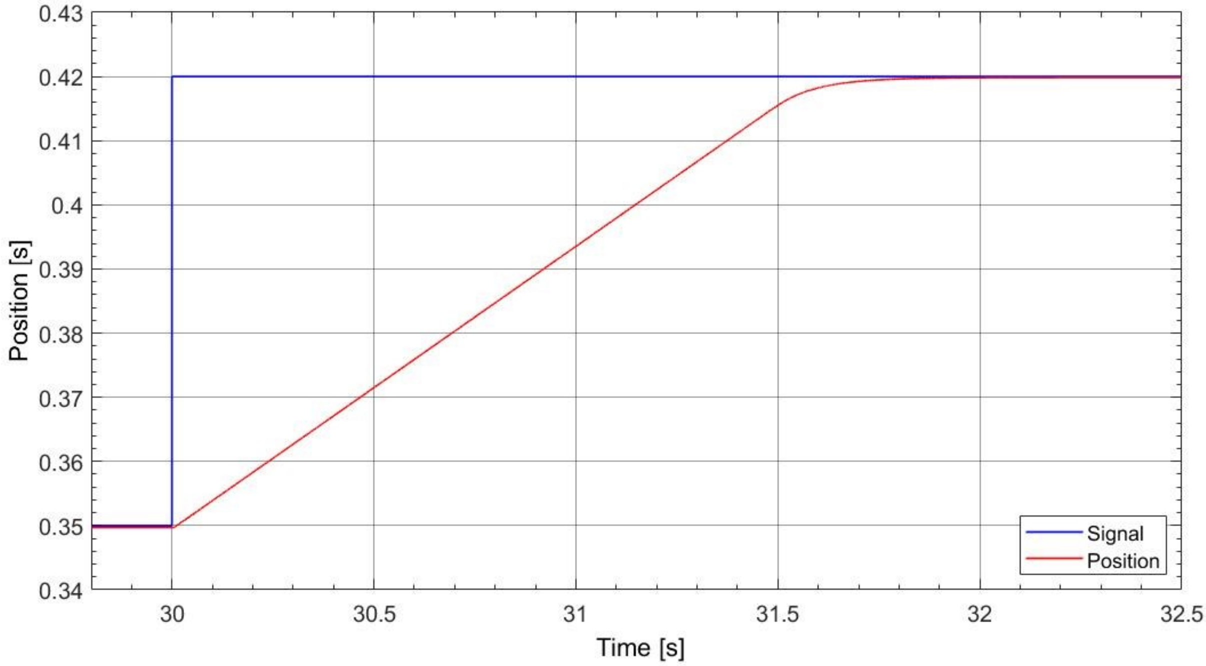

Source: Author (2024).

Figure 55 - Swash plate position for the analysis using a step input of 10% of the actuator stroke after positioning it at the its mid-stroke in dead water.

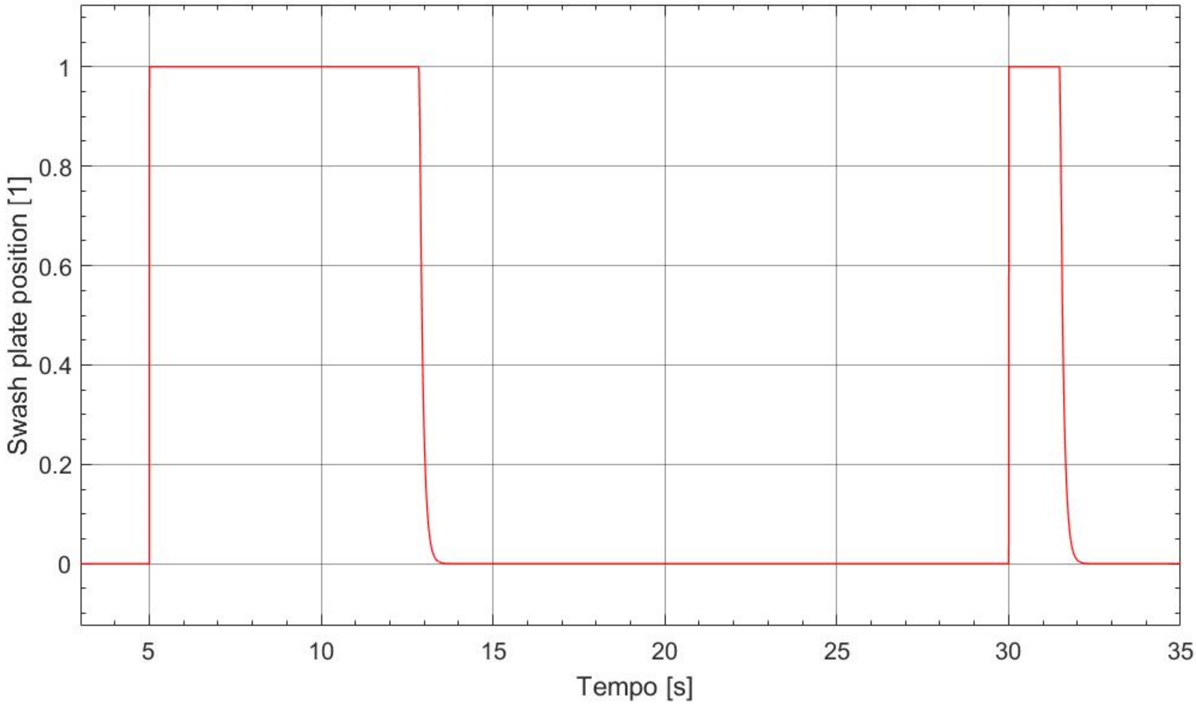

Source: Author (2024).

Figure 56 - Pump flow rate for the analysis using a step input of 10% of the actuator stroke after positioning it at the its mid-stroke in dead water.

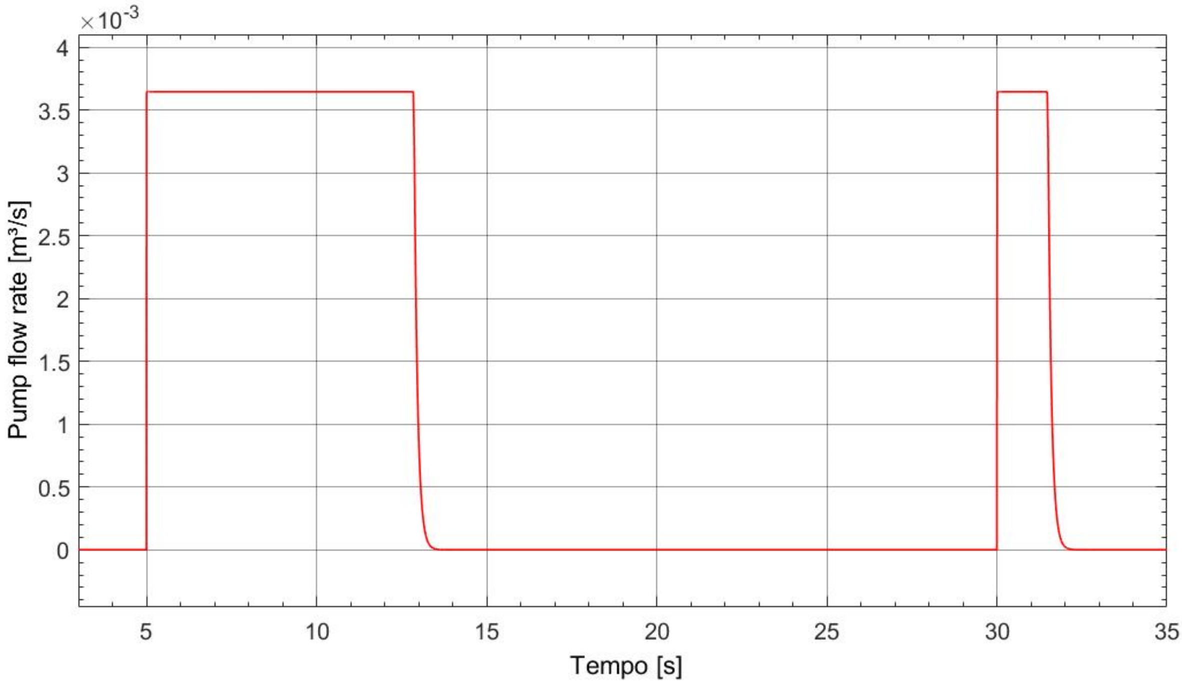

Source: Author (2024).

Figure 57 - Position error for the analysis using a step input of 10% of the actuator stroke after positioning it at the its mid-stroke in dead water.

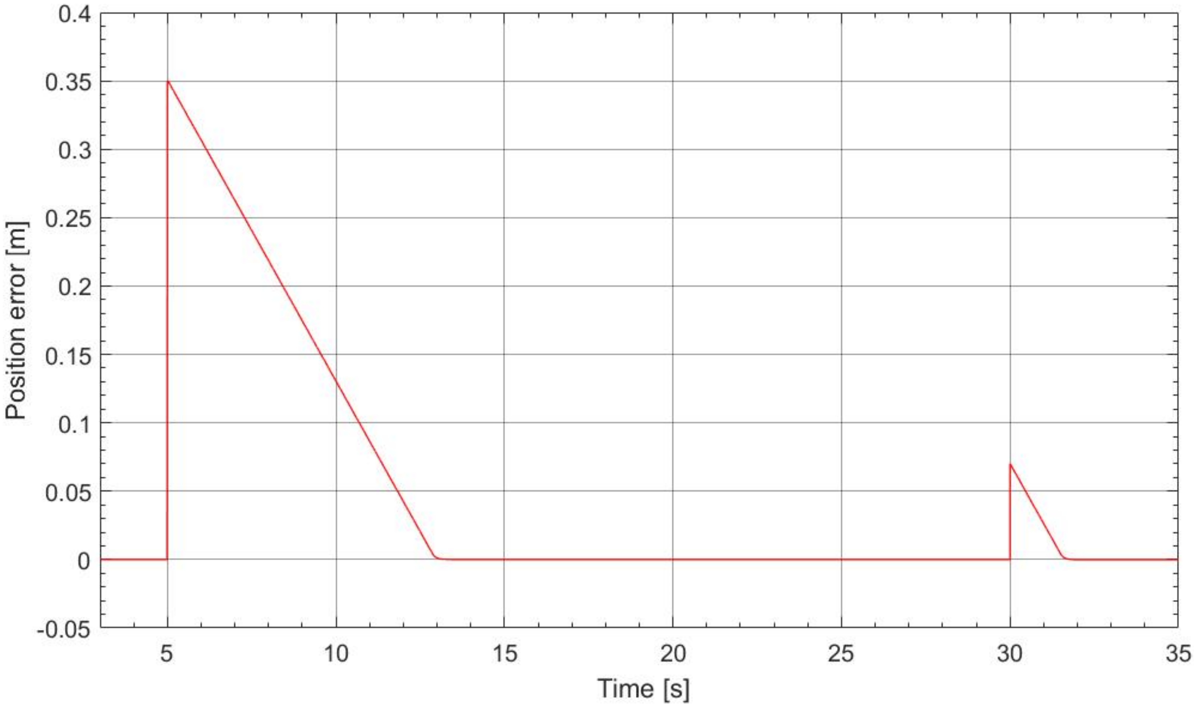

Source: Author (2024).

Table 14 presents both the experimental data from the original power plant and the proposed system simulation data for a position step input of 10% of the cylinder's stroke. As can be seen, although the proposed system has a longer rise time, its shorter settling time makes it appropriate for the intended application.

The pressures during the simulation at both sides of the pump/hydraulic cylinder are available in Figure 58. As Figure 58 demonstrates, the pressures never fall below 6×10^{-7} Pa, indicating that cavitation does not occur in the pump.

Table 14 - Performance parameters of the original power plant speed governor and the proposed system speed governor during the second input signal of 10% of the stroke.

Parameter		Original system	Proposed system
Position step input	%	10	10
Rise time	s	1.06	1.27
Settling time	s	1.65	1.53
Steady-state error	m	N.A.	4.11×10^{-4}

Source: Author (2024).

Figure 58 - System pressures during the simulation of a step input of 10% of the cylinder stroke after positioning it at its mid-stroke in dead water.

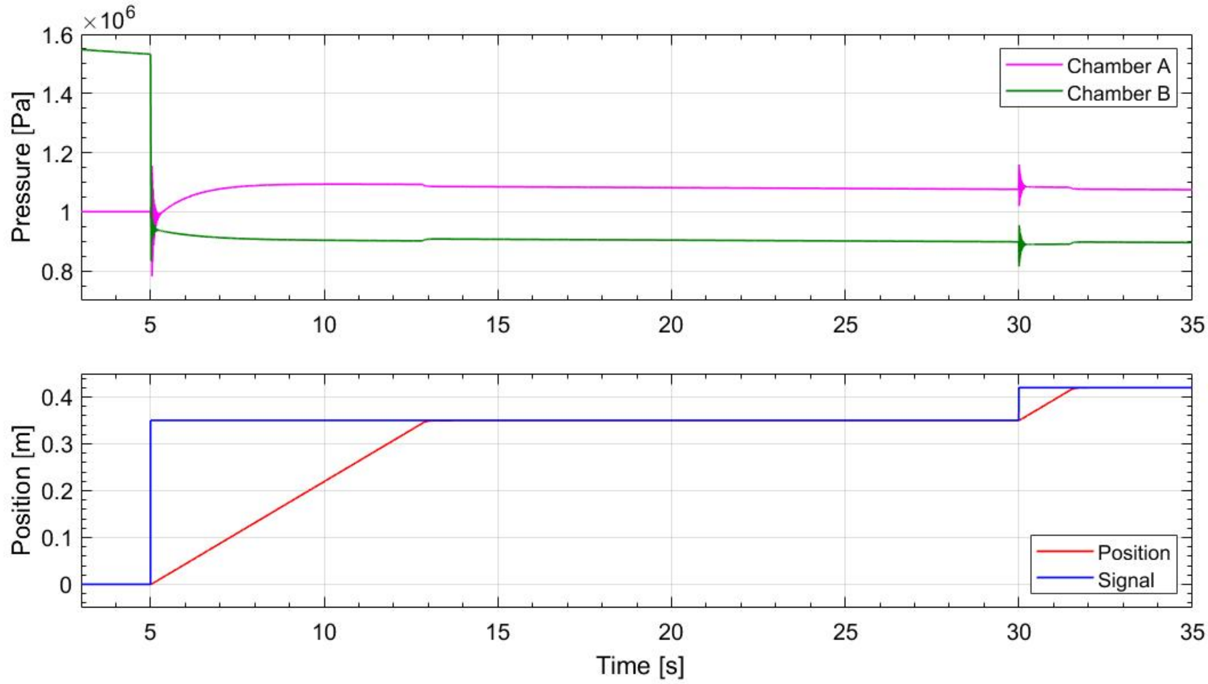

Source: Author (2024).

4.4.2 System response analysis to a step of 5% of the actuator stroke

Just as for the analysis of the step input of 10% of the actuator stroke step input was followed, nonetheless, a 5% position step was added to the simulation instead of 10% of the hydraulic cylinder stroke. The complete position response is shown in Figure 59, and Figure 60 focuses on the 5% position input signal. The rise time is 0.64 s and the settling time, or the time for the piston to reach a position error within 0.3% of the total stroke, is 0.79 s. Due to the smaller input signal the pump remained less time in its maximum volumetric displacement when compared to the previous simulation in Section 4.4.1 (Figure 61). The flow rate is shown in Figure 62.

The simulation rendered a steady-state error of 2.5×10^{-4} m, which is equivalent to 0.71% of the 5% step input. The position error for the simulation in this section is presented in Figure 63. At 5 s and at 30 s it is possible to observe the position error resulting from the step inputs that decreases until the piston reach the desired position.

Table 15 summarizes the performance parameters of the experimental tests from the original system and the new speed governor simulation for the input signal of 5% of the hydraulic cylinder stroke. In the same way as the simulation of a position step input of 10% of the total stroke, the simulation of the 5% stroke rendered a longer rise time, however, with a smaller settling time. Therefore, the system is capable of handling position changes of 5% of the total cylinder's stroke even faster than the original system.

Figure 59 - System position response to a step input of 5% of the cylinder stroke after positioning it at its mid-stroke in dead water.

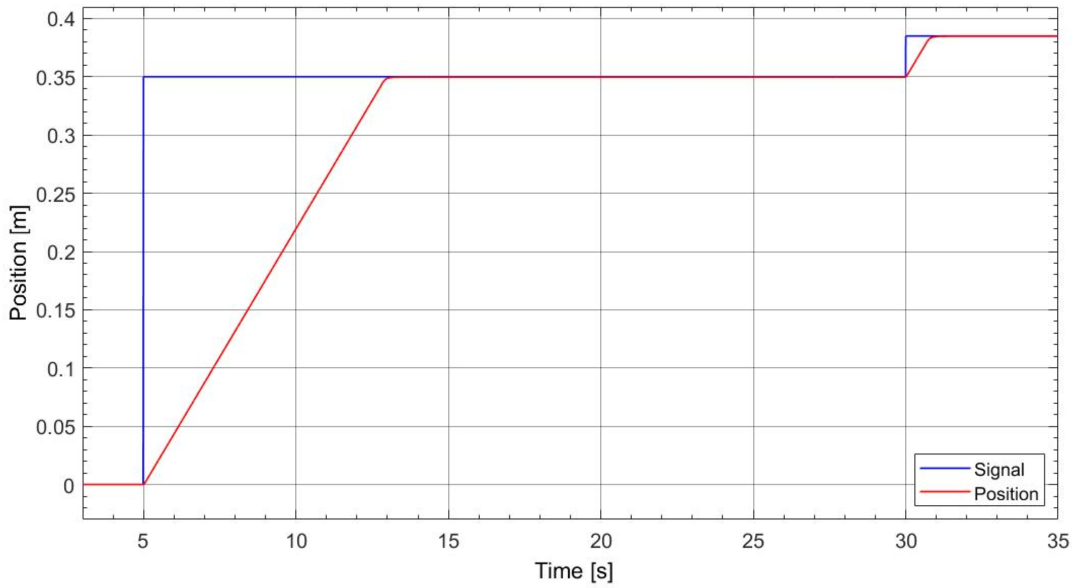

Source: Author (2024).

Figure 60 - Highlighted system position response to a step input of 5% of the cylinder stroke after positioning it at the its mid-stroke in dead water.

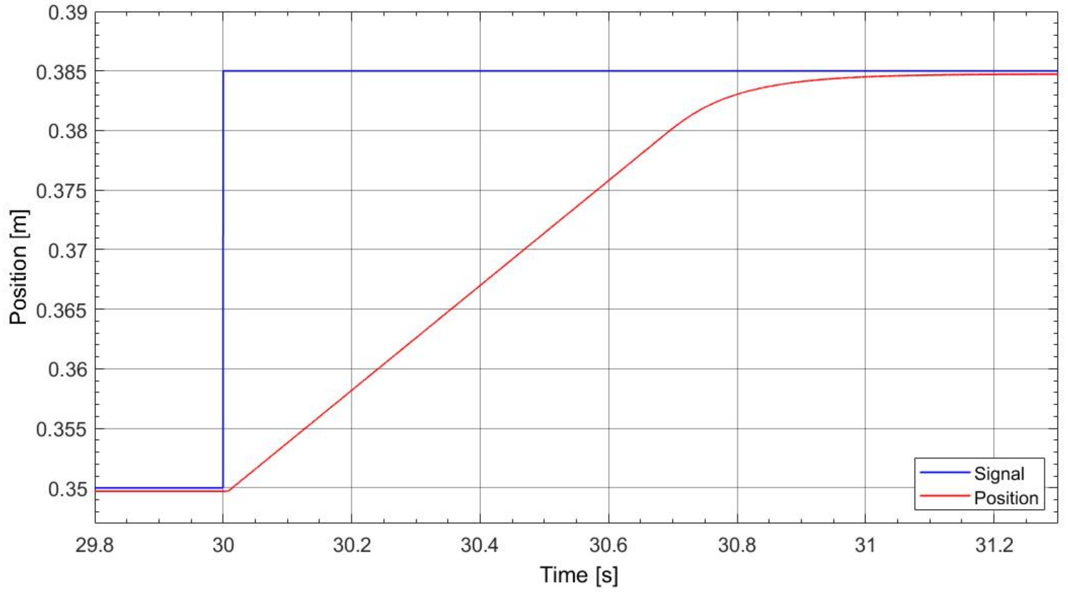

Source: Author (2024).

Figure 61 - Swash plate position for the analysis using a step input of 5% of the actuator stroke after positioning it at mid-stroke in dead water.

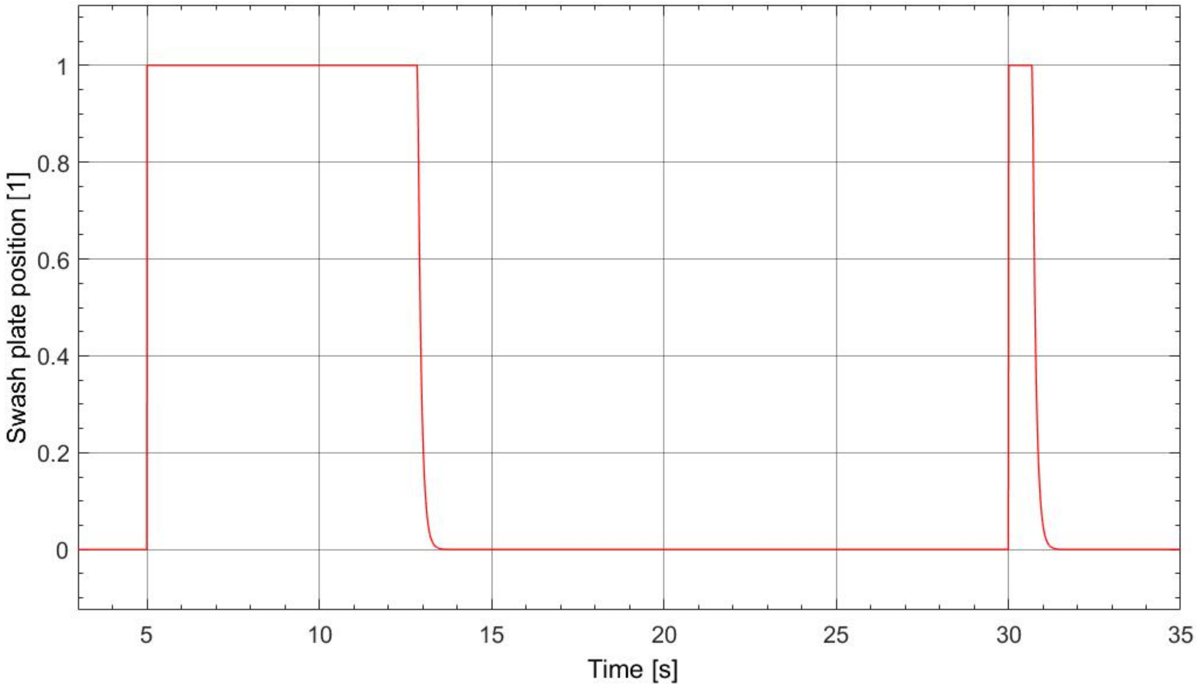

Source: Author (2024).

Figure 62 – Pump flow rate for the analysis using a step input of 5% of the actuator stroke after positioning it at mid-stroke in dead water.

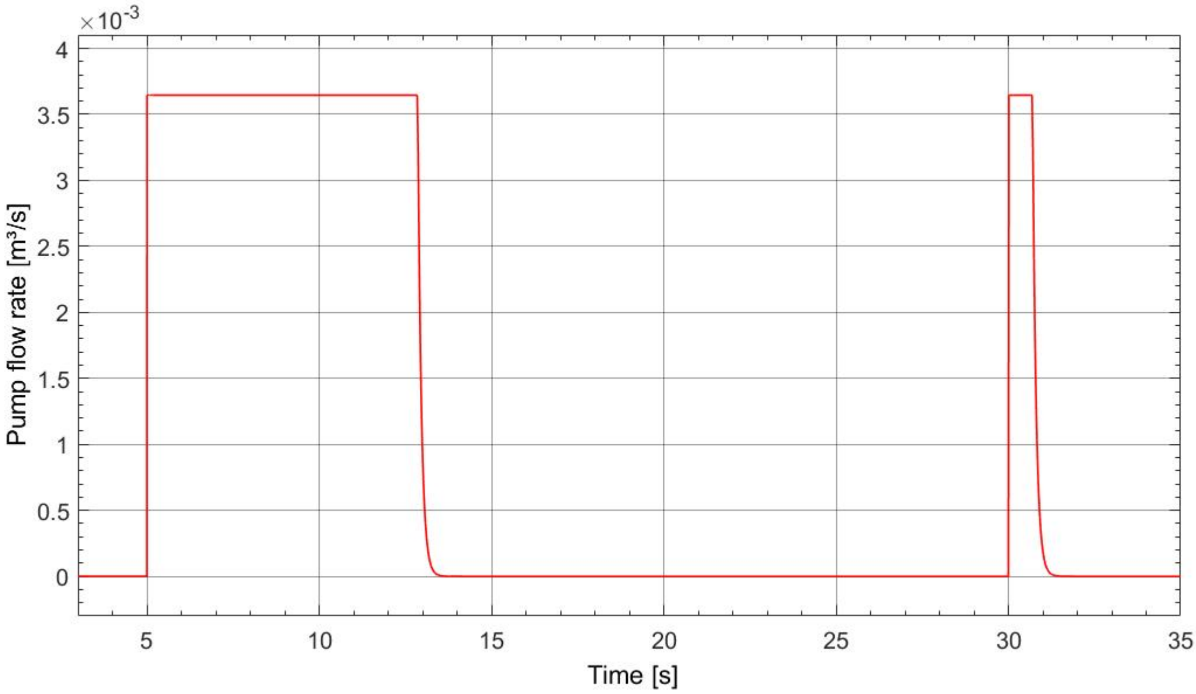

Source: Author (2024).

Figure 63 - Position error for the analysis using a step input of 5% of the actuator stroke after positioning it at mid-stroke in dead water.

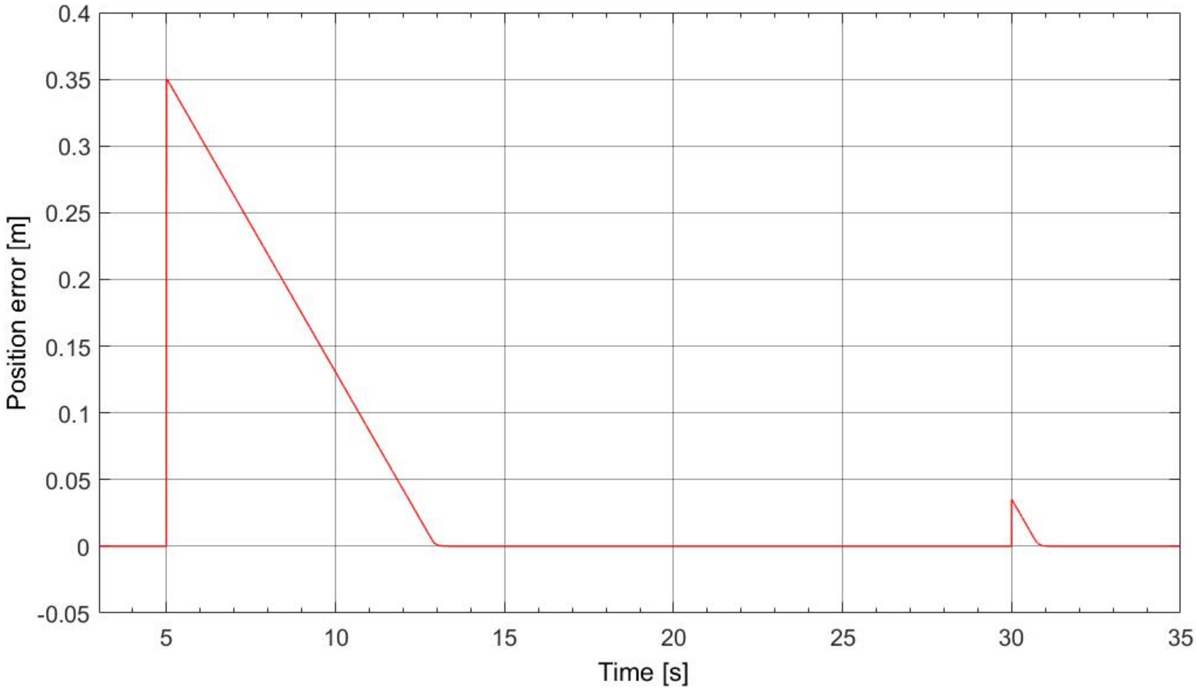

Source: Author (2024).

Table 15 - Performance parameters of the original power plant speed governor and the proposed system speed governor during the second input signal of 5% of the stroke after positioning it at mid-stroke in dead water.

Parameter		Original system	Proposed system
Position step input	%	5	5
Rise time	s	0.63	0.64
Settling time	s	1.08	0.79
Steady-state error	m	N.A.	2.5×10^{-4}

Source: Author (2024).

Figure 64 shows that the pressure in any of the cylinder chambers never falls below 6×10^{-7} Pa so that cavitation is not present in the system for position step inputs of 5% of the total stroke.

Figure 64 - System pressures during the simulation of a step input of 5% of the cylinder stroke after positioning it at its mid-stroke in dead water.

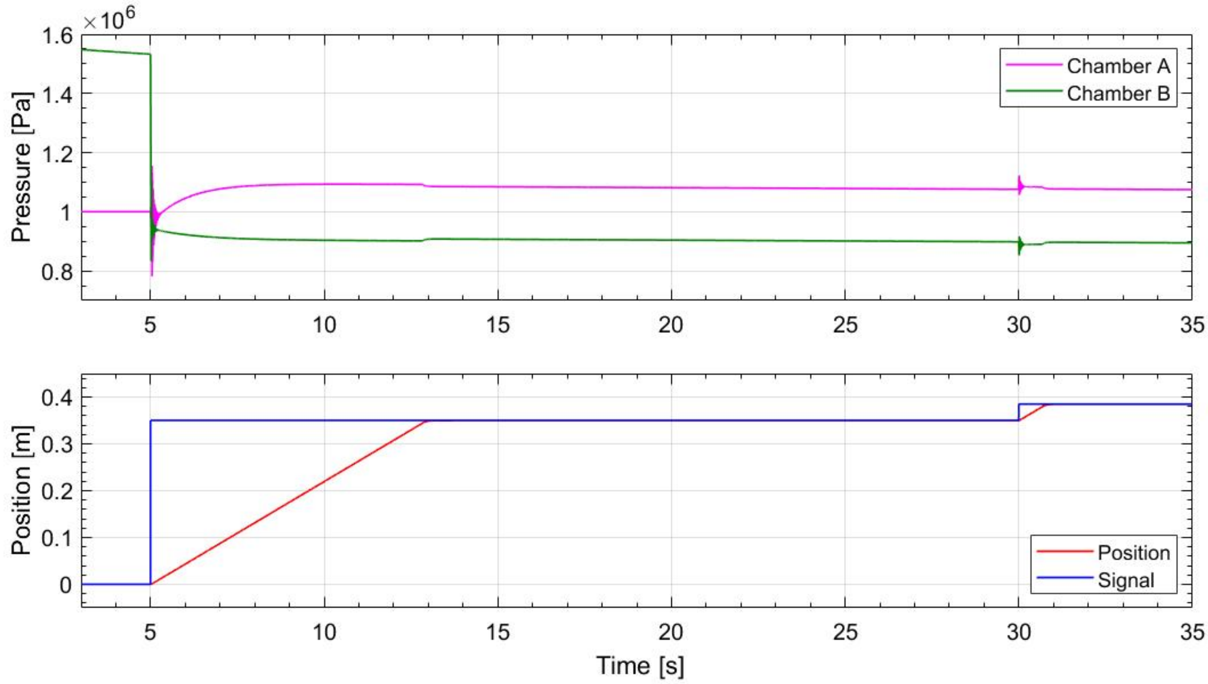

Source: Author (2024).

4.4.3 System response analysis to a step of 3% of the actuator stroke

Now, the system response to a position step of 3% of the total stroke in dead water is evaluated. In the same way as in the previous simulations (Sections 4.4.1 and 4.4.2), the piston travels to mid-stroke through an input signal, then a step of 3% of the total stroke is added. The overall behavior is shown in Figure 65 and the 3% position response step is highlighted in Figure 66. At 30 s the pump goes from approximately zero volumetric displacement to its maximum displacement, then remains at its maximum displacement up to 30.4 s when the swash plate begins to return to the neutral position (zero volumetric displacement), although it keeps a minimum volumetric displacement to compensate for the leakage in the system (Figure 67). The flow rate for this simulation is shown in Figure 68.

The performance parameters from the experimental tests of the original system and the new speed governor simulation for the input signal of 3% of the hydraulic cylinder stroke are available in Table 16. The proposed system has shown a shorter rise time and settling time than the original servomotor, of 0.42 s and 0.52 s, respectively. Meanwhile, the original system has a rise time of 0.52 s and a settling time of 0.9 s. Therefore, the system is capable of handling position changes of 3% of the total cylinder stroke even faster than the original system. The settling time was measured for a position range of 0.2% of the cylinder stroke.

Figure 65 – System position response to a step input of 3% of the cylinder stroke after positioning it at its mid-stroke in dead water.

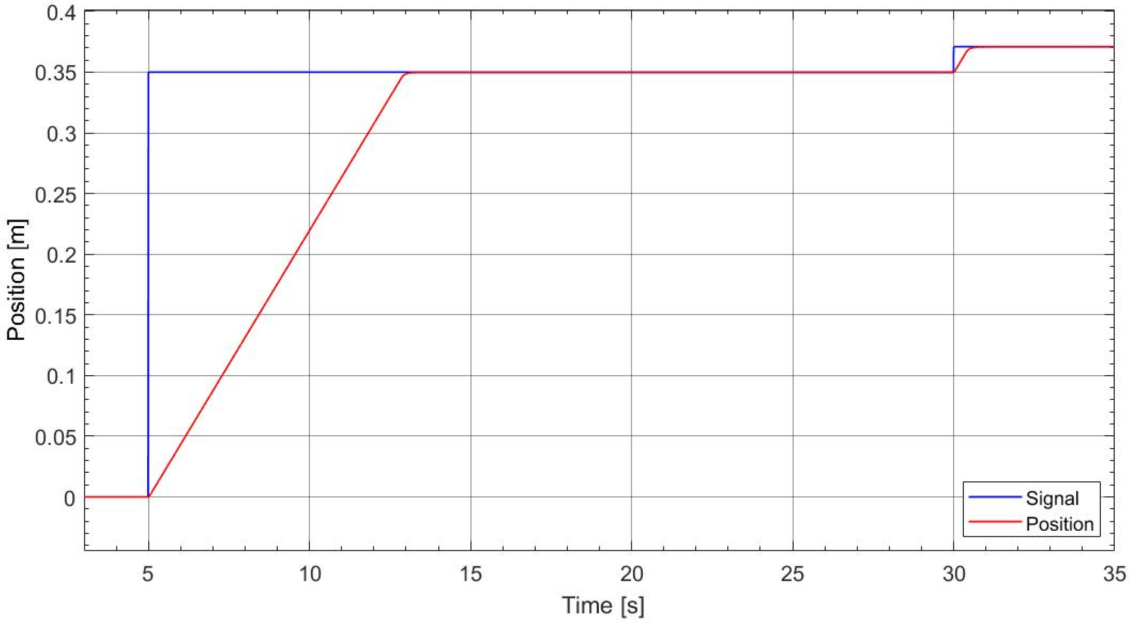

Source: Author (2024).

Figure 66 – Highlighted system position response to a step input of 3% of the cylinder stroke after positioning it at its mid-stroke in dead water.

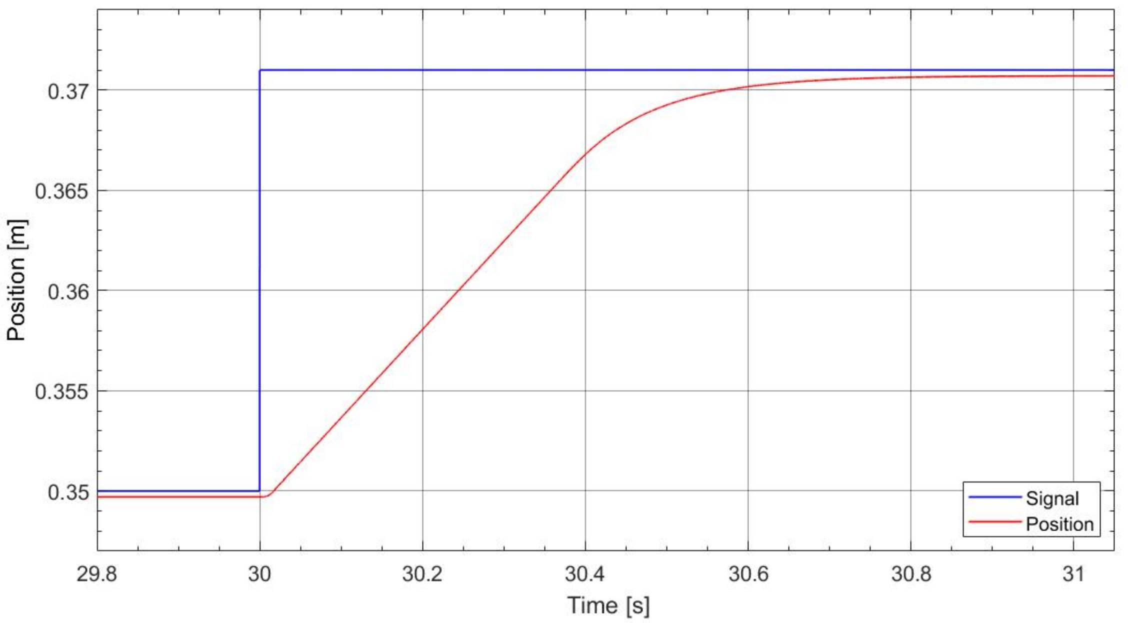

Source: Author (2024).

Figure 67 - Swash plate position for response analysis to a step of 3% of the actuator stroke after positioning it at mid-stroke in dead water.

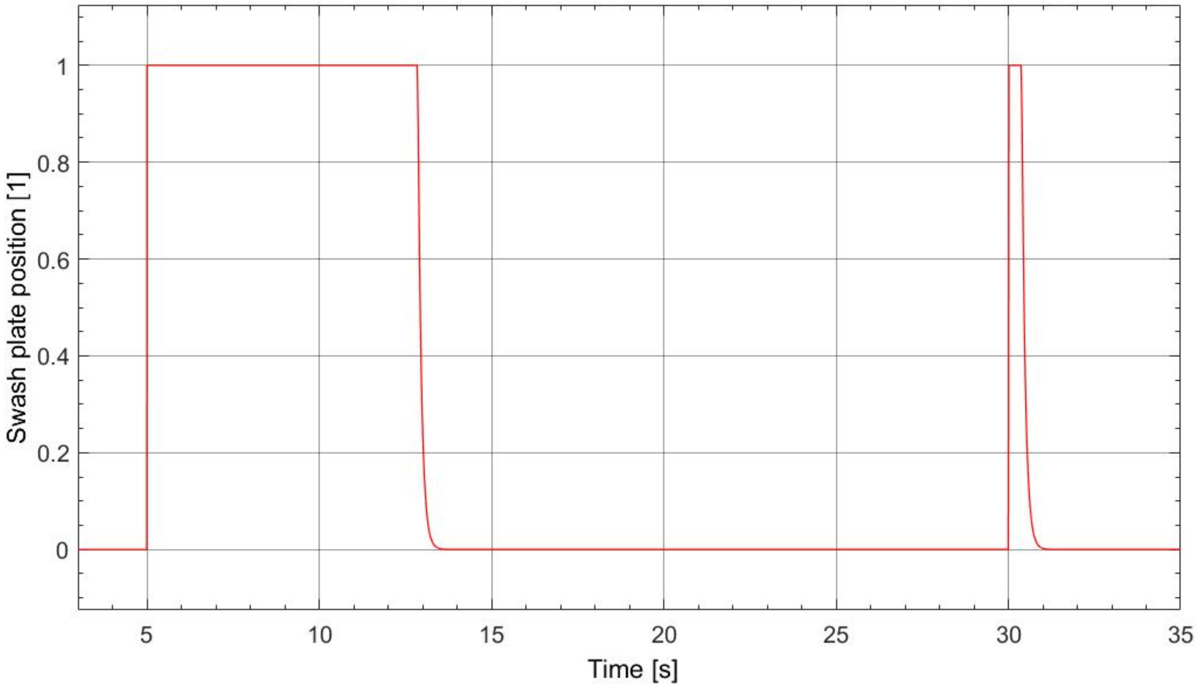

Source: Author (2024).

Figure 68 - Pump flow rate for the system response analysis to a step of 3% of the actuator stroke after positioning it at mid-stroke in dead water.

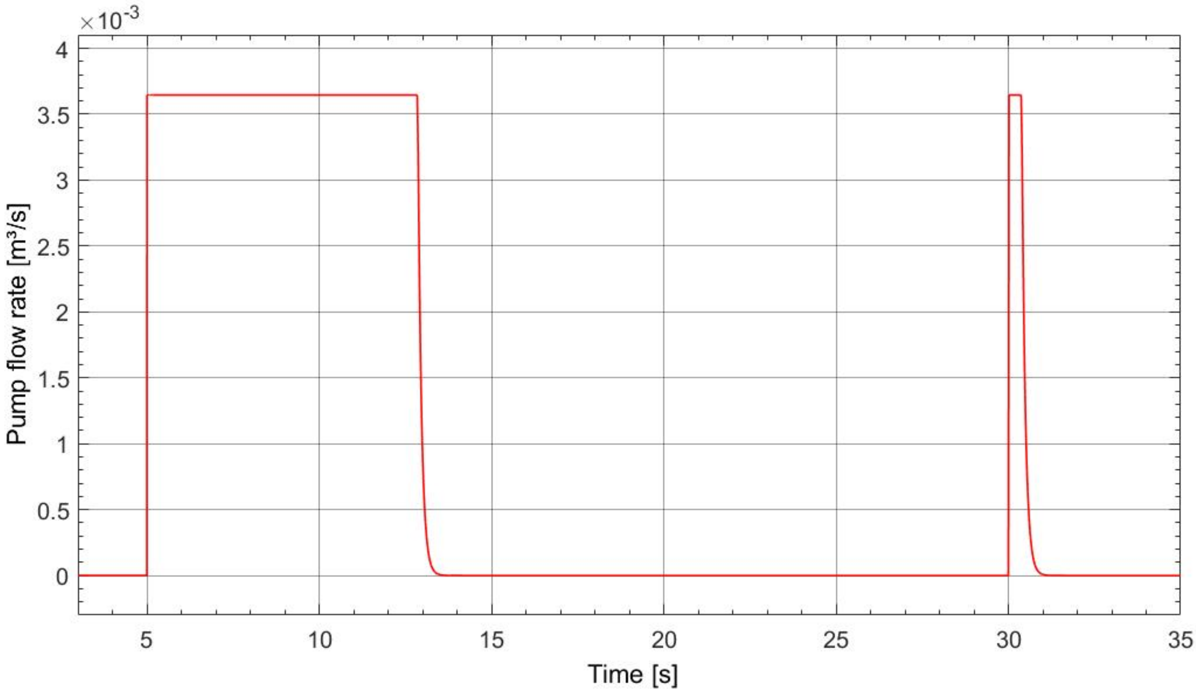

Source: Author (2024).

Table 16 - Performance parameters of the original power plant speed governor and the proposed system speed governor during the second input signal of 3% of the stroke after positioning it at mid-stroke in dead water.

Parameter		Original system	Proposed system
Position step input	%	3	3
Rise time	s	0.52	0.42
Settling time	s	0.90	0.52
Steady-state error	m	N.A.	2.7×10^{-4}

Source: Author (2024).

The simulated system has a steady state error of 2.7×10^{-4} m, representing 1.28% of the 3% of the stroke step input. The position error for the present simulation is presented in Figure 69. As expected, the position error is at its maximum when the step input is applied and decreases almost linearly up to the point when the swash plate begins to return to a position close to its neutral position.

Figure 69 - Position error for the system response analysis to a step of 3% of the actuator stroke after positioning it at mid-stroke in dead water.

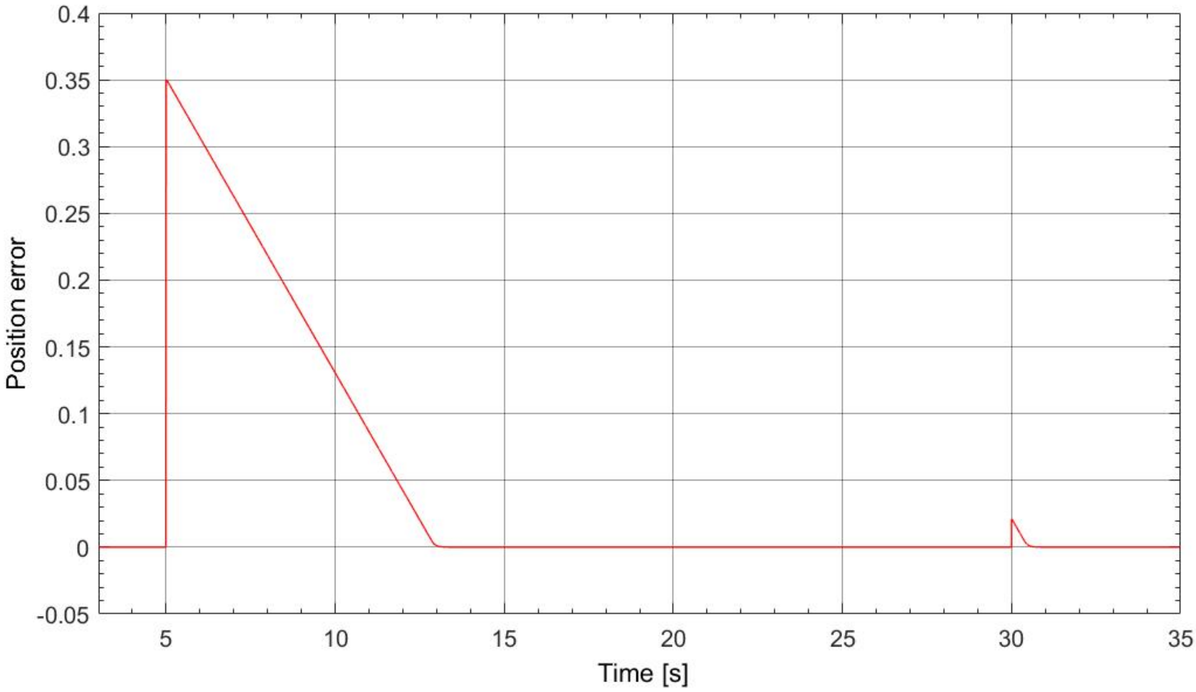

Source: Author (2024).

Figure 70 shows that the pressure in any of the cylinder's chambers never falls under 6×10^{-7} Pa so that cavitation is not present in the system for position step inputs of 3% of the total stroke.

Figure 70 - System pressures during the simulation of a step input of 3% of the cylinder stroke after positioning it at its mid-stroke in dead water.

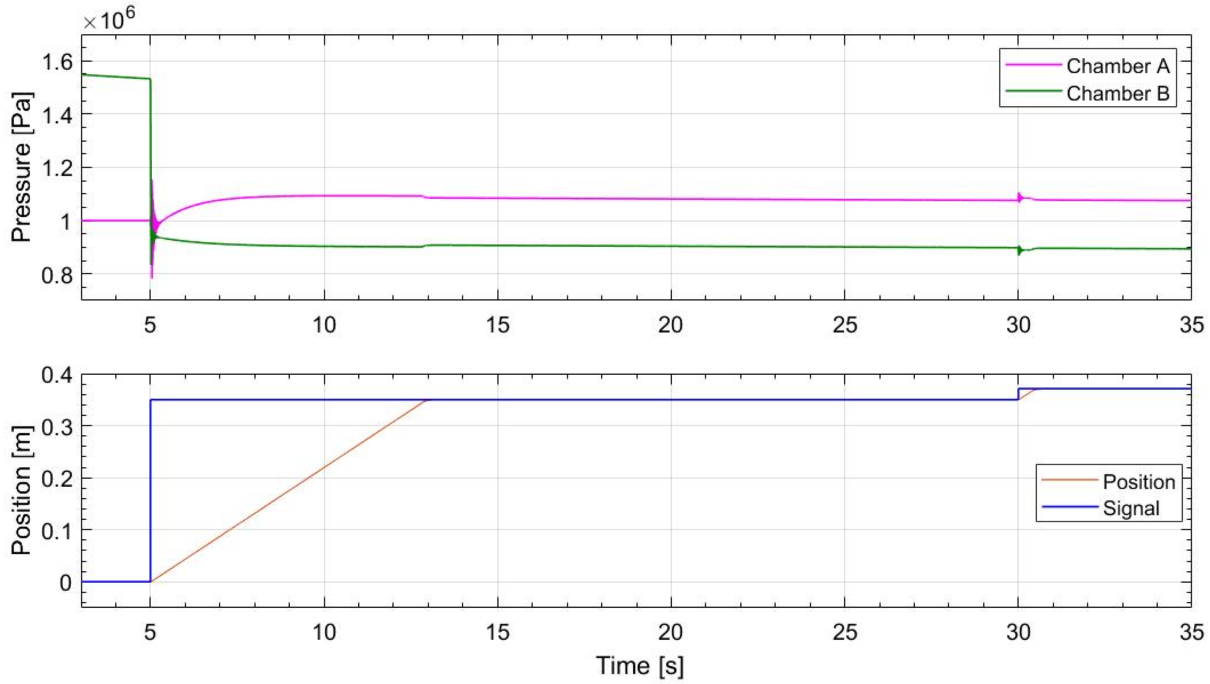

Source: Author (2024).

5 CONCLUSIONS

This master's thesis presents an overview of a hydroelectric power plant and its main components, with emphasis on the speed governor. After analyzing a typical hydraulic system for this type of machine, a modern and decentralized system is proposed, allowing each function to operate independently. To achieve this, an electro-hydrostatic actuator is employed for each function of the power plant and at a higher pressure than that of the analyzed plant.

A review of hydrostatic actuators was provided to offer the necessary background for selecting the best design for the application. A new architecture is proposed, whose performance analysis comprises the opening time evaluations, as well as the dynamic response and its emergency response capability. All simulations and analyses were conducted via simulation using the Hopsan and Matlab/Simulink softwares, with the main models described in this work.

Therefore, it is possible to conclude that the system can handle small variations in electrical power supply in the same manner as the original system, to open the distributor wicket gates in due time, and safely perform emergency shutdowns.

Another significant contribution is the reduction in oil consumption, the new system architecture significantly reduces the accumulator oil volume from 4.054 m^3 (4054 l) to 0.087 m^3 (87 l). Furthermore, as an electrohydrostatic actuator in a decentralized architecture, it can be installed close to the servomotor, leading to a considerable reduction in the piping volume, originally 0.848 m^3 (848 L). The increased pressure also reduces the combined servomotor volume from 0.617 m^3 (617 L) to 0.058 m^3 (58 L).

Furthermore, the reduced number of components as well as their size decrease makes maintenance easier. In addition, there is no need for special components exclusively manufactured for the speed governor, such as a distribution valve, which enhances the overall reliability of the system's components.

Additionally, this thesis introduces a method to avoid excessive intermittency in pilot-operated check valves used to compensate for area differences in hydraulic cylinders and compensate for leaks. This is achieved through the pilot-operated directional valves 2V5 and 2V6, illustrated in Figure 29.

Finally, a complete hydraulic circuit is presented, demonstrating the feasibility of the project using commercially available components.

5.1 FUTURE WORKS

After a further analysis in this thesis the following works are proposed:

- To create a test bench and scale the system to apply in a power plant since this thesis covers only simulation results. Therefore, to validate it through experimental results would greatly contribute for understanding of these systems.
- As the present work employed a PI control with a specific load profile the development of control strategies for electro-hydrostatic actuators commanded via pump volumetric displacement with different load profiles and circuit configurations.
- To enhance the method for selecting variable displacement pumps for application in electro-hydrostatic actuators to incorporate a more suitable swash plate dynamics.
- To investigate and develop a solution for the hydraulic fluid maintainability regarding the filtration and thermal control since the system woks with a reduced amount of confined fluid.

BIBLIOGRAPHY

ABNT NBR 06445:2016. **Turbinas hidráulicas, turbinas-bombas e bombas de acumulação Hydraulic turbines, turbines-pump and accumulation pumps**. 2. ed. Rio de Janeiro: Associação Brasileira de Normas Técnicas, 2016. Disponível em: www.abnt.org.br.

AGÊNCIA NACIONAL DE ENERGIA ELÉTRICA. **Atlas de Energia elétrica do Brasil**. 3. ed. Brasília: ANEEL, 2008. Disponível em: http://www.aneel.gov.br/documents/656835/14876406/2008_AtlasEnergiaEletricaBrasil3ed/297ceb2e-16b7-514d-5f19-16cef60679fb. Acesso em: 29 jan. 2022.

AGOSTINI, Thales *et al.* Effect of Energy Recovery on Efficiency in Electro-Hydrostatic Closed System for Differential Actuator. **Actuators**, [*s. l.*], v. 9, n. 1, p. 1–16, 2020a. Disponível em: https://www.mdpi.com/2076-0825/9/1/12/htm. Acesso em: 3 mar. 2022.

AGOSTINI, Thales *et al.* Effect of energy recovery on efficiency in electro-hydrostatic closed system for differential actuator. **Actuators**, [*s. l.*], v. 9, n. 1, p. 1–16, 2020b.

ALLE, Navatha *et al.* Review on electro hydrostatic actuator for flight control. **International Journal of Fluid Power**, [*s. l.*], v. 17, n. 2, p. 125–145, 2016.

ARMSTRONG-HÉLOUVRY, Brian; DUPONT, Pierre; DE WIT, Carlos Canudas. A survey of models, analysis tools and compensation methods for the control of machines with friction. **Automatica**, [*s. l.*], v. 30, n. 7, p. 1083–1138, 1994.

ASAFF, Yesid; DE NEGRI, Victor Juliano; SOARES, João Marcos Castro. Pneutronic speed governor for small hydropower plants: a new application for pneumatics. **Journal of the Brazilian Society of Mechanical Sciences and Engineering**, [*s. l.*], v. 38, n. 8, p. 2621–2633, 2016.

BATISTA, Thales Agostini Ribeiro. **MODELING AND ANALYSIS OF AN ELECTRO-HYDROSTATIC SYSTEM USING ASYMMETRICAL CYLINDER FOR INDUSTRIAL AND MOBILE MACHINERY**. 2019. 1–119 f. Dissertação - Universidade Federal de Santa Catarina, Florianópolis, 2019.

BEECHER, B. J. Hydraulic turbines. *In*: BRITISH ELECTRICITY INTERNATIONAL. TURBINES, GENERATORS AND ASSOCIATED PLANT: INCORPORATING MODERN POWER SYSTEM PRACTICE. 3. ed. London: Pergamon, 1991. v. C, p. 422–445. Disponível em: https://linkinghub.elsevier.com/retrieve/pii/B9780080405131500130. Acesso em: 20 fev. 2022.

BOSCH REXROTH. **Axial piston variable pump A4VSG Series 1x and 3x**. Horb am Neckar: Bosch Rexroth, 2018.

BOSCH REXROTH. **Electro-hydraulic control with proportional solenoid EP**. Horb am Neckar: Bosch Rexroth, 2021.

BOSCH REXROTH. **Hydraulic Cylinders Mill Type**. Pomerode: [*s. n.*], 2022.

BOSSCHE, Dominique van den. THE A380 FLIGHT CONTROL ELECTROHYDROSTATIC ACTUATORS, ACHIEVEMENTS AND LESSONS LEARNT. *In*: , 2006, Hamburg. **25th International Congress Of The Aeronautical Sciences**. Hamburg: ICAS, 2006. p. 1–8.

BOSTANCI, Emine *et al.* Opportunities and Challenges of Switched Reluctance Motor Drives for Electric Propulsion: A Comparative Study. **IEEE Transactions on Transportation Electrification**, [*s. l.*], v. 3, n. 1, p. 58–75, 2017. Disponível em: Acesso em: 17 jan. 2023.

BRAVO, Rafael Rivelino da Silva *et al.* APLICAÇÃO DE TÉCNICAS DE ANÁLISE DE RISCO EM UM REGULADOR DE VELOCIDADE ELETRO-HIDRÁULICO DE TURBINAS DE CENTRAIS HIDRELÉTRICAS. *In*: 2012, São Luís. **VII Congresso Nacional de Engenharia Mecânica**. São Luís: Associação Brasileira de Engenharia e Ciências Mecânicas, 2012. p. 1–10.

BREEZE, Paul. Hydropower Turbines. **Hydropower**, [*s. l.*], p. 35–46, 2018. Disponível em: Acesso em: 20 fev. 2022.

CANUDAS DE WIT, C *et al.* A new model for control of systems with friction. **IEEE Transactions on automatic control**, [*s. l.*], v. 40, n. 3, p. 419–425, 1995.

CAO, Wenping *et al.* Overview of electric motor technologies used for more electric aircraft (MEA). **IEEE Transactions on Industrial Electronics**, [*s. l.*], v. 59, n. 9, p. 3523–3531, 2012. Disponível em: Acesso em: 17 jan. 2023.

CORÀ, Emiliano *et al.* **Hydropower Technologies: the state-of-the-art**. [*S. l.: s. n.*], 2020.

COSTA, Gustavo Koury; SEPEHRI, Nariman. **HYDROSTATIC TRANSMISSIONS AND ACTUATORS: OPERATION, MODELLING AND APPLICATIONS**. 1. ed. Winnipeg: Wiley, 2015.

COZ, Federico *et al.* **Manual de mini microcentrales hidraulicas: una guía para el desarrollo de proyetos**. 1. ed. Lima: Intermidiate Technology Development Group, ITDG - Perú, 1995.

DE NEGRI, Victor; RAMOS FILHO, José; SOUZA, Alisson. A Design Method for Hydraulic Positioning Systems. *In*: , 2008, Las Vegas, USA. **Proceedings of the 51st National Conference on Fluid Power**. Las Vegas, USA: National Fluid Power Association, 2008. p. 669–679.

DUPONT, Pierre; ARMSTRONG, Brian; HAYWARD, Vincent. Elasto-plastic friction model: contact compliance and stiction. *In*: , 2000. **Proceedings of the 2000 American control conference. ACC (IEEE cat. no. 00CH36334)**. [*S. l.*]: IEEE, 2000. p. 1072–1077.

EICK, Guilherme. **VIABILIDADE ECONÔMICA E FINANCEIRA DE UMA PEQUENA CENTRAL HIDRELÉTRICA NO BRASIL**. 2010. 1–69 f. Trabalho de conclusão de curso - UNIVERSIDADE FEDERAL DE SANTA CATARINA, Florianópolis, 2010.

EKMAN, Anna; BÖRJESSON, Pal. Life cycle assessment of mineral oil-based and vegetable oil-based hydraulic fluids including comparison of biocatalytic and conventional production methods. **International Journal of Life Cycle Assessment**, [*s. l.*], v. 16, n. 4, p. 297–305, 2011.

ELBULUK, Malik E.; KANKAM, M. David. Motor drive technologies for the power-by-wire (PBW) program: options, trends and tradeoffs. **IEEE Proceedings of the National Aerospace and Electronics Conference**, [*s. l.*], v. 1, p. 511–522, 1995. Disponível em: Acesso em: 17 jan. 2023.

EPE, EMPRESA DE PESQUISA ENERGÉTICA. **BALANÇO ENERGÉTICO NACIONAL 2021: Ano base 2020**. Rio de Janeiro: [*s. n.*], 2021. Disponível em: https://www.epe.gov.br/sites-pt/publicacoes-dados-abertos/publicacoes/PublicacoesArquivos/publicacao-601/topico-596/BEN2021.pdf. Acesso em: 1 nov. 2021.

FASOL, Karl Heinz. A Short History of Hydropower Control. **IEEE Control Systems**, [*s. l.*], v. 22, n. 4, p. 68–76, 2002.

FURST, Fernando Luiz. **Sistematização do projeto preliminar de circuitos hidráulicos de controle de posição**. 2001. 1–149 f. Dissertação - UNIVERSIDADE FEDERAL DE SANTA CATARINA, Florianópolis, 2001.

GELINSKI, Sabrina *et al.* Development and testing of a novel glycerol/chitosan based biocide-free hydraulic fluid. **Journal of Cleaner Production**, [*s. l.*], v. 112, p. 3589–3596, 2016.

GENE, Franklin; POWEL, J. David; EMAMI-NAEINI, Abbas. **Sistemas de Controle para Engenharia**. 6. ed. Porto Alegre: Bookman, 2013.

HADJIPASCHALIS, Ioannis; POULLIKKAS, Andreas; EFTHIMIOU, Venizelos. Overview of current and future energy storage technologies for electric power applications. **Renewable and Sustainable Energy Reviews**, [*s. l.*], v. 13, n. 6–7, p. 1513–1522, 2009.

HELDUSER, S. Electric-hydrostatic drive—an innovative energy-saving power and motion control system:. **http://dx.doi.org/10.1243/0959651991540250**, [*s. l.*], v. 213, n. 5, p. 427–437, 1999. Disponível em: https://journals.sagepub.com/doi/10.1243/0959651991540250. Acesso em: 2 mar. 2022.

HENN, Érico Antônio Lopes. **MÁQUINAS DE FLUIDO**. 2. ed. Santa Maria: Ed. da UFSM, 2006. Disponível em: www.ufsm.br/ed1torn.

HIDROENERGIA. **Tipos de Turbinas Hidráulicas: Conheça os principais modelos**. [*S. l.*], 2021. Disponível em: https://www.hidroenergia.com.br/blog/tipos-turbinas-hidraulicas/. Acesso em: 4 dez. 2021.

IEC 61362:2012. **Guide to specification of hydraulic turbine governing systems**. [*S. l.: s. n.*], 2012.

IEEE 125:2007. **IEEE Recommended Practice for Preparation of Equipment Specifications for Speed-Governing of Hydraulic Turbines Intended to Drive Electric Generators**. New York: The Institute of Electrical and Electronics Engineers, Inc., 2007.

JACK, Alan G; MECROW, Barrie C; HAYLOCK, James A. A Comparative Study of Permanent Magnet and Switched Reluctance Motors for High-Performance Fault-Tolerant Applications. **IEEE TRANSACTIONS ON INDUSTRY APPLICATIONS**, [*s. l.*], v. 32, n. 4, p. 889–895, 1996.

KÄRNELL, Samuel *et al.* Pump-Controlled Actuators with Dump Valves. *In*: , 2021, Linköping. **The 17th Scandinavian International Conference on Fluid Power**. Linköping: [*s. n.*], 2021. p. 150–160.

KETELSEN, Søren *et al.* **Classification and review of pump-controlled differential cylinder drives**. [*S. l.*]: MDPI AG, 2019.

KRISHNAN, R. (Ramu). **Switched reluctance motor drives : modeling, simulation, analysis, design, and applications**. [*S. l.*]: CRC Press, 2001.

LINSINGEN, Irlan Von. **Fundamentos de Sistemas Hidráulicos**. 5. ed. Florianópolis: Editora UFSC, 2016.

LINSINGEN, Irlan Von; DE NEGRI, Victor J. **Handbook of hydraulic fluid technology**. 2. ed. Boca Raton: CRC Press, 2012.

MACINTYRE, Archibald Joseph. **Máquinas Motrizes Hidráulicas**. 1. ed. Rio de Janeiro: Guanabara Dois S.A., 1983.

MARÉ, Jean-Charles. **Aerospace Actuators**. [*S. l.*]: John Wiley & Sons, Incorporated, 2017.

MATAIX, Claudio. **Turbomáquinas Hidráulicas: Turbinas hidráulicas, Bombas, Ventiladores**. 1. ed. Madrid: Editorial ICAI, 1975.

MAZZORANA, Rafael Hilário Fonseca. **MODELAGEM DINÂMICA VIA FLUXO DE POTÊNCIA DE REGULADORES DE VELOCIDADE EM USINAS HIDRELÉTRICAS**. 2008. 1–140 f. Dissertação - Universidade Federal de Santa Catarina, Florianópolis, 2008.

MENDOZA, Yesid Ernesto Asaff. **DESENVOLVIMENTO DE UM SISTEMA SERVOPNEUMÁTICO PARA REGULAÇÃO DE VELOCIDADE DE TURBINAS EM PEQUENAS CENTRAIS HIDRELÉTRICAS**. 2006. 1–143 f. Dissertação - Universidade Federal de Santa Catarina, Florianópolis, 2006.

MICHEL, Sebastian; WEBER, Jürgen. Electrohydraulic compact-drives for low power applications considering energy-efficiency and high inertial loads. *In*: , 2012, Reggio Emilia. **The 7th FPNI PhD Symposium on Fluid Power**. Reggio Emilia: [*s. n.*], 2012. p. 869–888. Disponível em: https://www.researchgate.net/profile/Sebastian-Michel-4/publication/332119168_Electrohydraulic_compact-drives_for_low_power_applications_considering_energy-efficiency_and_high_inertial_loads/links/5f7d7cb8a6fdccfd7b4cabe6/Electrohydraulic-compact-drives-for-low-power-applications-considering-energy-efficiency-and-high-inertial-loads.pdf. Acesso em: 6 mar. 2022.

MUNOZ-HERNANDEZ, German Ardul; MANSOOR, Sa'ad Petrous; JONES, Dewi Ieuan. **Modelling and Controlling Hydropower Plants**. 1. ed. London: Springer London, 2013.

(Advances in Industrial Control). Disponível em: http://link.springer.com/10.1007/978-1-4471-2291-3.

MURARO, Irving; TEIXEIRA, Paulo Leonel; DE NEGRI, Victor Juliano. Effect of Proportional Valves and Cylinders on the Behavior of Hydraulic Positioning Systems. *In*: , 2013. **ASME/BATH 2013 Symposium on Fluid Power and Motion Control**. [*S. l.*]: American Society of Mechanical Engineers, 2013.

OBED, Adel A.; KADHIM, Abbas K. Speed and Current Limiting Control Strategies for BLDC Motor Drive System: A Comparative Study. **International Journal of Advanced Engineering Research and Science**, [*s. l.*], v. 5, n. 2, p. 119–130, 2018.

OFFICE OF ENERGY EFFICIENCY & RENEWABLE ENERGY. **Water Power Technologies Office: types of hydropower plants**. [*S. l.*], 2022. Disponível em: https://www.energy.gov/eere/water/types-hydropower-plants. Acesso em: 6 jan. 2022.

PATEL, Jainesh M.; HIRVANIYA, Hitesh v.; RATHOD, Mulav. Power Electronics and Motion Control Conference, 2009, IPEMC ’09, IEEE 6th International. **INTERNATIONAL JOURNAL OF INNOVATIVE RESEARCH IN ELECTRICAL, ELECTRONICS, INSTRUMENTATION AND CONTROL ENGINEERING**, [*s. l.*], v. 2, n. 3, p. 1236–1238, 2014.

PEREIRA, Giovane Gonçalves. **CONTROLE DE VELOCIDADE DE TURBINAS HIDRÁULICAS: aspectos teóricos e práticos**. 2020. 1–91 f. Trabalho de Conclusão de Curso - Universidade Federal de Santa Catarina, Florianópolis, 2020.

PERONDI, Eduardo André. Controle não-linear em cascata de um servoposicionador pneumático com compensação do atrito. [*s. l.*], 2002.

QUAN, Zhongyi; QUAN, Long; ZHANG, Jinman. Review of energy efficient direct pump controlled cylinder electro-hydraulic technology. **Renewable and Sustainable Energy Reviews**, [*s. l.*], v. 35, p. 336–346, 2014. Disponível em: Acesso em: 6 mar. 2022.

RAHMAN, Md Mustafizur *et al.* Assessment of energy storage technologies: A review. **Energy Conversion and Management**, [*s. l.*], v. 223, p. 1–28, 2020.

RETZLAFF, L *et al.* Performance of distributing valves in hydroelectric speed governors: analysis of the influence of the internal geometry. *In*: , 2009, Ubatuba. **THE 8th LATIN-AMERICAN CONGRESS ON ELECTRICITY GENERATION AND TRANSMISSION - CLAGTEE 2009**. Ubatuba: UNESP, 2009. p. 1–7. Disponível em: https://www.osti.gov/etdeweb/biblio/21461558. Acesso em: 3 fev. 2022.

SCHREIBER, Gerhard Paul. **Usinas Hidrelétricas**. 1. ed. São Paulo: Editora Edgard Blücher LTDA, 1977.

SOUZA, Zulcy de; SANTOS, Afonso Henriques M.; BORTONI, Edson da Costa. **Centrais Hidrelétricas: estudos para implantação**. 1. ed. Rio de Janeiro: Eletrobrás, 1999.

SU, Wenhai; JIANG, Jihai. Direct Drive Volume Control Electro-Hydraulic Servo Ship Rudder. **Key Engineering Materials**, [*s. l.*], v. 439–440, p. 1388–1392, 2010. Disponível em: https://www.scientific.net/KEM.439-440.1388. Acesso em: 1 mar. 2022.

SWEVERS, Jan *et al.* An integrated friction model structure with improved presliding behavior for accurate friction compensation. **IEEE Transactions on automatic control**, [*s. l.*], v. 45, n. 4, p. 675–686, 2000.

TAKESHI, SASAGAWA *et al.* **Hybrid servo system and water wheel operation mechanism equipped with the same**. JP6139041B1; JP2018135915A. Concessão: 2018.

TAO, Gang; KOKOTOVIC, Petar V. **Adaptive control of systems with actuator and sensor nonlinearities**. [*S. l.*]: John Wiley & Sons, Inc., 1996.

TAŠNER, Tadej; LOVREC, Darko. COMPARISON OF MODERN ELECTROHYDRAULIC SYSTEMS. *In*: , 2011, Nis. **34 th INTERNATIONAL CONFERENCE ON PRODUCTION ENGINEERING**. Nis: [*s. n.*], 2011. p. 253–256.

TEIXEIRA, Paulo Leonel. **ANÁLISE TEÓRICO EXPERIMENTAL DE PRENSA DOBRADEIRA HIDRÁULICA CONTROLADA POR BOMBA-MOTOR COM VELOCIDADE VARIÁVEL**. 2015. 1–154 f. Dissertação - Universidade Federal de Santa Catarina, Florianópolis, 2015.

VALDIERO, Antonio Carlos. Controle de robôs hidráulicos com compensação de atrito. [*s. l.*], 2005.

VIVIER, Lucien. **Turbines Hydrauliques et leur régulation**. Albin Micheled. [*S. l.: s. n.*], 1966.

WANG, Yan; GUO, Shengrong; DONG, Hongkang. Modeling and control of a novel electro-hydrostatic actuator with adaptive pump displacement. **Chinese Journal of Aeronautics**, [*s. l.*], v. 33, n. 1, p. 365–371, 2020.

YANG, Zhi *et al.* Comparative study of interior permanent magnet, induction, and switched reluctance motor drives for EV and HEV applications. **IEEE Transactions on Transportation Electrification**, [*s. l.*], v. 1, n. 3, p. 245–254, 2015.

ZIMMERMAN, Joshua; BUSQUETS, Enrique; IVANTYSYNOVA, Monika. 40% Fuel Savings by Displacement Control Leads to Lower Working Temperatures - A Simulation Study and Measurements. *In*: , 2011, Las Vegas. **52nd National Conference on Fluid Power**. Las Vegas: [*s. n.*], 2011. p. 23–25. Disponível em: https://www.researchgate.net/publication/276274955_40_Fuel_Savings_by_Displacement_Control_Leads_to_Lower_Working_Temperatures_-_A_Simulation_Study_and_Measurements. Acesso em: 3 mar. 2022.

ANNEX A

Free Buckling Length

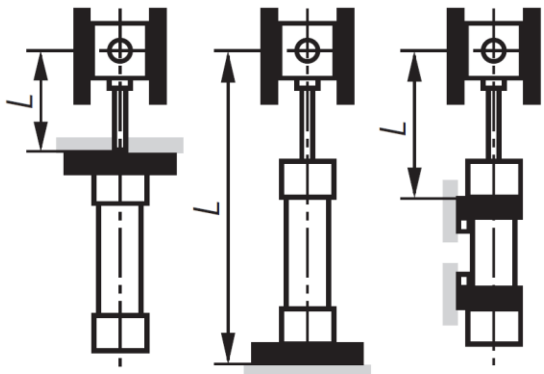

$L_K = 0{,}7\,L$

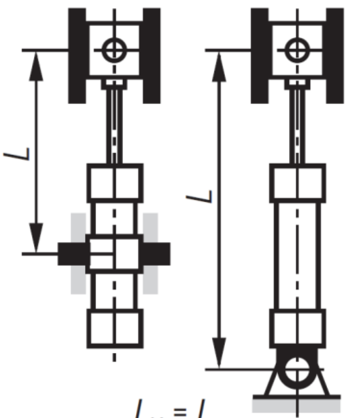

$L_K = L$

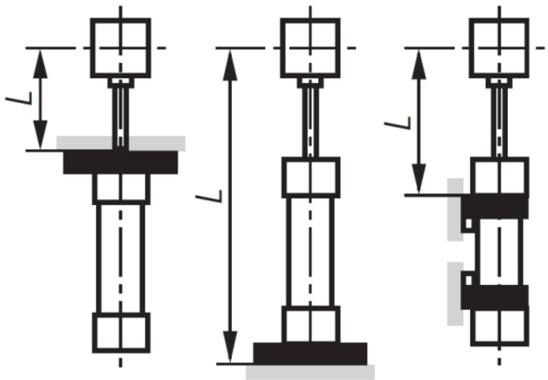

$L_K = 2\,L$

Source: Adapted from Bosch Rexroth (2022)

APPENDIX A
Motor selection and starting time estimation

- Required power

According to Linsingen (2016) the power required by a hydraulic pump considering an efficiency of 100% is:

$$P_h = p \cdot q_V \ ,$$

where:

P_h = Required power [W];

p = Pressure [Pa];

q_V = Flow rate [m³/s].

Taking in account the overall efficiency we have:

$$P_h = \frac{p \cdot q_V}{\eta_T} \ ,$$

where:

P_h = Required power [W];

p = Pressure [Pa];

q_V = Flow rate [m³/s];

η_T = Total efficiency [%].

Taking into account a pump the same size as the one dimensioned in Section 3.6, i.e., 125cm³/rev., its flow rate at 1750 rpm is 3.6458×10^{-3} m³/s. Assuming the system's maximum working pressure of 350×10^5 Pa and an overall efficiency of 92%, we need at least 138.699 KW to power the main circuit.

$$P_h = \frac{350 \times 10^5 \cdot 3.6458 \times 10^{-3}}{0.92} = 138699 \ W$$

Therefore, it is possible to use a motor of 150 KW, whose efficiency is about 94.9% for partial load, to power the main circuit. This three phase induction motor (squirrel cage) provides 800 N·m of rated torque and has a moment of inertia of 3.55 kg·m².

According to Linsingen (2016), The torque needed to drive the pump disregarding its efficiency is given by the equation:

$$T_h = \frac{D \cdot \Delta p}{2\pi} = \frac{125 \times 10^{-6} \cdot 350 \times 10^{5}}{2\pi} = 696.3\ N \cdot m$$

where:

T_h = Required torque [N·m];

p = Pressure [Pa].

From Newton's second law we have:

$$T = J \cdot \alpha,$$

Rearranging it:

$$\alpha = \frac{T}{J},$$

where:

α = Acceleration [rad/s²];

T = Torque [N·m];

J = Moment of inertia [kg·m²].

Then, assuming the acceleration to be constant we have:

$$\alpha = \frac{T_m - T_h}{J_m + J_p},$$

where:

α = Acceleration [rad/s²];

T_m = Motor torque [N·m];

T_h = Required torque [N·m];

J_m = Motor's moment of inertia [kg·m²];

J_p = Pump's moment of inertia [kg·m²].

Neglecting the pump inertia the average acceleration is:

$$\alpha = \frac{T_m - T_h}{J_m} = \frac{800 - 696.3}{3.55} = 29.21\ rad/s^2$$

Finaly, through the equation for constant angular acceleration we can estimate the minimum time for the motor to reach the rated angular speed.

$$\omega = \omega_0 + \alpha_c \cdot t\ ,$$

where:

ω = Final angular velocity [rad/s];

ω_0 = Initial angular velocity [rad/s];

α_c= Constant acceleration [rad/s²];

t = Time [s].

Therefore, we can find that even neglecting the pump moment of inertia, we have a considerable time to accelerate motors as big as 150 KW.

$$t = \frac{\omega - \omega_0}{\alpha_c} = \frac{183.259 - 0}{29.21} = 6.3\ s$$

APPENDIX B

Hydraulic Cylinder Selection

- Maximum Buckling force:

$$\lambda = \frac{4 \cdot l_k}{d} = \frac{4 \cdot 1400}{140} = 40$$

$$\lambda_0 = \sqrt{\frac{\pi^2 \cdot E}{0.8 \cdot R_e}} = \sqrt{\frac{\pi^2 \cdot 210000}{0.8 \cdot 350}} = 86$$

$$\lambda < \lambda_0$$
$$40 < 86$$

$$F_{cr} = \frac{d^2 \cdot \pi(335 - 0.62 \cdot \lambda)}{4 \cdot \nu} = \frac{140^2 \cdot \pi(335 - 0.62 \cdot 40)}{4 \cdot 3}$$
$$F_{cr} = \mathbf{1591719.3\ N}$$

- Hydraulic force when the cylinder is retracting:

$$F_r = p \cdot A_r = p \cdot \frac{\pi \cdot ({d_p}^2 - {d_r}^2)}{4} = 350 \times 10^5 \cdot \frac{\pi \cdot (0.25^2 - 0.14^2)}{4}$$

$$F_r = \mathbf{1179275.3\ N,}$$

where:

F_r = Maximum force while retracting [N];

p = System pressure [Pa];

A = Area of the piston rod side [m²];

d_p = Piston diameter [m];

d_r = Piston rod diameter [m].

- Total force of both cylinders:

$$F_T = F_{cr} + F_r$$
$$F_T = 1591719.3 + 1179275.3$$

$$F_T = \mathbf{2770994.6\ N}$$

- Validation whether the new hydraulic cylinder is equivalent to the original:

$$\lambda = \frac{4 \cdot l_k}{d} = \frac{4 \cdot 1400}{250} = 22.4$$

$$\lambda_0 = \sqrt{\frac{\pi^2 \cdot E}{0.8 \cdot R_e}} = \sqrt{\frac{\pi^2 \cdot 210000}{0.8 \cdot 350}} = 86$$

$$\lambda < \lambda_0$$
$$22.4 < 86$$

$$F_{cr} = \frac{d^2 \cdot \pi(335 - 0.62 \cdot \lambda)}{4 \cdot \nu} = \frac{250^2 \cdot \pi(335 - 0.62 \cdot 22.5)}{4 \cdot 3}$$
$$F_{cr} = \mathbf{5253168.3\ N}$$

However, as the cylinder slenderness is small its force is limited by the pressure since the original system works with a pressure of only 3.1×10^6 Pa (31 bar). So that the maximum force during extension is computed as following.

$$F_{ex} = p \cdot A_p = p \cdot \frac{\pi \cdot {d_p}^2}{4} = 31 \times 10^5 \cdot \frac{\pi \cdot 0.77^2}{4}$$
$$F_{ex} = \mathbf{1443554\ N,}$$

where:

F_{ex} = Maximum force while extending [N];

p = System pressure [Pa];

A_p = Area of the piston side [m²];

d_p = Piston diameter [m].

- Hydraulic force when the cylinder is retracting:

$$F_r = p \cdot A_r = p \cdot \frac{\pi \cdot ({d_p}^2 - {d_r}^2)}{4} = 31 \times 10^5 \cdot \frac{\pi \cdot (0.77^2 - 0.25^2)}{4}$$

$$F_r = \mathbf{1291383.1}\ \mathbf{N},$$

where:

F_r = Maximum force while retracting [N];

p = System pressure [Pa];

A_r = Area of the piston rod side [m²];

d_p = Piston diameter [m];

d_r = Piston rod diameter [m].

- Total force of both cylinders:

$$F_0 = F_{ex} + F_r$$

$$F_0 = 1443554 + 1291383.1$$

$$F_0 = \mathbf{2734937.1}\ \mathbf{N},$$

where:

F_0 = Maximum force of the original system [N];

F_{ex} = Maximum force while extending [N];

F_r = Maximum force while retracting [N];

As the original system maximum force is smaller than the proposed system maximum force one can proceed with the design of the hydraulic system for the speed governor.

APPENDIX C

LuGre friction block diagram

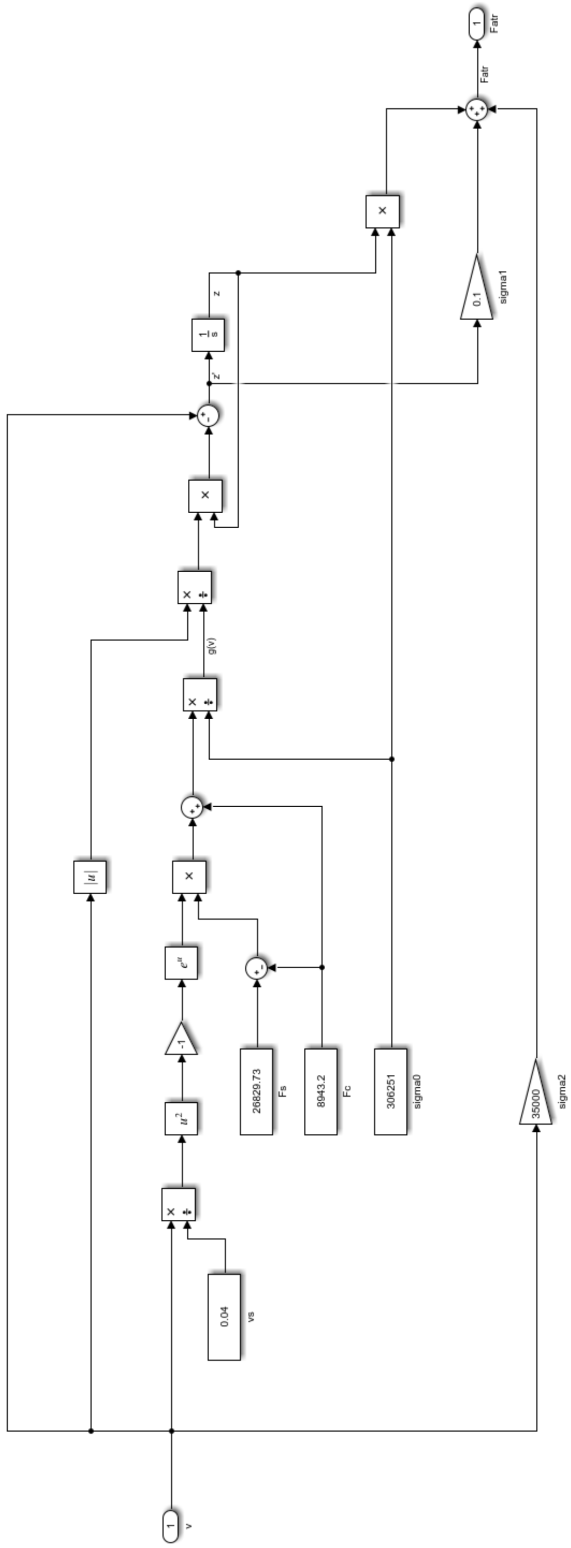

APPENDIX D

Servomotor external load block diagram

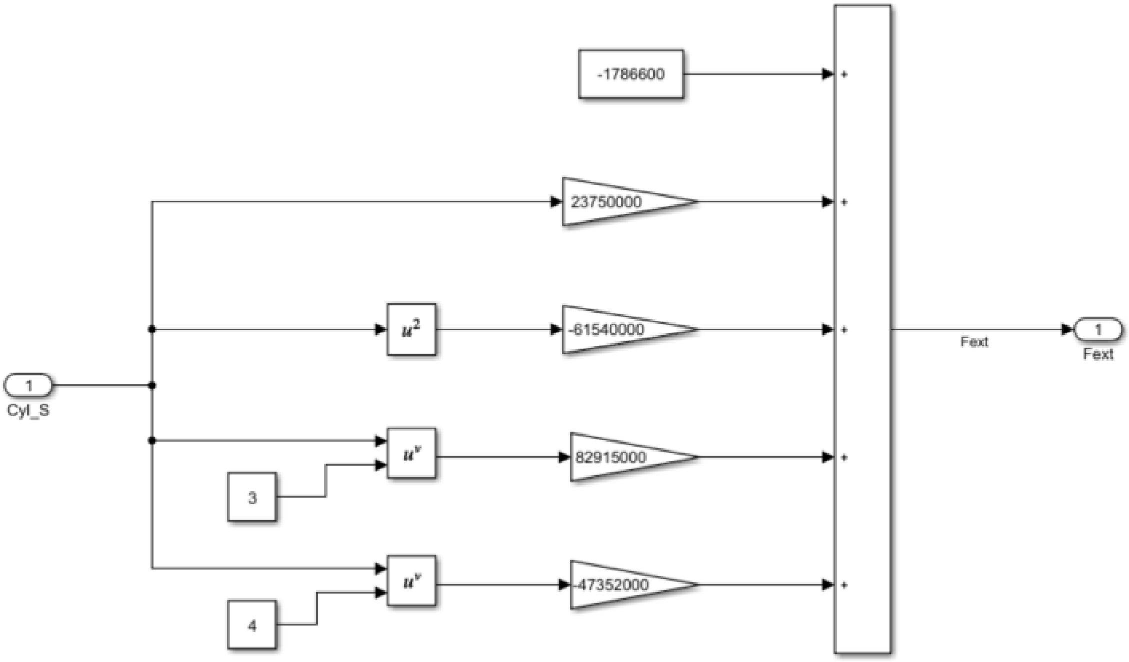

APPENDIX E

Hopsan model for the servomotor positioning control

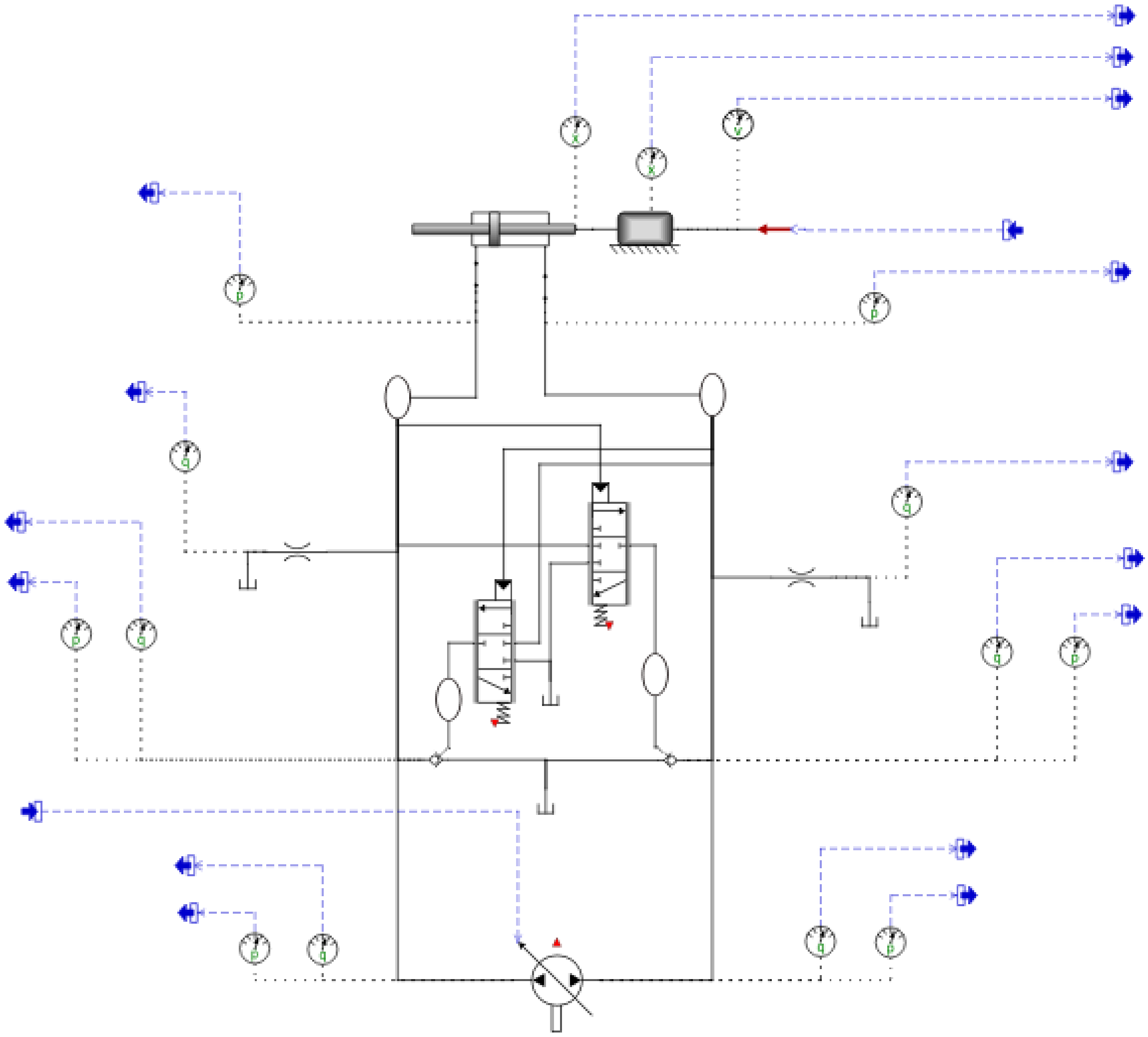

APPENDIX F

Complete Simulink model for the servomotor positioning control

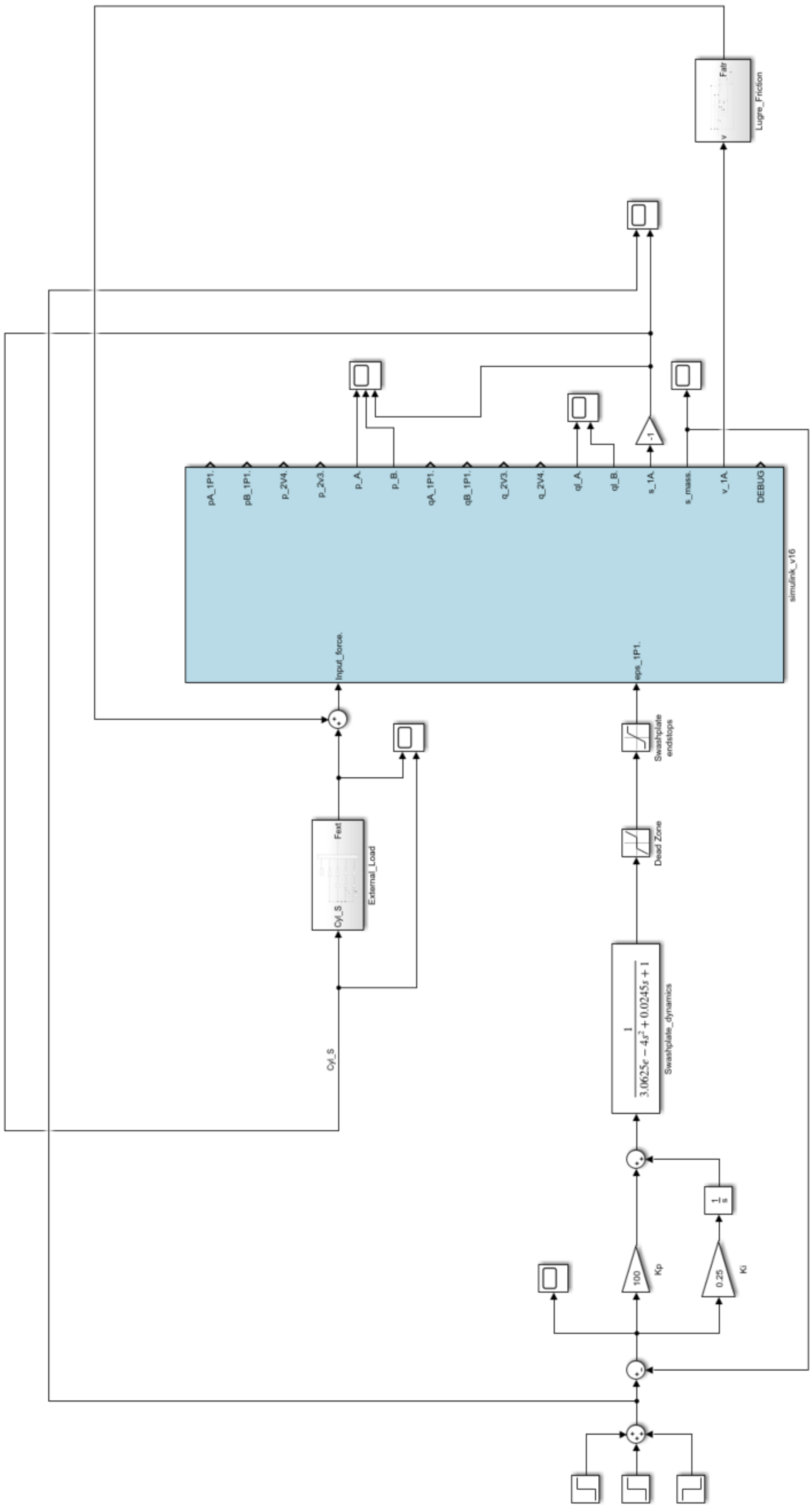

APPENDIX G

Hopsan model for the assessment of the emergency mode.

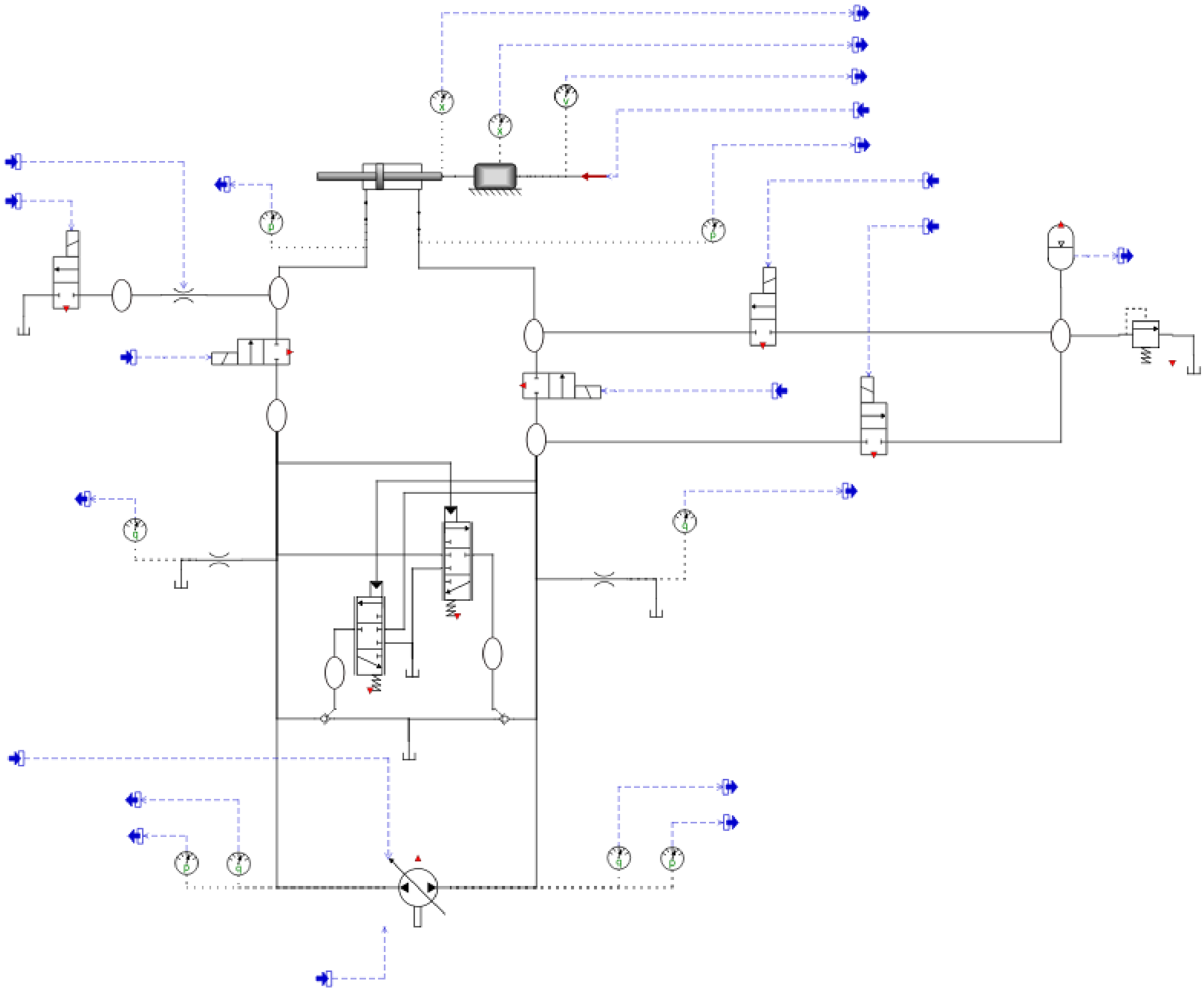

APPENDIX H

Simulink model for the assessment of the emergency mode.

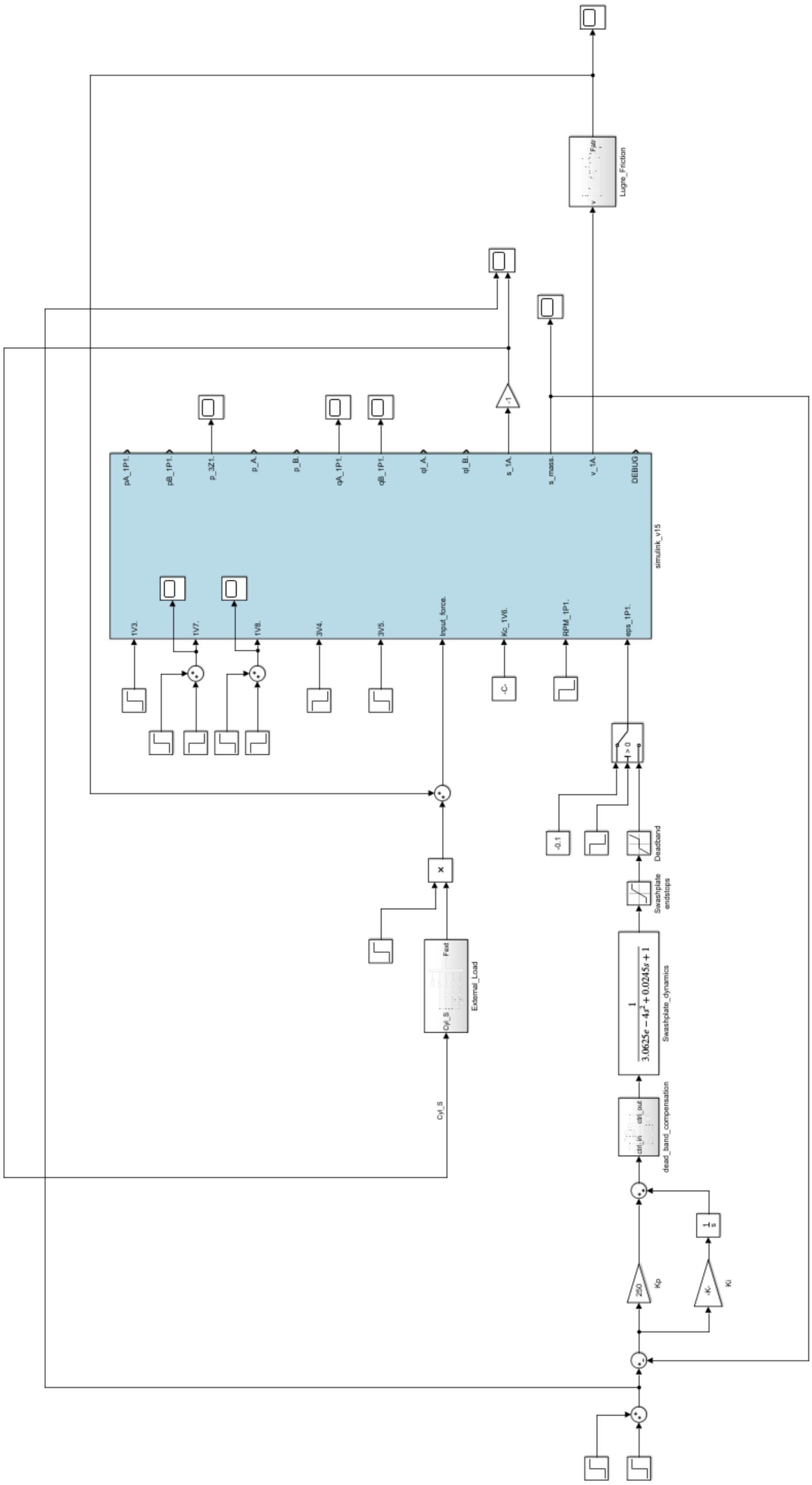

APPENDIX I

Complete Simulink model for the servomotor positioning control in still water

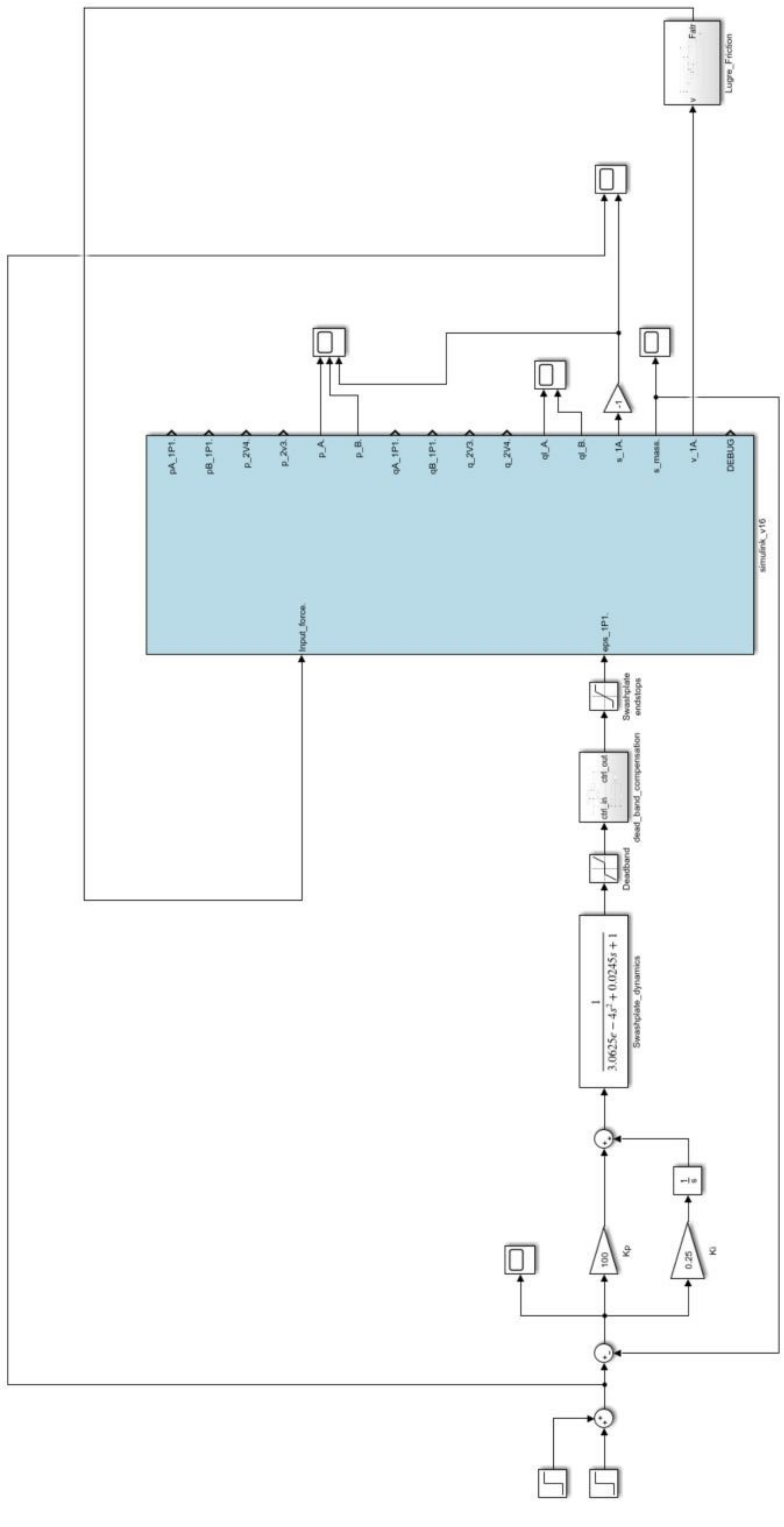

APPENDIX J

Simulation parameters

VALVE	SIMULATION PARAMETERS	UNIT	VALUE
Global	Oil density	kg/m^3	870
	Bulk Modulus	Pa	1.4×10^{9}
	viscosity	Ns/m2	0.03
	Kp	1	150
	Ki	1	0.25
1P1	Angular velocity	RPM	1750
	Displacement	cm^3/rev	125
	Leakage coefficient	(m^3/s)/Pa	1×10^{-12}
1V3	Resonance Frequency	rad/s	100
	Damping Factor	1	1
	Flow Coefficient	1	0.67
	Spool Diameter	m	0.05
	Spool Fraction of the Diameter	1	1
	Maximum Spool Displacement	m	0.01
1V4	Pressure-Flow Coefficient	m^5/Ns	1×10^{-10}
1V5	Resonance Frequency	rad/s	100
	Damping Factor	1	1
	Flow Coefficient	1	0.67
	Spool Diameter	m	0.05
	Spool Fraction of the Diameter	1	1
	Maximum Spool Displacement	m	0.01
1V6	Resonance Frequency	rad/s	100
	Damping Factor	1	1
	Flow Coefficient	1	0.67
	Spool Diameter	m	0.05
	Spool Fraction of the Diameter	1	1
	Maximum Spool Displacement	m	0.01
2V2	Restrictor Coefficient	1	3×10^{-5}
	Pilot Ratio	1	3.5
	Cracking Pressure	bar	10
2V3	Restrictor Coefficient	1	3×10^{-5}
	Pilot Ratio	1	3.5
	Cracking Pressure	bar	10
2V5	Reference pressure	bar	15
	Flow coefficient.	1	0.67
	spool diameter	m	0.01
	Spool cricle fraction(P-A)	1	1
	Spool cricle fraction(A-T)	1	1
	Underlap	m	0
	Underlap	m	0
	Turbulence onset pressure	Pa	10000
	Damping	N/(m s)	100
	Max spool displacement	m	-0.01

	Max spool displacement	m	0.01
	Stream angle	rad	0.03
	Spring constant	N/m	10
2V6	Reference pressure	bar	15
	Flow coefficient.	1	0.67
	spool diameter	m	0.01
	Spool cricle fraction(P-A)	1	1
	Spool cricle fraction(A-T)	1	1
	Underlap	m	0
	Underlap	m	0
	Turbulence onset pressure	Pa	10000
	Damping	N/(m s)	100
	Max spool displacement	m	-0.01
	Max spool displacement	m	0.01
	Stream angle	rad	0.03
	Spring constant	N/m	10
3Z1	Ackumulator Volume	m^3	0.617216
	Ack. inlet coeff.	m^3/(s Pa)	1.00E-08
	polytropic exp. of gas	1	1.2
	Preload pressure	N/m^2	3×10^7
	Momentary gas volume	m^3	0.001
	Ackumulator oil pressure	Pa	1×10^7
3V3	Reference pressure	bar	360
	Spool diameter	m	0.05
	Fraction of spool opening	1	0.1
	Damping	N/(m s)	1000
	Max spool displacement	m	0.002
	Flow coefficient	1	0.67
	Stream angle	rad	1.17
	Spring constant	N/m	10000
	Turbulent pressure trans.	Pa	100000
3V4	Resonance Frequency	rad/s	100
	Damping Factor	1	1
	Flow Coefficient	1	0.67
	Spool Diameter	m	0.05
	Spool Fraction of the Diameter	1	1
	Maximum Spool Displacement	m	0.01
3V5	Resonance Frequency	rad/s	100
	Damping Factor	1	1
	Flow Coefficient	1	0.67
	Spool Diameter	m	0.05
	Spool Fraction of the Diameter	1	1
	Maximum Spool Displacement	m	0.01